WL-TR-94-7039

DEBRIS CLOUD MATERIAL CHARACTERIZATION FOR HYPERVELOCITY IMPACTS OF SINGLE- AND MULTI-MATERIAL PROJECTILES ON THIN TARGET PLATES

Dr. William P. Schonberg

Civil & Environmental Engineering Department
University of Alabama in Huntsville
Huntsville Alabama 35899

May 1994

FINAL REPORT FOR PERIOD JUNE 1993 - SEPTEMBER 1993

Approved for Public Release; Distribution unlimited.

WRIGHT LABORATORY ARMAMENT DIRECTORATE
Air Force Materiel Command ▮ United States Air Force ▮ Eglin Air Force Base

NOTICE

When Government drawings, specifications, or other data are used for any purpose other than in connection with a definitely Government-related procurement, the United States Government incurs no responsibility or any obligation whatsoever. The fact that the Government may have formulated or in any way supplied the said drawings, specifications, or other data, is not to be regarded by implication, or otherwise as in any manner construed, as licensing the holder, or any other person or corporation; or as conveying any rights or permission to manufacture, use, or sell any patented invention that may in any way be related thereto.

This technical report has been reviewed and is approved for publication.

FOR THE COMMANDER

WALTER O. MAINE
Chief, Assessment and Instrumentation Division

Even though this report may contain special release rights held by the controlling office, please do not request copies from the Wright Laboratory, Armament Directorate. If you qualify as a recipient, release approval will be obtained from the originating agency by DTIC. Address your requests for additional copies to:

Defense Technical Information Center
Cameron Station
Alexandria VA 22304-6145

If your address has changed, if you wish to be removed from our mailing list, or if your organization no longer employs the addressee, please notify WL/MNSA, 101 West Eglin Blvd Ste 326, Eglin AFB FL 32542-6810, to help us maintain a current mailing list.

Do not return copies of this report unless contractual obligations or notice on a specific document requires that it be returned.

REPORT DOCUMENTATION PAGE

Form Approved
OMB No. 0704-0188

1. AGENCY USE ONLY (Leave blank)	2. REPORT DATE	3. REPORT TYPE AND DATES COVERED
	May 1994	Final June 1998 to September 1993

4. TITLE AND SUBTITLE
Debris Cloud Material Characterization for Hypervelocity Impacts of Single- and Multi-Material Projectiles on Thin Target Plates

5. FUNDING NUMBERS
C: F49620-90-C-0076
PE: N/A
PR:
TA:
WU:

6. AUTHOR(S)
William P. Schonberg

7. PERFORMING ORGANIZATION NAME(S) AND ADDRESS(ES)
University of Alabama in Huntsville
Civil and Environmental Engineering Department
Huntsville AL 35899

8. PERFORMING ORGANIZATION REPORT NUMBER

9. SPONSORING/MONITORING AGENCY NAME(S) AND ADDRESS(ES)
Wright Laboratory, Armament Directorate
Assessment and Instrumentation Division
Technology Assessment Branch (WL/MNSA)
101 W. Eglin Blvd., Ste 326
Eglin AFB FL 32542-6810

10. SPONSORING/MONITORING AGENCY REPORT NUMBER
WL-TR-94-7039

11. SUPPLEMENTARY NOTES
Availability of report is specified on verso of front cover.

12a. DISTRIBUTION/AVAILABILITY STATEMENT
Approved for public Release; distribution is unlimited.

12b. DISTRIBUTION CODE
A

13. ABSTRACT (Maximum 200 words)

The response of a target to a KEW impact can be said to consist of 'local' and 'global' phenomena. For KEW impacts, damage associated with local response occurs very quickly and is limited to a volume immediately adjacent to the impact site. Global response can refer to any one of a number of phenomena that occur over a longer period of time, under less intense loads, and over a much larger area of the target. In KEW impacts, one or more debris clouds are created during the initial impact on the outer wall of a target. These debris clouds can contain solid, melted, and vaporized projectile and target materials. The levels of melt and vaporization within the debris clouds determine the loads transmitted to various internal target components. To accurately determine total target damage, a lethality assessment scheme must include the effects of discrete impacts by solid fragments as well as impulsive loadings due to molten and vaporous debris cloud material. Thus, the amount of material in each of the three states of matter must be known to accurately assess total target damage and break-up. This report presents a first-principles method to calculate 1) the amount of material in a debris cloud created by a perforating hypervelocity impact that is solid, molten, and vaporous, 2) the debris cloud leading edge, trailing edge, center-of-mass, and expansion velocities, and 3) the angular spread of the debris cloud material. The method presented can be used for single- and multi-material solid rod projectiles impacting thin target plates. The methodology presented in this report includes, improves, and expands upon the debris cloud characterization scheme presented in WL-TR-93-7028. The predictions of this methodology are compared against those of empirically-based lethality assessment schemes and against numerical and empirical results.

14. SUBJECT TERMS
Hypervelocity Impact, Lethality, Vulnerability, Shock Waves, Mie-Gruneisen, Tillotson, Equation of State, Debris Clopd, Kinetic Energy Weapon, Vaporization, Penetration, Perforation

15. NUMBER OF PAGES
158

16. PRICE CODE

17. SECURITY CLASSIFICATION OF REPORT	18. SECURITY CLASSIFICATION OF THIS PAGE	19. SECURITY CLASSIFICATION OF ABSTRACT	20. LIMITATION OF ABSTRACT
UNCLASSIFIED	UNCLASSIFIED	UNCLASSIFIED	SAR

PREFACE

This program was conducted by the University of Alabama in Huntsville, Department of Civil and Environmental Engineering, Huntsville, AL 35899 under Contract No. F49620-90-C-0076 with the Wright Laboratory Armament Directorate (WL/MN), Eglin AFB FL, 32542-6810. Mr. Ron Hunt managed the program for the Armament Directorate. This work performed during the period from June 1993 to September 1993. This report is intended to supersede WL-TR-93-7028.

The author would like to acknowledge the support of the Air Force Office of Scientific Research Summer Faculty Research Program. In addition, the author is grateful to Mr. Scott Mullin of the Southwest Research Institute and to Ms. Kathy Holian of Los Alamos National Laboratory for their assistance with the implementation of the Tillotson equation-of-state. The assistance of Mr. Danny Brubaker and Mr. Bruce Patterson in performing the CTH runs for this study and in analyzing the output is also gratefully acknowledged. Finally, thanks to Mr. Ronald Hunt within the Technology Assessment Branch (WL/MNSA) for his guidance and assistance during the course of the research project.

TABLE OF CONTENTS

LIST OF FIGURES

LIST OF TABLES

1.0 INTRODUCTION

For the past eight years, the Wright Laboratory Armament Directorate at Eglin Air Force Base has conducted a Lethality/Vulnerability program to evaluate the effectiveness of kinetic energy weapons (KEWs) against ballistic missiles. This program, part of the Lethality and Target Hardening (LTH-5) Program of the Strategic Defense Initiative, has focused on the response of ballistic missile boosters, post-boost vehicles, and their associated warheads to KEW impacts. The evaluation and selection of the systems to advance from the conceptual phase of design to demonstration/validation, engineering/manufacturing development, production, and deployment requires the assessment of candidate weapons effectiveness against their intended threat spectrum.

The response of a target to a KEW impact can be said to consist of two basic and distinct types of response: 'local response' and 'global response'. For KEW impacts, material damage associated with local response occurs very quickly (i.e. within the first 100-200 μsec) and is limited to a volume immediately adjacent to the impact site. At sufficiently high impact velocities, shatter, melting, and/or vaporization of the materials can occur. For an aluminum-on-aluminum impact, the projectile and target materials will begin to shatter, melt, and vaporize at impact velocities of approx. 3.2, 5.6, and 10.4 km/sec, respectively [1,2].

Global response can refer to any one of a number of global phenomena that occur over a longer period of time (on the order of milliseconds), under less intense loads, and over a much larger area of the target. In KEW impacts, one or more debris clouds are created during the initial impact on the outer wall of a target. These debris clouds spread out as they move through target voids and eventually impact an inner wall or interior component of the target structure. Depending on the impact velocity and the relative material properties of the projectile and target, these debris clouds can contain solid, melted, and vaporized projectile and target materials. The levels of melt and vaporization within the debris clouds in turn determine the nature of the loads transmitted to various target components. Typical global

responses include the denting, buckling, tearing or catastrophic dismemberment of internal missile components.

To accurately determine total target damage, a lethality assessment methodology (see, e.g. [3-12]) must include the effects of discrete impacts by solid debris cloud fragments as well as impulsive loadings due to molten and vaporous debris cloud material. Clearly, the amount of debris cloud material in each of the three states of matter must be known to accurately assess total target damage and break-up due to a KEW impact. This report presents a first-principles method to calculate 1) the amount of material in a debris cloud created by a perforating hypervelocity impact that is solid, molten, and vaporous, 2) the debris cloud leading edge, trailing edge, center-of-mass, and expansion velocities, and 3) the angular spread of the debris cloud material. The method presented can be used for single- and multi-material solid rod projectiles impacting an array of target plates. The methodology presented in this report includes, improves, and expands upon the debris cloud characterization scheme presented in WL-TR-93-7028 [13]. As such, the information this report is intended to supersede the information in [13] and, with the exception of the portions that have been modified, the information in [13] is reproduced in its entirety in this report for completeness and to maintain continuity. At this point, no adjustments have been made to account for differences in response due to projectile yaw or impact obliquity. The predictions of this methodology are compared against those of empirically-based lethality assessment schemes as well as against numerical and empirical results obtained in previous studies of hypervelocity impact debris cloud formation.

2.0 LETHALITY ASSESSMENT MODEL REQUIREMENTS

The key to conducting an accurate lethality assessment is the use of a robust assessment methodology. The methodology should incorporate all the significant response and damage mechanisms which result from all hypervelocity weapon-target interactions. To accurately determine the total damage level sustained by an impacted target, a lethality assessment methodology must include the effects of discrete and simultaneous debris cloud fragment impacts, as well as impulsive target debris cloud loadings. Discrete or simultaneous impacts by individual fragments can pose a lethal threat to the inner wall or to an interior component of a target, depending on the fragments' speed, density, and trajectory, and on the density and strength of the target inner wall or interior component material. Individually, the molten and/or vaporous fragments in a debris cloud may not do significant damage; however, as a whole, they can produce a significant impulsive loading over a relatively large area inside the target. This in turn can result in further damage to the target at later times. Clearly then, to accurately assess the total damage to a target impacted by a KEW, the amounts and types of debris in a debris cloud produced by a hypervelocity impact must be known.

A number of empirical and semi-analytical procedures have been developed over the past decade to determine the lethal effectiveness of KEW systems. While these procedures are capable of assisting engineers and system architects in optimizing weapon designs and in performing cost trade- off studies, they are significantly limited in their characterization of the material in the debris clouds created by hypervelocity impacts. Unfortunately, very little impact test data for relatively massive projectiles (on the order of 10 gms or more) is available at speeds above 8 km/sec. This makes it difficult to properly characterize the nature of the material in the debris clouds over the entire impact velocity regime of interest. Electrostatic devices which can launch small particles to speeds as high as 100 km/sec exist, but these systems can only launch micron-size particles [14,15]. Other electric gun systems have launched Kapton flyer plates to speeds of 11 km/sec, but cannot reach that velocity with

chunky projectiles [16]. Thus, existing lethality assessment models must be used with a fair amount of caution, especially in scenarios involving impact velocities greater than those attainable in experiments.

Current semi-analytical lethality assessment models usually fall into one of two broad groups: discrete particle models [3-12,17,18] and expanding shell models [19-23]. Discrete particle models typically account for only solid fragments [3-8,17,18], or track only a small number of discrete fragments [9-12] in the debris cloud created by a high speed impact. These models are best suited for applications in which the debris clouds generated by the initial impact contain only a relatively small number of fragments and in which melting or vaporization of the projectile and target materials do not occur.

The expanding shell models typically assume that all of the debris cloud material is homogeneously distributed over a uniformly expanding spherical shell. These models are applicable only in those impact situations where complete projectile and target material vaporization occurs. Flash X-ray photographs of the debris clouds created in lead-on-lead impacts at speeds high enough to cause melting and vaporization do show that the assumptions of the spherical shell model are valid at least for the leading portion of the debris clouds [24]. However, when a debris cloud is comprised primarily of solid fragments, then similarly obtained photographs show the debris clouds to be elliptical with an eccentricity of approximately 1.6 [24].

It is evident, therefore, that the need exists to bridge the gap between the discrete particle models, which consider only a finite number of solid fragments, and the expanding shell models, which are most accurate when complete vaporization occurs. Specifically, a lethality assessment model that considers the creation and subsequent effects of debris clouds containing all three matter states is needed. FATEPEN2 [3-6], PEN-4 [7,8], and KAPP-II [10-12] are discrete particle lethality assessment models which can be modified to include the effects of non-solid debris cloud constituents.

The FATE family of codes was developed for the Naval Surface Warfare Center (NSWC) for analyzing the impacts of warhead fragments against aircraft structures over a range of impact velocities from 2.5 to 5.0 km/sec. Initially called FATE [3], later FATE-2 [4], and now FATEPEN2 [5,6], the code has been modified to include projectile tip erosion even at impact velocities below shatter velocity. The equations within the FATEPEN2 code predict the number of plates perforated in a multi-plate target configuration as well as the holes in the perforated plates. In addition, FATEPEN2 also predicts the number, size, trajectories, and velocities of the fragments in the various debris clouds created as the projectile or its remains move through a multi-plate target.

The PEN-4 lethality assessment model was developed for the NSWC in an attempt to model fragment impact against thin plates over a wider range of impact velocities [7,8]. This model is similar to the FATEPEN2 model in that the equations used in the model require a number of simplifying assumptions and experimentally derived factors. By restricting the lower limit of the impact velocity to 3.6 km/sec, PEN-4 is able to neglect shear failures in the projectile material; by restricting its upper limit to 7.6 km/sec, PEN-4 neglects material melting and vaporization. In more recent versions, PEN-4 has been updated to incorporate advanced fragmentation models. These fragmentation models are considerable improvements over the models used in earlier versions of the code.

KAPP-II was developed for the Defense Nuclear Agency to predict damage to complex three-dimensional aerospace targets impacted by multiple hypervelocity projectiles, including chunky fragments, rods, and hollow cylinders [10]. It is the fusion of the previously developed KAPP and KNAPP computer codes [11,12] and has been calibrated with an experimental database covering an impact velocity range of approx. 1-9 km/sec. The empirical relationships within KAPP-II allow the user to characterize the state of the projectile as it passes through the target as well as the response of the target system to the impact loadings of the initial projectile and the debris created by the initial impact. Unless otherwise noted, version 1.1 of KAPP-II was utilized in the study whose results are presented herein.

3.0 SHOCK LOADING AND RELEASE ANALYSIS

3.1 Introductory Comments

Consider the normal impact of a right circular cylindrical projectile on a flat target plate. In this study, the projectile is assumed to be made of one or more perfectly bonded dissimilar layers or disks. Upon impact, shock waves are set up in the projectile and target materials. The pressures associated with these shocks typically exceed the strengths of the projectile and target materials by several orders of magnitude. For example, in an 8 km/sec aluminum-on-aluminum impact, the ratio of the impact pressure (116.5 GPa=1.15 MBar) to the strength of the material (310 MPa for aluminum 6061-T6) is approximately 375, or roughly 2.5 orders of magnitude. As the shock waves propagate, the projectile and target materials are heated adiabatically and non-isentropically. The release of the shock pressures occurs isentropically through the action of rarefaction waves that are generated as the shock waves interact with the free surfaces of the projectile and target. This process leaves the projectile and target materials in high energy states and can cause either or both to fragment, melt or vaporize, depending on the material properties, geometric parameters, and the velocity of impact. At very early times during the impact event, only the area in the immediate vicinity of the impact site is affected by the impact. For the projectile and target geometries considered in this study, the shock waves can be considered to be initially planar. This simplification allows one-dimensional relationships to be used for analyzing the creation and release of shock pressures.

The shock pressures, energies, etc., in the projectile and target materials were calculated using the three 1-D shock-jump conditions, a linear relationship between the shock wave velocity and particle velocity in each material, and continuity of pressure and velocity at the projectile/target interface. If we consider the 1-D impact of a projectile with velocity v_o on a stationary target, conservation of mass, momentum, and energy across the shock fronts in the projectile and in the target yields

Projectile	Target	
$u_{sp}/V_{op} = (u_{sp}-u_{pp})/V_p$	$u_{st}/V_{ot} = (u_{st}-u_{pt})/V_t$	(1a,b)
$P_{Hp} = u_{sp}u_{pp}/V_{op}$	$P_{Ht} = u_{st}u_{pt}/V_{ot}$	(2a,b)
$E_{Hp} = P_{Hp}(V_{op}-V_{Hp})/2$	$E_{Ht} = P_{Ht}(V_{ot}-V_{Ht})/2$	(3a,b)

where $V=1/\rho$ is specific volume, u_s and u_p are shock and particle velocity, respectively, and P_H and E_H are the pressure and energy state associated with the initial impact. In equations (1-3), the subscripts 'p', and 't' refer to projectile and target quantities, respectively. Furthermore, in the development of equations (1-3), the initial conditions ahead of the projectile and target shock waves were taken to be zero (with the exception of density which is $\rho_o=1/V_o$) and the shock velocity in the projectile is taken relative to a 'stationary' projectile.

The linear shock velocity-particle velocity relationships for the projectile and target materials are in the form

$$u_s = c_o + ku_p \tag{4}$$

where $c_o=\sqrt{(KV_o)}$ is the material bulk speed of sound, $K=E/3(1-2\nu)$ is the adiabatic bulk modulus, E and ν are Young's modulus and Poisson's ratio, respectively, and k is an empirically-derived constant. At the projectile/target interface, pressure equilibrium implies that

$$P_{Hp} = P_{Ht} \tag{5}$$

while material continuity at the interface implies that

$$v_o = u_{pp} + u_{pt} \tag{6}$$

Solving equations (1-6) simultaneously yields expressions for projectile and target particle velocities which can then be used to calculate shock velocities, pressures, internal energies, and material densities after the passage of a shock wave.

The shock loading of a material is an irreversible process that results in an increase of the internal energy of the shocked material. However, the release of a shocked material occurs isentropically along an 'isentrope' or 'release adiabat'. The difference between the area

under the isentrope and the energy of the shocked state is the amount of residual energy that remains in the material and can cause the material to melt or even vaporize. A sketch of a generic Hugoniot and a generic release isentrope with initial, shocked, and final material states highlighted is shown in Figure 1. In order to calculate the release of the projectile and target materials from their respective shocked states (each characterized by P_H, E_H, and V_H), an appropriate equation-of-state is needed for each material. To keep the analysis relatively simple, the Mie-Gruneisen [25] and Tillotson [26] equations-of-state were examined for suitability for use in this study.

3.2 Mie-Gruneisen Equation-of-State

The Mie-Gruneisen equation-of-state (EOS) is an accurate thermodynamic description of most metals in the solid regime and is relatively easy to use. It has the form

$$P = P_H + \rho\Gamma(E-E_H) \tag{7}$$

where the time-dependent Gruneisen coefficient Γ is given for most metals as

$$\Gamma = \Gamma_o\rho_o/\rho \tag{8}$$

where $\Gamma_o=K\beta/\rho_oC_p$ is the ambient Gruneisen coefficient, K is the adiabatic bulk modulus, $\beta=3\alpha$ is the volumetric coefficient of thermal expansion, and C_p is specific heat at constant pressure. Invoking the Second Law of Thermodynamics

$$dE = TdS - PdV \tag{9}$$

along with the isentropic constraint dS=0 for the release process allows us to construct the release isentrope in P-V space for a material referenced to the material Hugoniot in P-V space and a given initial shocked state defined by P_H, V_H, E_H. Using the procedure outlined by McQueen, et.al. [25], the pressure P_i and internal energy E_i at a specific position 'i' along the isentrope can be shown to be given by

$$P_i = [P_{Hi} + (\Gamma/V)_i(E_{i-1} - P_{i-1}\Delta V/2 - E_{Hi})]/[1+(\Gamma/V)_i\Delta V/2] \tag{10}$$

where ΔV is the incremental change in volume used to create the release isentrope, and P_{Hi} and E_{Hi} are the pressure and energy along the Hugoniot corresponding to the i-th position in the release process. The release process is continued using equation (10) until the release

isentrope so determined crosses the V-axis (i.e. until P_i becomes zero).

Based on its thermodynamic origins, the Mie-Gruneisen EOS cannot be expected to give accurate results in the expanded liquid regime or in the vapor regime. This is because as impact energy increases, the assumption that the Gruneisen coefficient is a function of density alone is no longer valid. At high impact energies, the Gruneisen coefficient is a function of internal energy as well as density. Experience has shown, however, that it does yield fairly accurate end-state results even when there is a small percentage of molten material present [1].

3.3 Tillotson Equation-of-State

The Tillotson EOS has a more complicated form. In its original form [26], it is has two parts. The choice of which part to use depends on the location of the release isentrope within P-V-E space. The first part applies when the material is in compression regardless of the internal energy (i.e. for $V<V_0$ and for all $E>0$) and in the small region of expansion in which $V_0<V<V_s$ provided that $E<E_s'=E_s+H_v$ where E_s is the total heat needed to produce incipient vaporization and H_v is the latent heat of vaporization. The quantity $V_s=1/\rho_s$ corresponds to the volume (or density) of a material that completes its release process with an internal energy $E=E_s$. In these two regions, the Tillotson EOS has the form

$$P_1 = [a + b/f(E,\rho)]E\rho + A\mu + B\mu^2 \qquad (11)$$

where $\mu=V_0/V-1$ and

$$f(E,\rho) = (E/E_0)(\rho_0/\rho)^2 + 1 \qquad (12)$$

Equation (11) applies in particular to shock loadings in which the material remains a solid after it isentropically returns to ambient pressure. In equation (11), $A=\rho_0 c_0^2$ and $a+b=\Gamma_0$. For most metals, a value of $a=0.5$ will yield satisfactory results. In his report, Tillotson states that the constants E_c and B should adjusted to give the best fit for the EOS surface [26]. However, recent efforts by Mullin, et.al. [27] show that the constant B can be approximated reasonably well as

$$B=\rho_0 c_0^2(2k-1-\Gamma_0/2) \qquad (13)$$

but that E_0 still has to be treated as a curve-fitting parameter.

One of the dangers of improperly guessing a value for E_o is that the isentrope would actually curve up from its starting point (P_H,V_H,E_H) instead of curving down as would be expected. If this were to occur, the release process would have to be terminated, another value of E_o would have to be specified (usually a lower one), and the release process would have to start over again. The following empirical relationship was obtained as part of this investigation for E_o as a function of other material parameters to serve as a guide in the selection of an appropriate starting value for E_o.

$$E_o/E_s' = 0.819\Gamma_o^{-0.768}k^{6.594}(T_m/T_v)^{-0.021}(H_f/H_v)^{0.572} \qquad (14)$$

where H_f is the latent heat of fusion. This equation is based on the materials considered in this study (see Tables 1 and 2 for mechanical and thermal properties, respectively) and has a correlation coefficient of 87.21%. When compared with the given values of E_o used to derive it, equation (14) had an average error of 2.6% with a standard deviation of 30%.

In a highly expanded state (i.e. for $V>V_s$ regardless of internal energy) or if the internal energy is high enough to cause complete vaporization even in a moderately expanded state (i.e. for $V_o<V<V_s$ and if $E>E_s'$), the second part of the EOS is invoked:

$$P_2 = aE\rho + \{[bE\rho/f(E,\rho) + A\mu\exp[-\beta(V/V_o-1)]\}\exp[-\alpha(V/V_o-1)^2] \qquad (15)$$

where the constants α and β are adjusted to control the rate of convergence of the EOS to that of an ideal gas. The exponential factors force the second term in equation (15) to approach zero at large expansion volumes. The remaining first term is then equivalent to the ideal gas term $(\gamma-1)E\rho$ with $\gamma=1.5$, which is a reasonable value for real gases [26].

In this two-part form, the Tillotson EOS is asymptotically correct in the compression and expansion regimes and reproduces many of the isentropic release features observed with much more complicated equations-of-state [27]. It should be noted that the release process as described by the Tillotson EOS does not always terminate in a simple, clear cut manner as it does with the Mie-Gruneisen EOS. For impact conditions in which the material remains in a solid state upon release, the isentrope generated with the Tillotson EOS will in fact cross the V-axis in a manner analogous to that which is observed when using the Mie-Gruneisen EOS.

However, for impact conditions that lead to material melt and vaporization, instead of crossing the V-axis, the isentrope created with the Tillotson EOS approaches the V-axis asymptotically and never crosses it. Therefore, an additional user-supplied parameter must be a cut-off point for the release process in the event of extreme gaseous expansion.

Table 1. Material Mechanical Properties

Material	c_0 (km/s)	k	ρ (gm/cm^3)	BHN (kg/mm^2)	E (GPa)	ν
Aluminum	5.380	1.34	2.71	120	71.0	0.35
Beryllium	7.975	1.12	1.82	120	290.0	0.08
Cadmium	2.307	1.64	8.64	24	46.2	0.33
Copper	3.940	2.49	8.93	37	131.0	0.34
Gold	3.060	1.57	19.24	33	85.5	0.42
Iron	4.580	1.49	7.87	95	200	0.30
Lead	2.030	1.47	11.34	7	13.8	0.45
Magnesium	4.490	1.24	1.74	45	44.1	0.29
Molybdenum	5.173	1.22	10.20	200	317.2	0.31
Nickel	4.667	1.53	8,86	200	227.5	0.30
Platinum	3.680	1.50	21.37	70	191.0	0.39
Silver	3.230	2.50	10.49	25	82.7	0.37
4340 Steel	4.570	1.55	7.83	290	200.0	0.30
Tantalum	3.374	1.20	16.65	200	179.3	0.35
Tin	2.560	1.52	7.28	4	41.4	0.33
Titanium	4.786	1.05	4.51	330	124.1	0.30
Tungsten	4.150	1.24	19.17	400	406.8	0.30
Zinc	3.042	1.50	7.14	82	74.5	0.33

Table 2. Material Thermal Properties

Material	Γ_o	α ($\times 10^{-4}$/°C)	C_p (cal/gm°C)	T_m (°C)	T_v (°C)	H_f (cal/gm)	H_v (cal/gm)
Aluminum	2.13	0.240	0.235	660	2450	95	2450
Beryllium	1.16	0.140	0.570	1281	2884	260	8195
Cadmium	2.27	0.343	0.058	321	765	13	212
Copper	2.00	0.170	0.097	1083	2590	49	1150
Gold	3.10	0.161	0.034	1063	2960	16	413
Iron	1.57	0.120	0.120	1539	3035	65	1591
Lead	2.77	0.293	0.031	327	1740	6	210
Magnesium	1.50	0.300	0.295	650	1110	88	1326
Molybdenum	1.52	0.061	0.079	2610	5555	70	1242
Nickel	1.80	0.143	0.130	1454	2865	74	1523
Platinum	2.94	0.110	0.037	1769	4349	26	632
Silver	2.50	0.211	0.062	961	2210	25	554
4340 Steel	1.67	0.112	0.110	1510	3070	65	1590
Tantalum	1.69	0.065	0.033	2996	5425	38	1007
Tin	1.85	0.269	0.058	235	2450	14	580
Titanium	1.10	0.100	0.150	1676	3260	99	2182
Tungsten	1.48	0.040	0.035	3410	5900	53	1054
Zinc	2.15	0.274	0.100	420	907	25	420

Closed-form expressions for P_i along the isentrope described by equations (11) and (15) can also be obtained using the procedure described in [26] and used in deriving P_i for the Mie-Gruneisen EOS. Three different variations of the incremental form of equation (9) with $dS=0$ were considered in the development of the expressions for P_i. These variations are

(#1) $E_i - E_{i-1} = -(P_i + P_{i-1})\Delta V/2$ (16a)

(#2) $E_i - E_{i-1} = -P_{i-1}\Delta V$ (16b)

(#3) $E_i - E_{i-1} = -P_i\Delta V$ (16c)

These three forms were considered in an attempt to simplify the final expression for P_i. In the procedure described in [25] equation (11) needs to be manipulated so that the unknown pressure P_i at the current increment is written in terms of quantities at the previous increment, including the previous pressure P_{i-1}. This is relatively easy to do using variation (#1), the most sensible of the three, for the Mie-Gruneisen EOS because the pressure terms in the Mie-Gruneisen EOS are easily separable. In the Tillotson EOS, the complexity arises from the fact $dE=-PdV$ is used in the denominator of only one term on the right-hand-side in equations (11) and (15). This makes the separation of the pressure terms somewhat more cumbersome.

After deriving the expressions for P_i using each of the three proposed variations, the predictions of the three variations for the impact velocity required to produce melt and vaporization in materials for which such quantities were known were compared against known velocity values. It was found that variations (#2) and (#3) did not reproduce the known values very well. Thus, variation (#1) was selected for further use in the development of the equations for P_i. The final expressions using equation (16a) are presented below.

$$(P_1)_i = [C_2 - \sqrt{(C_2^2 - 4C_1C_3)}]/2C_1V_i \quad (17)$$

$$C_1 = V_i(\Delta V')[1+a(\Delta V'/V_i)] \quad (18)$$

$$C_2 = C_1R_i/V_i(\Delta V') + (\Delta V'/V_i)R_i' + Q_iV_i^2(\Delta V') - P_{i-1}(\Delta V')V_i^2[1+a(\Delta V/V_i)] \quad (19)$$

$$C_3 = (aE_{i-1}+Q_iV_i)R_i + bE_{i-1}E_oV_o^2 - P_{i-1}(\Delta V')[(1+a)E_{i-1}V_i^2 + (1+b)E_oV_o^2 + Q_iV_i^3] + [P_{i-1}(\Delta V')]^2V_i^2 \quad (20)$$

$$Q_i = A\mu_i + B\mu_i^2 \quad (21)$$

$$R_i = E_{i-1}V_i^2 + E_oV_o^2 \quad (22)$$

$$R_i' = aE_{i-1}V_i^2 + bE_oV_o^2 \quad (23)$$

and $\Delta V' = \Delta V/2$. Although a substantial amount of algebra is required to derive equations

(17-23), the manipulations involved in deriving a closed-form expression for $(P_2)_i$ can be reduced significantly if equation (15) is re-written in the following form:

$$P_2 = [a + b'/f(E,\rho)]E\rho + Q' \qquad (24)$$

where $f(E,\rho)$ is still given by equation (12), $b'=bU$ and $Q'=US$ where

$$S = A\mu\exp[-\beta(V/V_0-1)] \qquad (25)$$

$$U = \exp[-\alpha(V/V_0-1)^2] \qquad (26)$$

Thus, the expression for P_2 can be written in exactly the same form as the expression for P_1. As a result, we can use the expressions that were derived for $(P_1)_i$ can be used to give us $(P_2)_i$ as well provided that in every instance b is replaced with bU_i and Q_i is replaced with U_iS_i where U_i and S_i are found using equations (25) and (26).

3.4 Modified Tillotson Equation-of-State

If we examine equations (11,15) in more detail, we note that they are continuous across $V=V_0$, which implies that the Tillotson EOS is continuous across $V=V_0$ for very high impact energies. However, at $V=V_s$, there is an abrupt jump in the release isentrope for moderate impact energies, that is, when $E_s<E<E_s'$ at $V=V_s$. This jump occurs because according to the original formulation proposed by Tillotson, whenever $E<E_s'$ equation (11) is used, even in the $V_0<V<V_s$ region of the curve. However, once we move across $V=V_s$, equation (15) is invoked regardless of the impact energy. Since these two equations are not continuous at $V=V_s$, neither is the isentrope. Table 3 shows values of V_s calculated using the Tillotson EOS and the EOS parameters used to obtain them. Examination of the last column in Table 3 reveals that the ratio V_s/V_0 is relatively insensitive to the choice of material: the average value of V_s/V_0 is 1.138 with a standard deviation of only 4.3% of the average value.

The effect of this discontinuity in the Tillotson EOS is that it over predicts the amount of expansion that occurs in the release of a material from a moderately energetic state, that is, one that is not sufficiently energetic to cause an appreciable amount of vaporization to occur. For example, in the case in which E is only slightly greater than E_s at $V=V_s$, the original form of the Tillotson EOS dictates that the release isentrope for $V>V_s$ would follow a path similar

to the one in the event of complete vaporization, that is, it would become asymptotic to the V-axis and would terminate at an unrealistically high value of specific volume.

Table 3. Values of V_s for Materials Considered

Material	Initial E_0 Multiplier	α	β	v_0 (km/s)	V_0 (cm^3/gm)	V_s (cm^3/gm)	V_s/V_0
Aluminum	1.1	5.0	5.0	10.2	0.369	0.424	1.149
Beryllium	1.0	5.0	5.0	17.3	0.549	0.620	1.129
Cadmium	1.0	5.0	5.0	3.2	0.116	0.128	1.106
Copper	1.0	10.0	10.0	7.1	0.112	0.130	1.161
Gold	0.3	10.0	10.0	5.3	0.052	0.060	1.154
Iron	1.0	10.0	10.0	7.8	0.127	0.145	1.141
Lead	0.3	10.0	10.0	3.5	0.088	0.101	1.148
Magnesium	1.0	5.0	5.0	7.4	0.575	0.626	1.089
Molybdenum	0.5	10.0	10.0	9.4	0.098	0.109	1.112
Nickel	1.0	10.0	10.0	8.5	0.113	0.133	1.177
Platinum	0.2	10.0	10.0	6.1	0.047	0.053	1.128
Silver	1.0	10.0	10.0	4.6	0.095	0.122	1.284
Tantalum	0.2	10.0	10.0	6.0	0.060	0.067	1.116
Tin	1.0	10.0	10.0	4.9	0.137	0.163	1.187
Titanium	0.3	10.0	10.0	9.0	0.222	0.238	1.072
Tungsten	0.3	10.0	10.0	6.6	0.052	0.057	1.096
Zinc	1.0	10.0	10.0	4.5	0.140	0.155	2.207

Note: Initial E_0 guess based on E_0 (J/kg) = $2.56 \times 10^{-4} A^{0.94}$, $A = \rho_0 c_0^2$ [56]

Generic release isentropes obtained by implementing the Tillotson EOS in its original

formulation are illustrated in Figures 2a-c. In Figure 2a, the energy as the isentrope crosses $V=V_O$ is less than E_S. No vaporization is expected to occur and calculation of the isentrope continues using equation (11). The isentrope in this case terminates at a specific volume $V_f<V_S$. In Figure 2b, the energy as the isentrope crosses V_O is greater than E_S but less than E_S'. Since E is already larger than E_S, the isentrope in this case must terminate at a value of specific volume greater than V_S as shown in Figure 2b. In Figure 2c, the energy as the isentrope crosses V_O is already greater than E_S'. In this case, a significant amount of vaporization is expected to occur. Equation (15) is invoked automatically, the isentrope is continuous across $V=V_O$, and there is no jump at $V=V_S$.

A modification in the form of a 'Mixed Phase Formulation' of the Tillotson EOS was proposed in an attempt to lessen the effects of the discontinuity at $V=V_S$ [28,29]. The Mixed Phase Formulation states that if $E_S<E<E_S'$ as the release isentrope crosses $V=V_O$, then for $V>V_O$ the pressure is to be calculated using the equation

$$P_3 = [P_2(E-E_S) + P_1(E_S'-E)]/(E_S'-E_S) \qquad (27)$$

This ensures that the EOS and the release isentrope are continuous if $E=E_S$ or if $E=E_S'$ at $V=V_O$. This modification was motivated by the fact that if $E>E_S$ as the isentrope crossed $V=V_O$, then enough energy would be present to cause partial vaporization. Thus, rather than continue to use equation (11) if $E_S<E<E_S'$ when $V=V_O$, equation (27) is to be implemented to account for some additional expansion of the material.

An alternative means of eliminating the discontinuity in the Tillotson EOS then $V>V_S$ and $E_S<E<E_S'$ (i.e. in moderately high energy impacts) is uniformly subtracting the magnitude of the jump at $V=V_S$ from the pressure values calculated when $V>V_S$ using equation (15), that is, the original Tillotson EOS equation applicable when $V>V_S$ [13]. Thus, if $E_S<E<E_S'$ as the isentrope crosses $V=V_S$, then for $V>V_S$ the pressure is to be calculated using the equation

$$P_4 = P_2 - [P_2(V=V_S)-P_3(V=V_S)] \qquad (28)$$

in which P_2 is calculated using equation (15) and P_3 is calculated using equation (27). As can be seen from equation (28), this correction is not intended to replace the Mixed Phase

Formulation of the Tillotson EOS, but rather to complement its use in the region $V>V_S$.

The quantity within the square brackets of equation (28) is the amount of the jump in the release isentrope; it is largest if $E=(E_S)^+$ at $V=V_S$ and decreases as $E \rightarrow E_S'$. In the event that $E \geq E_S'$ at $V=V_S$, the proposed modification in the Tillotson EOS disappears, the EOS reverts back to its original form (i.e. $P_4=P_2$), and continuity at $V=V_S$ is maintained. If $E<E_S$ as the isentrope crosses $V=V_O$, then the isentrope never reaches $V=V_S$ so that in such cases, the correction is never invoked. Thus, the proposed correction is only invoked when needed, that is, if $E_S<E<E_S'$ as the isentrope crosses $V=V_S$.

The effect of implementing the subtraction jump correction in the Tillotson EOS on the nature of the release isentrope is shown in Figures 3a,b, and c for impact scenarios in which $E=(E_S)^+$, E is between E_S and E_S', and $E=(E_S')^-$, respectively, as the isentrope crosses $V=V_S$. In Figures 3a-c, $V_{f,MT}$ refers to the final specific volume obtained using the jump subtraction correction formulation of the Tillotson EOS. As can be seen in Figures 3a-c, the proposed modification gives an appropriate amount of expansion when E is near E_S' and does not over predict the amount of expansion when E is only slightly greater than E_S.

In this report, the version of the Tillotson EOS in which the jump at $V=V_S$ is eliminated by the uniform subtraction approach is referred to as the Tillotson/SJC formulation while the mixed phase formulation of the Tillotson EOS is referred to as the Tillotson/MPF formulation. Unless otherwise specified, the Tillotson/SJC formulation was used in the remainder of this effort. Table 4 presents a summary of which equation to use in which regime of P-V-E space to generate a release with the Tillotson/SJC and Tillotson/MPF equations-of-state.

Table 4. Equations for Generating Release Isentrope as a Function of Location in P-V-E Space

V-Region	E-Region	Tillotson/SJC	Tillotson/MPF
$V<V_0$	all $E>0$	(11)	(11)
$V_0<V<V_s$	$E<E_s$	(11)	(11)
$V_0<V<V_s$	$E_s<E<E_s'$	(27)	(27)
$V_0<V<V_s$	$E_s'<E$	(15)	(15)
$V_s<V$	$E_s<E<E_s'$	(28)	(27)
$V_s<V$	$E_s'<E$	(15)	(15)

3.5 Propagation of Shock Pressures in a Multi-Material Projectile

As the shock wave generated by the impact on the target propagates through the projectile, it encounters the various interfaces between material layers. At each interface between two dissimilar materials, a transmitted shock wave and a reflected wave are generated. The properties of the reflected and transmitted waves are found using a technique based on the method of impedance matching (see, e.g., [30-32]). In this technique, continuity of pressure and particle velocity are enforced at each interface. If the reflected pressure is greater than the incident pressure, then the reflected wave is a shock wave. Conversely, if the reflected pressure is less than the incident pressure, the reflected wave is a rarefaction wave. The equations governing the reflection and transmission of shock waves at projectile material interfaces are derived as follows.

Figure 4a shows an incoming shock wave in material A, a reflected wave from the A/B interface, and a transmitted shock wave into material B. Shock wave I is shown moving into undisturbed material (denoted with a '0' subscript). The shocked state of the material in its wake is denoted by a '1' subscript. The reflected wave II moves back into this shocked

material and leaves behind it material whose state is denoted by a subscript of '2'. The transmitted shock wave III moves into undistributed material (denoted by a '4' subscript); the condition of the shocked material behind it is labeled with a '3' subscript. Figure 4b shows the same configuration only all motion is shown under steady conditions.

Across shock front I we have

$$\rho_1(U_1-u_1) = \rho_o{}^A(U_1-u_0) \tag{29}$$

$$P_1-P_0 = \rho_o{}^A(U_1-u_0)(u_1-u_0) \tag{30}$$

as well as the constitutive relationship between the shock wave speed U_1 and the particle velocity u_1 induced in the shocked material

$$U_1 = c_o{}^A + k^A u_1 \tag{31}$$

In equations (29,30), ρ_o has been replaced by $\rho_o{}^A$, the ambient density of material A. Assuming stationary conditions at zero pressure ahead of the shock wave (i.e. $u_0=P_0=0$) and that P_1 is known (as it will be in impact problems), equations (29-31) can be used to solve for u_1 and ρ_1 as follows:

$$u_1 = -(c_o{}^A/2k^A)\{1-[1+4k^A p_1/\rho_o{}^A(c_o{}^A)2]1/2\} \tag{32}$$

$$\rho_1 = \rho_o{}^A U_1/(U_1-u_1) \tag{33}$$

This completely defines the state of the material behind shock wave I. For shock wave II we have

$$\rho_1(U_2+u_1) = \rho_2(U_2+u_2) \tag{34}$$

$$P_2-P_1 = \rho_1(U_2+u_1)(u_1-u_2) \tag{35}$$

and for shock wave III we have

$$\rho_3(U_3-v_3) = \rho_o{}^B(U_3-u_4) \tag{36}$$

$$P_3-P_4 = \rho_o{}^B(U_3-u_4)(u_3-u_4) \tag{37}$$

$$U_3 = c_0^B + k^B u_3 \tag{38}$$

where ρ_4 has been replaced by ρ_0^B, the ambient density of material B. Assuming stationary conditions at zero pressure ahead of shock wave III and enforcing pressure and velocity continuity at the A/B material interface (i.e. $P_3=P_2$ and $u_3=u_2$) reduces equations (36-38) to

$$\rho_3(U_3-u_2) = \rho_0^B U_3 \tag{39}$$

$$P_2=\rho_0^B U_3 u_2 \tag{40}$$

$$U_3 = c_0^B + k^B u_2 \tag{41}$$

Equations (34,35,39-41) are a system of 5 equations in 6 unknowns (P_2,ρ_2,U_2,u_2, ρ_3,U_3). The elimination of one unknown is illustrated graphically in Figure 5. In Figure 5, Curves A and B are the Hugoniots of materials A and B, and Curve A' is the Hugoniot of materials A reflected about point C which denotes the initial shocked state in material A (i.e. prior to the passage of the reflected wave). The shocked state of material B must lie at the intersection of its Hugoniot (Curve B) and the reflected Hugoniot for material A (Curve A'). This state is denoted by point D. The particle velocity corresponding to point D is the interface velocity $u_2=u_3$ while the pressure corresponding to point D is the interface pressure $P_2=P_3$.

Knowing that curve A' is the reflection of Curve A, that is, it passes throughout the points ($u_p=u_1$,$P=P_1$), ($u_p=2u_1$,$P=0$), and ($u_p=0$,$P=2\rho_0^A u_1(c_0^A+2k^A u_1)$), allows us to obtain the following functional form for Curve A' in P-u_p space:

$$P_{A'} = 2\rho_0^A u_1(c_0^A+2k^A u_1) - \rho_0^A(c_0^A+4k^A u_1-k^A u_p)u_p \tag{42}$$

Thus, when we set $p_{A'}$ equal to the functional form of Curve B, we have an equation for the particle velocity that corresponds to point D. Solving for this particle velocity yields:

$$u_D = [\beta-(\beta^2-4\alpha\gamma)^{1/2}]/2\alpha \tag{43}$$

where

$$\alpha = \rho_o{}^A k^A - \rho_o{}^B k^B \tag{44}$$

$$\beta = \rho_o{}^A c_o{}^A + \rho_o{}^B c_o{}^B + 4\rho_o{}^A k^A u_1 \tag{45}$$

$$\gamma = 2\rho_o{}^A u_1 (c_o{}^A + 2k^A u_1) \tag{46}$$

in which u_1, of course, is known. Setting $u_2 = u_D$ in equations (34,35) and (39-41) allows us to solve for all the remaining quantities:

$$U_3 = c_o{}^B + k^B u_2 \tag{47}$$

$$P_3 = \rho_o{}^B U_3 u_2 \tag{48}$$

$$\rho_3 = \rho o^B U_3/(U_3 - u_2) \tag{49}$$

$$U_2 = (P_1 - P_2)/\rho_1(u_1 - u_2) - u_1 \tag{50}$$

$$\rho_2 = \rho_1(U_2 + u_1)/(U_2 + u_2) \tag{51}$$

An example of this technique is discussed in the next paragraph.

Figure 6, which consists of three Hugoniot curves drawn in pressure-particle velocity ($P\text{-}u_p$) space, shows what happens when a shock wave traveling in copper at 12 km/sec encounters an aluminum interface. Using the three one-dimensional shock jump conditions and the linear $P\text{-}u_p$ relationship for copper, it is found that a 12 km/sec shock wave in copper creates a pressure jump of 568 GPa and induces a particle velocity of 5.34 km/sec in its wake as it moves into copper at ambient conditions. To find the pressures and particle velocities of the reflected and transmitted waves, the Hugoniot for copper in $P\text{-}u_p$ space is reflected about the point defined by u_p=5.34 km/sec, P=568 GPa. Its point of intersection with the Hugoniot for aluminum yields the desired pressure (290 GPa) and particle velocity (7.15 km/sec) for the wave reflected back into the copper and transmitted into the aluminum.

Once the pressure and the particle velocity in a subsequent material layer are determined, the one-dimensional shock-jump conditions are used to calculate the specific volume and the energy of the shocked material. This procedure is repeated for each

successive projectile material layer. Thus, while the impact conditions are used to define the shocked states in the target and first projectile layer materials, the shocked states in subsequent projectile material layers are obtained using the impedance matching technique just described and illustrated.

3.6 Release of Shock Pressures

The target shock pressures are released by the action of the rarefaction wave that is created by the reflection of the shock wave in the target from the target rear free surface. This rarefaction wave propagates through the target material and into the shocked projectile layer materials. In doing so, it also releases the projectile materials from their respective shocked states. For the purposes of the model developed herein, this process of shocking and releasing continues until the rarefaction wave overtakes the shock wave. After this point in time, it is assumed that no additional shocking and release of projectile material occurs. In this manner, the model considers only material that is "fully shocked".

As mentioned previously, in some instances the relative impedance of two adjoining projectile layer materials may result in a shock wave being reflected back into a projectile material layer that has been shocked and released. However, it is assumed for the purposes of this study that this reflected shock wave does not "re-shock" the projectile material and that the material into which it is reflected remains released. This assumption is reasonable since as the reflected shock wave moves back into the released layer material, it continuously creates rarefaction waves at the projectile edge free surfaces which release any material shocking it produces. Thus, in the model developed herein, any projectile layer material that has been shocked and released will remain released regardless of the nature of the wave reflected from its interface with an adjoining layer.

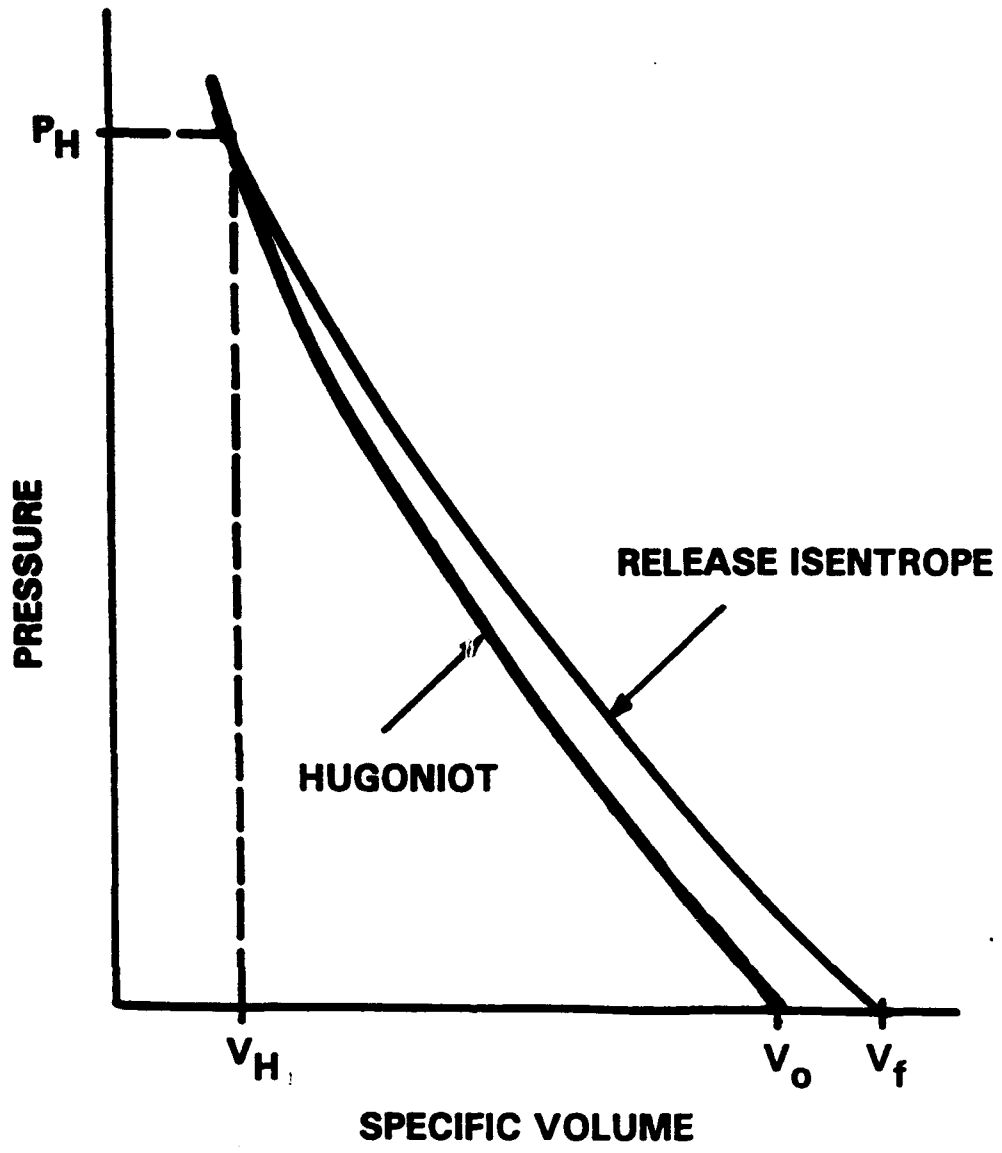

Figure 1. Generic Hugoniot and Release Isentrope

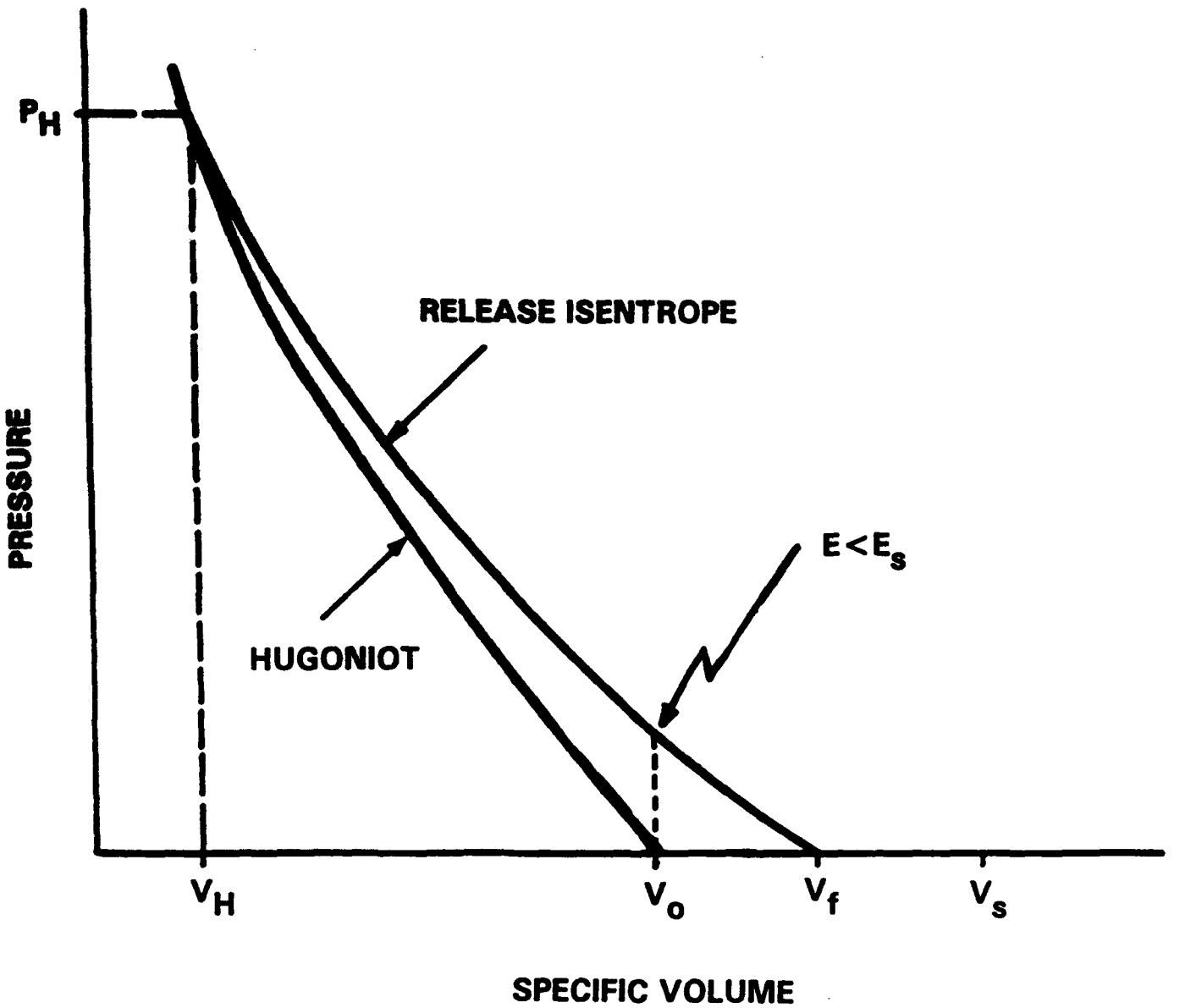

Figure 2a. Tillotson Equation-of-State with $E<E_s$ at $V=V_o$

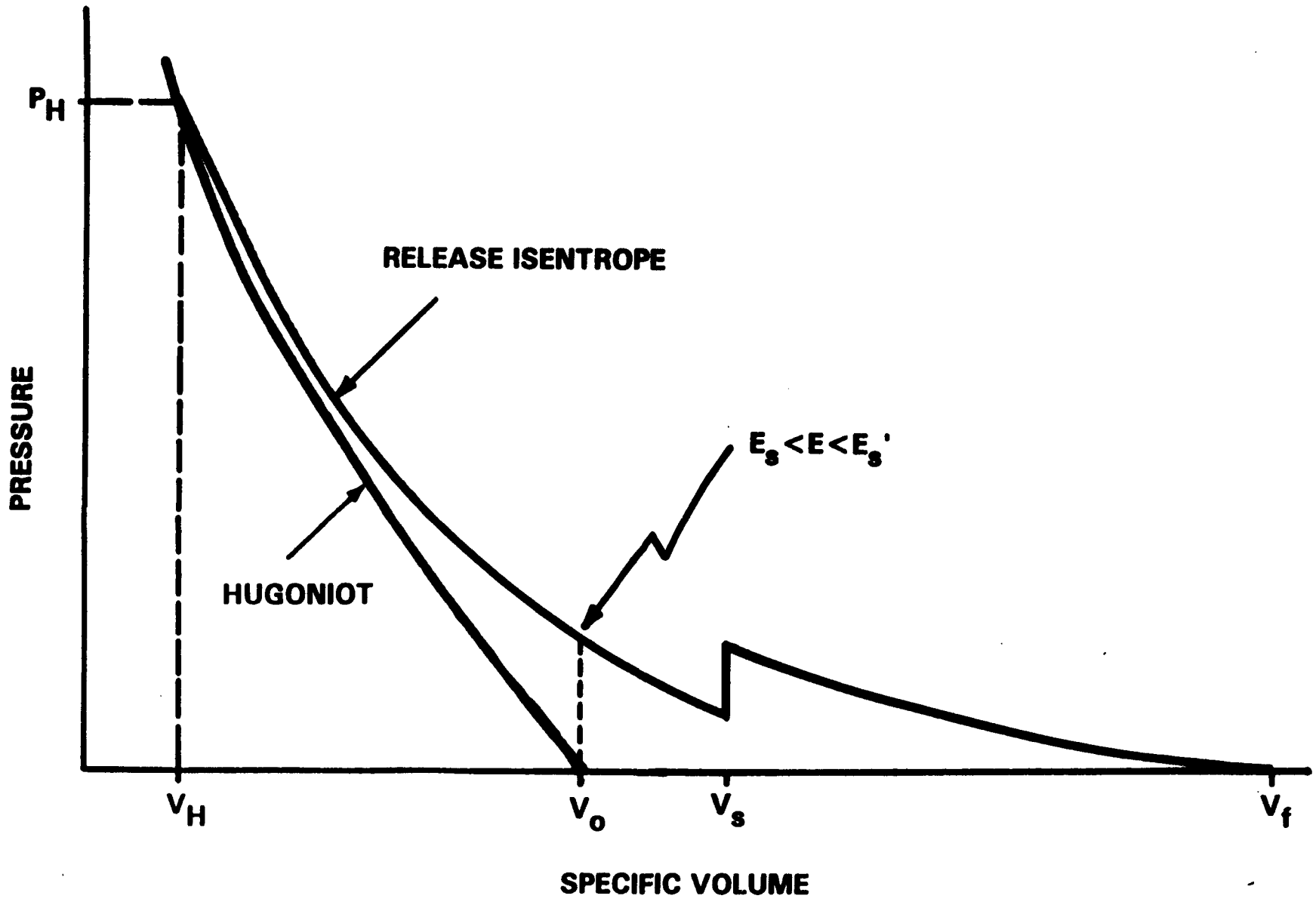

Figure 2b. Tillotson Equation-of-State with $E_s<E<E_s'$ at $V=V_o$

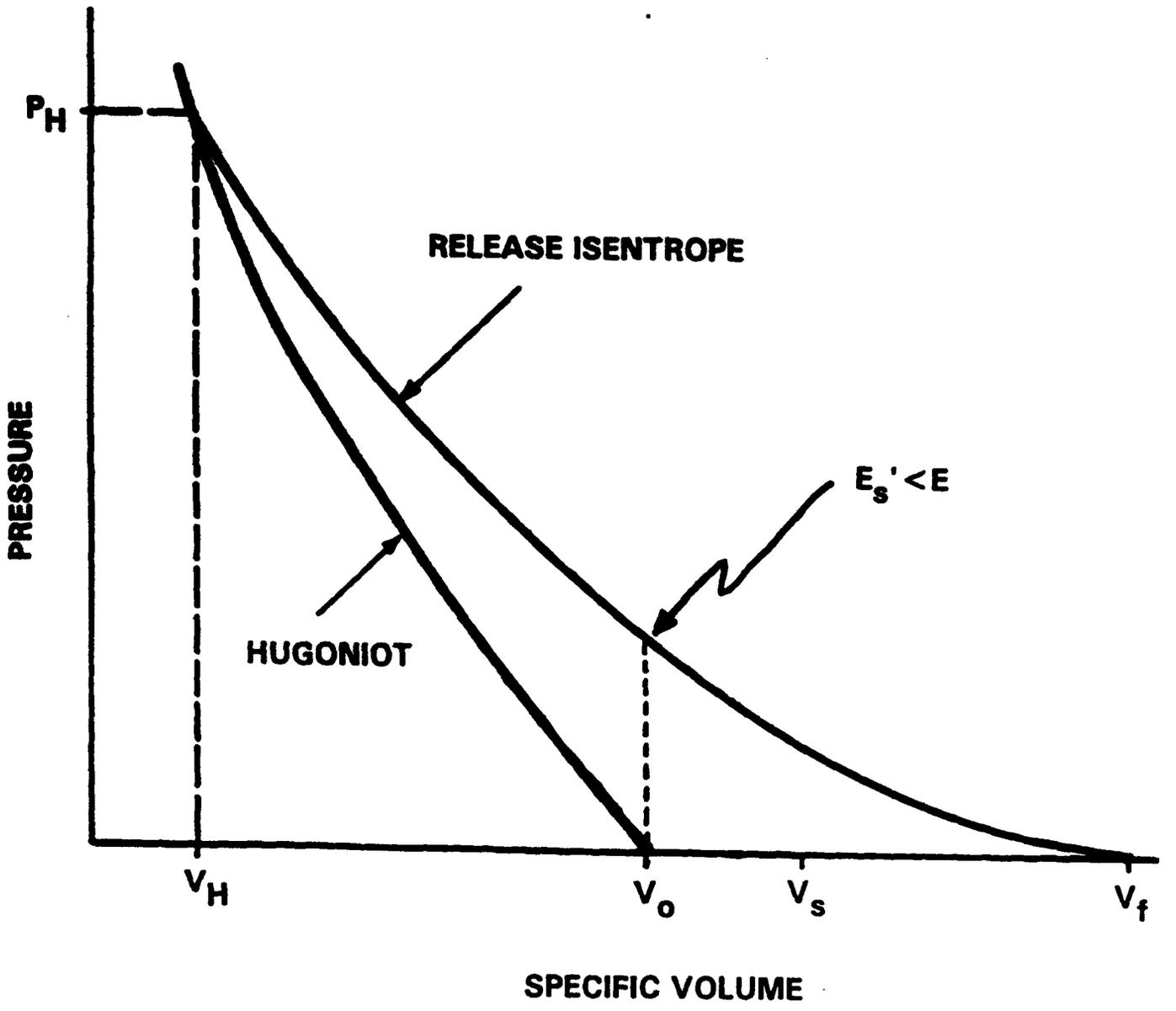

Figure 2c. Tillotson Equation-of-State with $E_s' < E$ at $V = V_o$

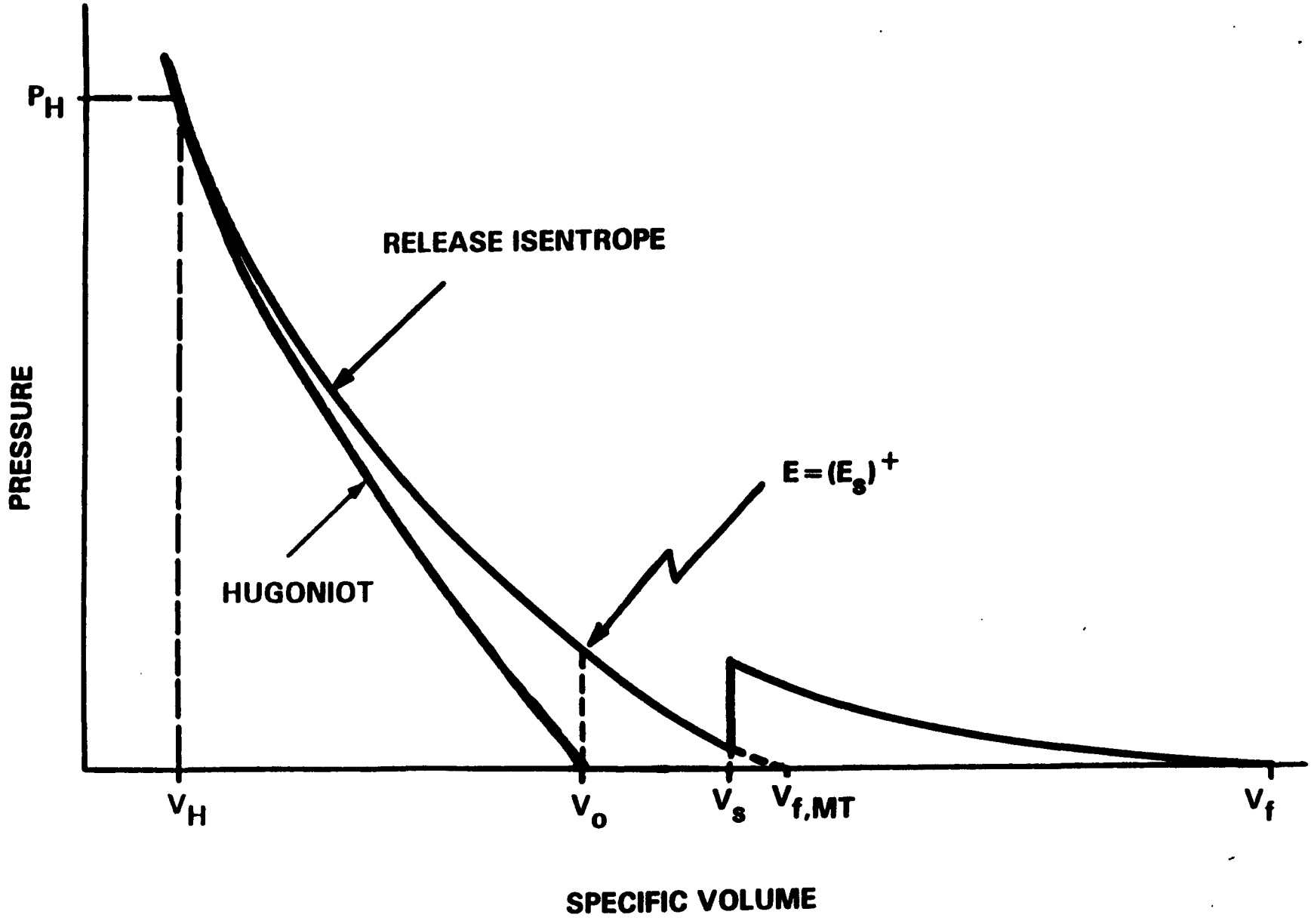

Figure 3a. Modified Tillotson Equation-of-State with $E=(E_s)^+$

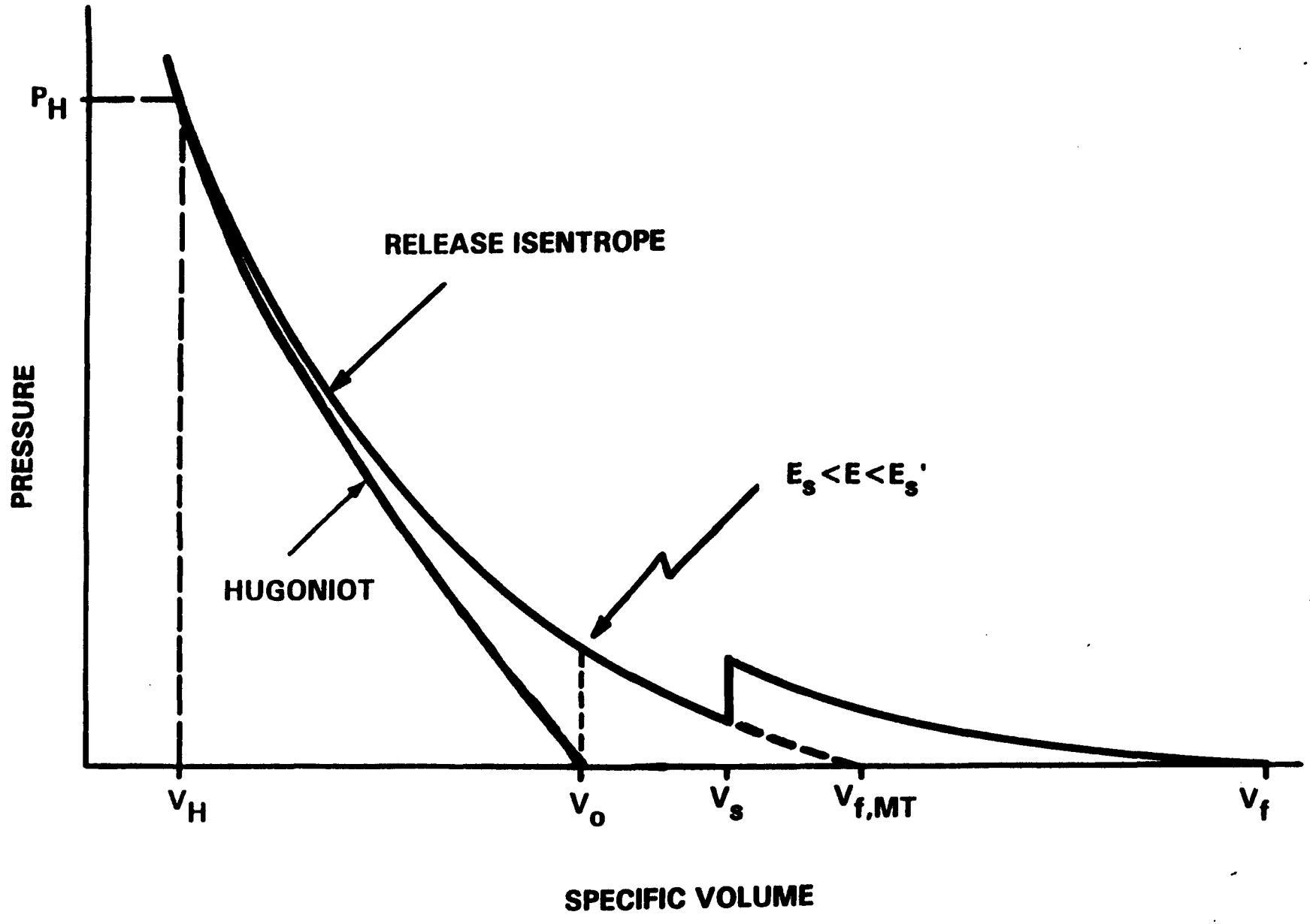

Figure 3b. Modified Tillotson Equation-of-State with and $E_s<E<E_s'$

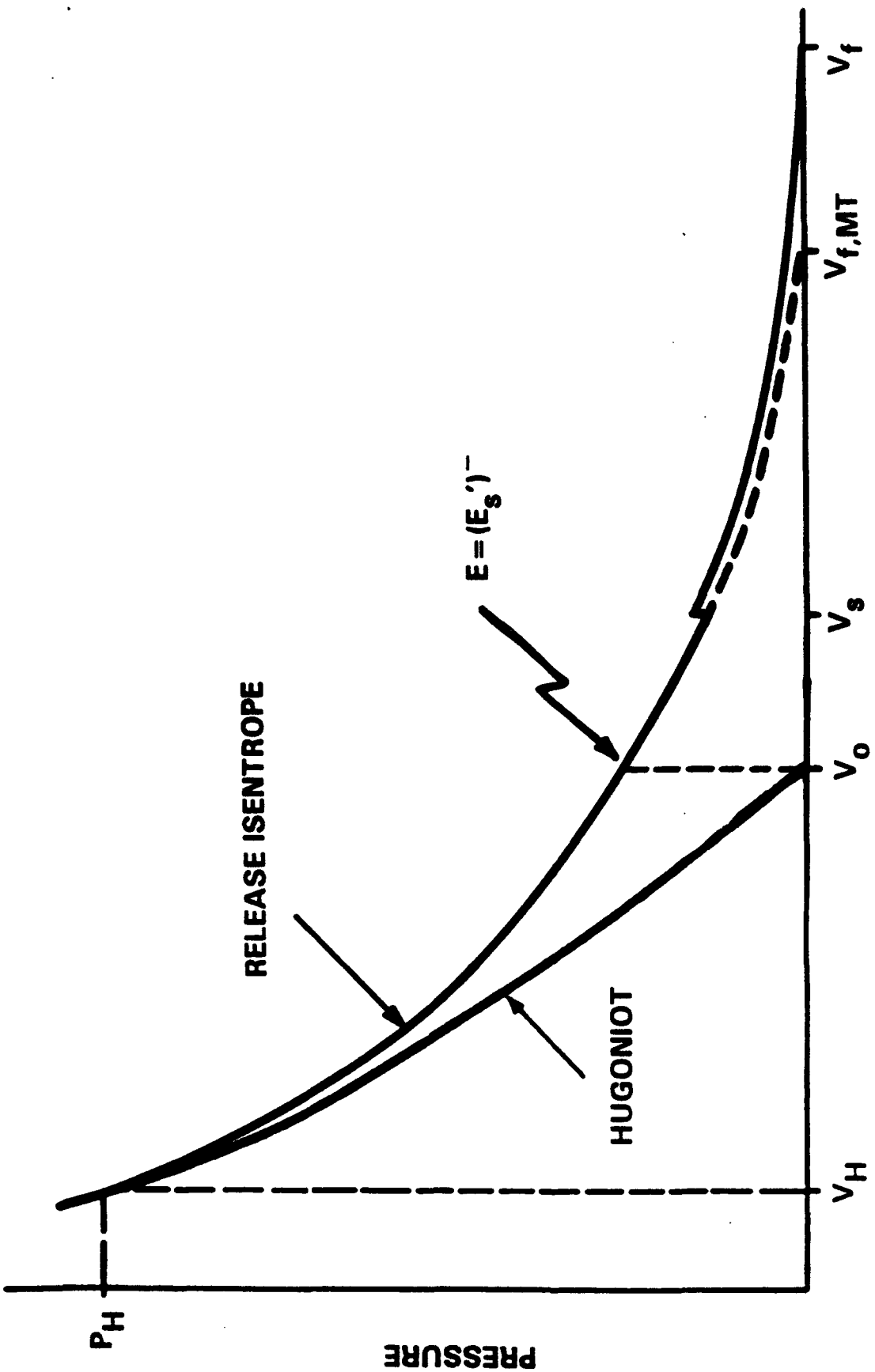

Figure 3c. Modified Tillotson Equation-of-State with $E=(E_s')^-$

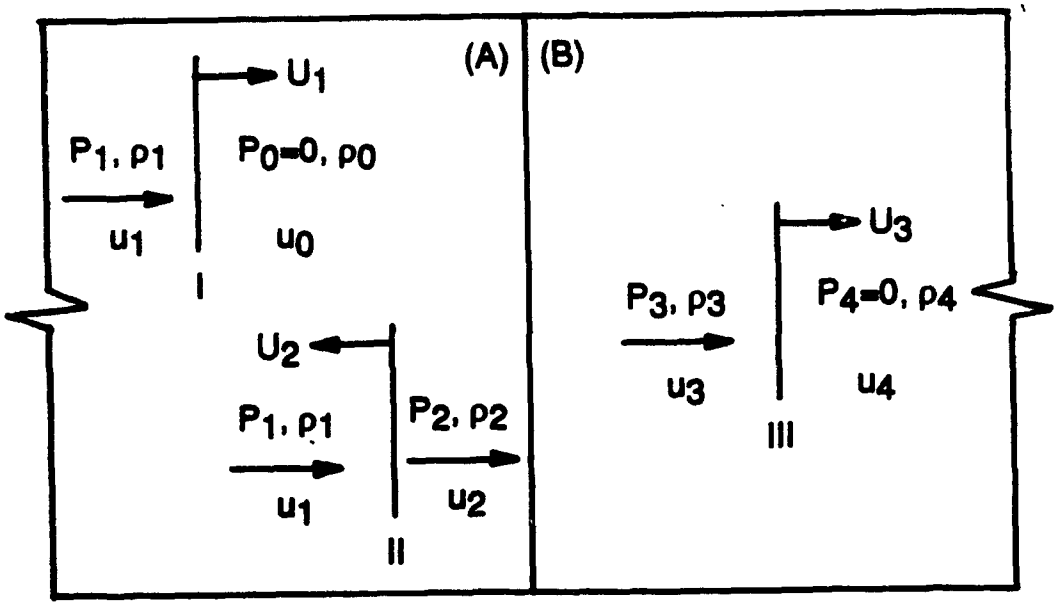

Figure 4a. Shock Wave Reflection and Transmission at a Material Interface -- Unsteady Conditions

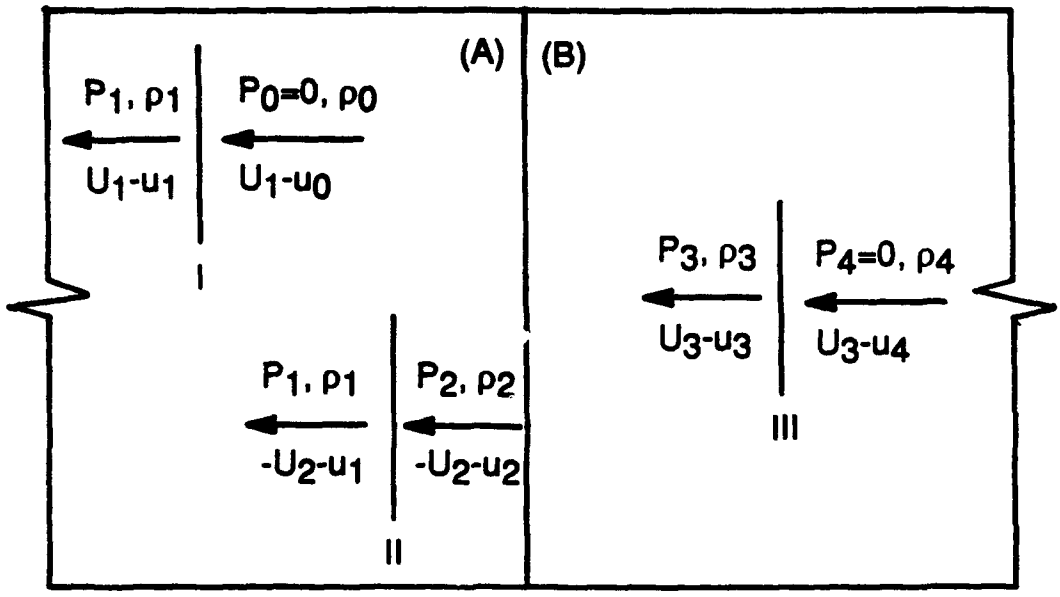

$P_2 = P_3$

$u_2 = u_3$

Figure 4b. Shock Wave Reflection and Transmission at a Material Interface -- Steady Conditions

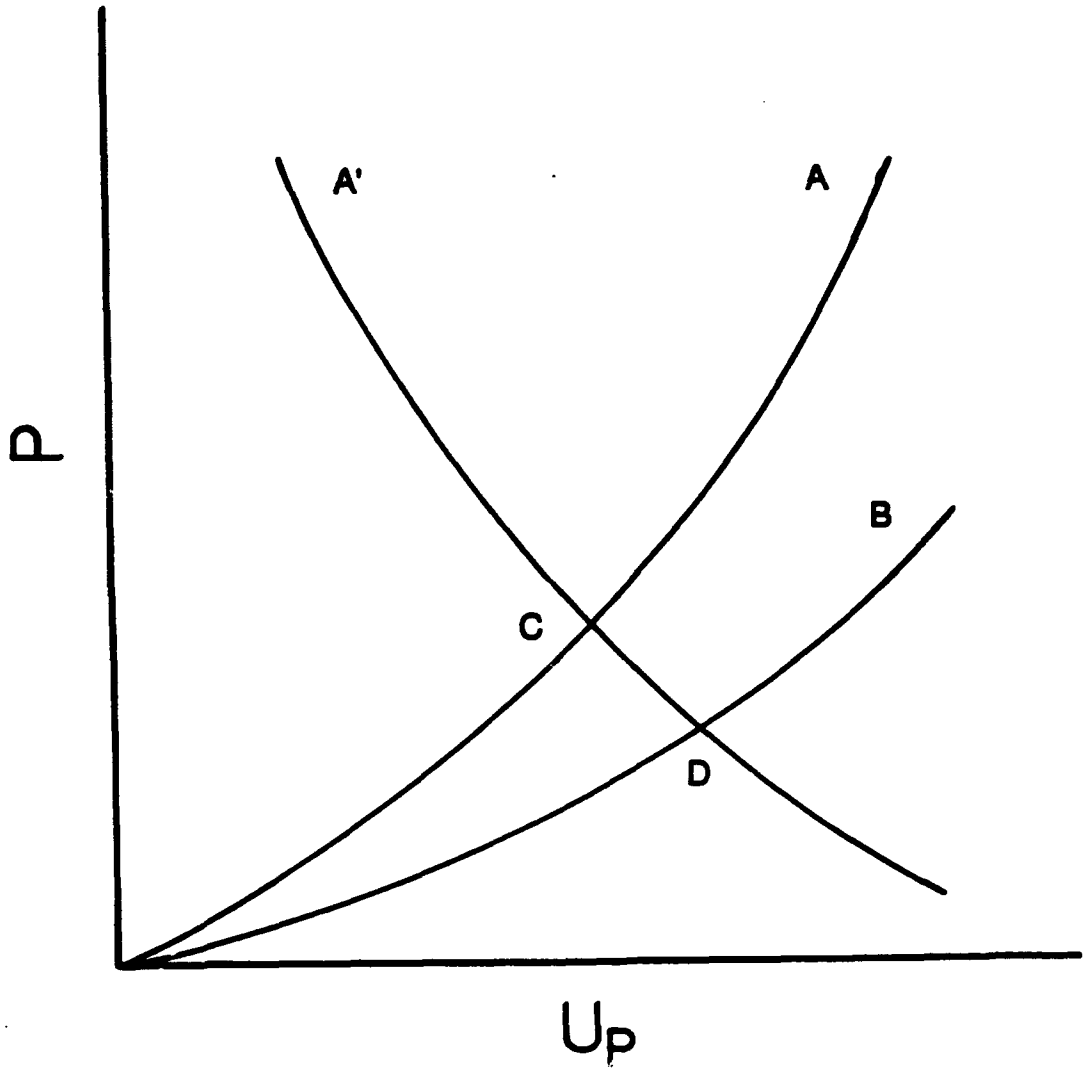

Figure 5. Impedance Mismatch at a Material Interface -- Generic Sketch

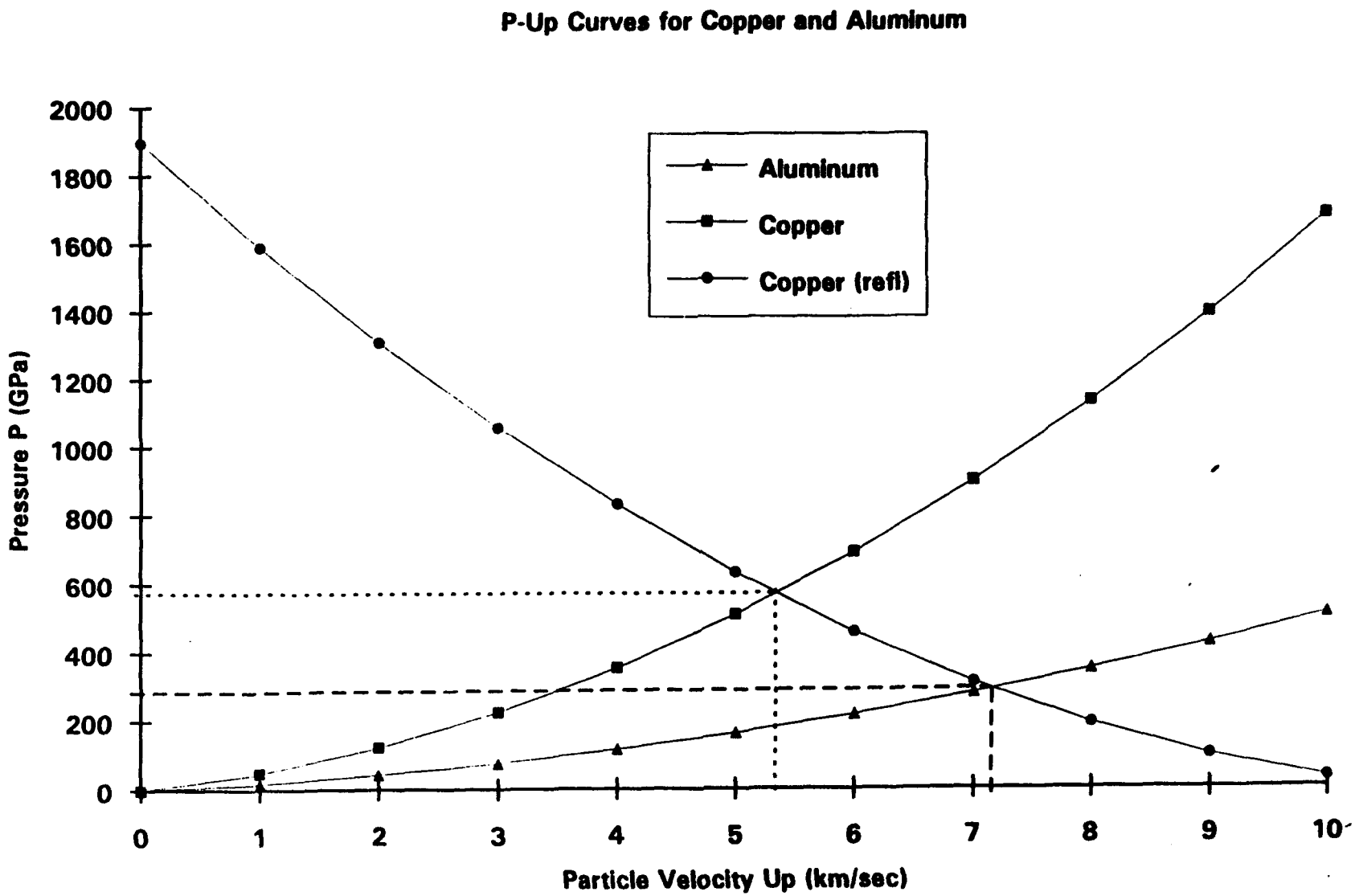

Figure 6. Impedance Mismatch at a Material Interface -- Specific Example

4.0 DEBRIS CLOUD MATERIAL CHARACTERIZATION

4.1 Computing the Percentages of Solid, Liquid, and Gaseous Debris Cloud Material

Once the residual internal energies in the shocked and released portions of the projectile and target materials had been obtained, the percentages of the various states of matter in the resulting debris cloud were estimated using the following procedure. This procedure requires the knowledge of the materials' solid and liquid specific heats (C_{ps},C_{pl}), their melting and boiling points (T_m,T_v), and their heats of fusion and vaporization (H_f,H_v) in addition to the residual internal energy (E_r).

If $E_r < C_{ps}T_m$, then all of the shocked and released materials was considered to remain in a solid matter state, that is,

$$P_s = 1.0$$
$$P_l = 0.0 \qquad (52a,b,c)$$
$$P_v = 0.0$$

If $C_{ps}T_m < E_r < C_{ps}+H_f$, then the quantity $(E_r - C_{ps}T_m)/H_f$ represented the fraction of the shocked and released material that was melted, while the remaining shocked and released material was assumed to be in solid form, that is,

$$P_s = 1.0 - (E_r - C_{ps}T_m)/H_f$$
$$P_l = (E_r - C_{ps}T_m)/H_f \qquad (53a,b,c)$$
$$P_v = 0.0$$

If $C_{ps}T_m + H_f < E_r < C_{ps}T_m + H_f + C_{pl}(T_v - T_m)$, then all of the shocked and released material was considered to be in a liquid state, that is,

$$P_s = 0.0$$
$$P_l = 1.0 \qquad (54a,b,c)$$
$$P_v = 0.0$$

If $C_{ps}T_m + H_f + C_{pl}(T_v - T_m) < E_r < C_{ps}T_m + H_f + C_{pl}(T_v - T_m) + H_v$, then the quantity $\{E_r - [C_{ps}T_m + H_f + C_{pl}(T_v - T_m)]\}/H_v$ represented the fraction of the shocked and released

material that was vaporized, while the remaining shocked and released material was considered to be in liquid form, that is,

$$P_s = 0.0$$

$$P_l = 1.0 - \{E_r-[C_{ps}T_m+H_f+C_{pl}(T_v-T_m)]\}/H_v \qquad (55a,b,c)$$

$$P_v = \{E_r-[C_{ps}T_m+H_f+C_{pl}(T_v-T_m)]\}/H_v$$

If $C_{ps}T_m+H_f+C_{pl}(T_v-T_m)+H_v<E_r$, then all of the shocked and released material was vaporized, that is,

$$P_s = 0.0$$

$$P_l = 0.0 \qquad (56a,b,c)$$

$$P_v = 1.0$$

4.2 Computing the Masses of the Solid, Liquid, and Gaseous Debris Cloud Material

The material in the debris cloud created by the initial impact consists of the target material removed by the impact and the impacting projectile mass. While the mass of the projectile material in the debris cloud was known a priori, the mass of the target material in the debris cloud had to be determined by multiplying the target hole-out area by the target thickness and the target material density.

4.2.1 Target Plate Hole Diameter

The diameter of the hole created in the target plate by the initial impact (D) can be calculated using any one of a number of empirical equations for hole diameter in a thin plate due to a high speed impact. Four such equations were considered and implemented in the debris cloud materials characterization scheme being developed herein. These equations are given below.

#1) KAPP-II/HSS01

$$D/d_p = \exp(a\rho_p)\{1+bv_o[1-\exp(-ct_s/d_p)]\} \qquad (57)$$

where a,b, and c are empirical constants [10].

#2) KAPP-II/HSS02

$$D = F_w(r_c/P)[T(2P-T)]^{1/2} \qquad (58)$$

where

$$T = k_t t_s + P\{1-[1-(d_p/2r_c)^2]^{1/2}\} \quad (59)$$

$$r_c = P/[d(\rho_p/r_t) + f]^{1/2} \quad (60)$$

$$P/d_p = \begin{cases} S(v_o)(\rho_p/\rho_t)^{1/2}(L_p/d_p - 1 + D_{inf}/2d_p) & \text{..... long rods} \\ S(v_o)(\rho_p/r_t)^{1/2}(D_{inf}/2d_s)(L_p/d_p)^{1/3} & \text{..... disks} \end{cases} \quad (61a,b)$$

$$S(v_o) = 1 - \exp\{-v_o^2(\rho_p/2Y_t)[u/(1+u)]\} \quad (62)$$

$$u = (\rho_p/\rho_t)^{1/2} \quad (63)$$

$$D_{inf}/d_p = a(\rho_p/\rho_t)^b(3L_p/2d_p)^c[(\rho_p v_o^2)/(2eB_t)]^{1/3} \quad (64)$$

where d_s is the diameter of an equivalent sphere, Y_t is the target material tensile yield strength, B_t is the target material Brinell Hardness Number, and a,b,c,d,e,f,k_t, and F_w are empirical constants [10].

#3) KAPP-II/HSA01

$$D/d_p = 1 + (D_{inf}/d_p - 1)\{1-\exp[-h(t_s/d_p)^{2/3}]\} \quad (65)$$

where D_{inf} is as defined in equation (64), and

$$h = a(B_t/\rho_p)^b \quad (66)$$

and a,b are empirical constants [10].

#4) PEN4.v10

$$D/t_s = 11.02\{1 - \exp[-(d_p/t_s)(\rho_p v_o^2/Y_t)^{0.415}(\rho_p/\rho_t)^{-0.15}/29.9]\} \quad (67)$$

While the empirical nature of these equations mandates their use only within the impact velocity regimes for which they were designed, the results obtained for velocities outside the prescribed regimes are in general not unreasonable. One of the implications of these equations is that the amount of target mass in the debris cloud and will continue to grow as the impact velocity is increased. This is because the velocity terms in equations (57,58,65,67) have a positive real number exponent; three of them state that hole diameter is proportional to $v_o^{2/3}$. However, this is not necessarily the case, especially in the case of a thin target. For a

thin target, one would expect the hole diameter to increase until a certain critical impact velocity (which depends on relative target and projectile material and geometric properties) and then level off as velocity continues to increase.

Up until the critical impact velocity, there would be substantial interaction between the projectile and the target as the projectile moves through the target; above the critical impact speed, the projectile would move through the target so fast (because of the relative thinness of the target) that there is only a minimal amount of projectile/target interaction. Hence, one would expect impact velocity to have a minimal effect on hole diameter in a thin target beyond a certain critical value. Unfortunately, equations (57,58,65,67) do not have this characteristic.

A brief study was made using equations (57,58,65,67) for aluminum projectiles impacting thin aluminum targets at speeds between 2 and 25 km/sec. The results are presented in Figures 7-10; each Figure corresponds to a different relative geometric configuration that was considered. In Figure 7, the projectile length-to-diameter ratio (L_p/d_p) was 2 while the ratio of the target thickness to the projectile diameter (t_s/d_p) was 0.1; in Figure 8, L_p/d_p=2 while t_s/d_p=0.5; in Figure 9, L_p/d_p=0.1 and t_s/d_p=0.1; and in Figure 10, L_p/d_p=0.1 and t_s/d_p=0.5.

Thus, in Figures 7,8 a relatively long rod impacted a relatively thin and thick plate, respectively, while in Figures 9,10 a relatively thin disk impacted and relatively thin and thick plate, respectively. A common feature of all four figures is than only the PEN4.v10 equation possessed the ability to level off in hole diameter beyond a certain impact velocity. However, the PEN4.v10 equation is for spheres only; the projectile diameter used in the equation was taken to be equal to d_p, and not some 'equivalent diameter' that would be larger than d_p and confuse the issue. Thus, the predictions of the PEN4.v10 equation are affected only by target thickness and not projectile length.

Another common feature of all four figures is that the predictions of all three KAPP-II equations continue to grow as impact velocity increases. Of these three equations, the one denoted by 'KII/HSS02' appears to have some tendency to flatten out as the impact velocity

increases. Thus, it would appear that KII/HSS02 offers some promise in being able to be modified to reflect what would be expected of hole diameter as a function of impact velocity.

A fifth hole diameter option was added to the debris cloud characterization scheme for thin disk projectiles. In this option, the diameter of the hole in a target plate impacted by a thin high speed projectile is merely set equal to the diameter of the impacting disk. This appropriateness of this approximation has been demonstrated in numerous experimental studies of high speed impacts (see, e.g. [33]).

4.2.2 Calculation of Shocked and Released Material Masses

To calculate the masses of the various states of the projectile and target materials in the debris cloud, the amounts of shocked and released target and projectile material had to be determined. These quantities were obtained by determining the locations in the target plate and in the projectile where the rarefaction waves had overtaken the corresponding shock wave [34]. It was the material through which both the shock wave and the release wave had traveled that was shocked and released and which was therefore either melted or vaporized, depending on the particulars of the impact event. Any material beyond the point at which the rarefaction wave had overtaken the shock wave was assumed, for the purposes of this study, not to have been shocked and to have remained in a solid matter state. If the point at which the release wave had overtaken the shock wave was beyond the thickness of the target plate or the length of the projectile, then all of the target and/or projectile material had been shocked and released.

For single-material projectiles, referring to Figures 11a,b and 12 and utilizing the results in [34], rarefaction wave R_1 overtakes the shock wave S_1 on the axis of symmetry at a point in the projectile given by

$$L_1 = 0.72d_p \tag{68}$$

where L_1 is measured from the front face of the initially uncompressed projectile. Furthermore, rarefaction wave R_4 will overtake the shock wave S_1 at a point in the projectile given by

$$L_4 = t_s[(c_{st}+u_{st}-u_{pt})/(c_{sp}-u_{sp}+u_{pp})](c_{sp}/c_{st})(u_{sp}/u_{st}) \quad (69)$$

where t_s is the target thickness, and c_{st},c_{sp} are the speeds of sound in the shocked target, projectile materials and are given by [34]

$$c_{s(t,p)}^2 = u_{s(t,p)}^2\{0.49 + [(u_{s(t,p)}-u_{p(t,p)})/u_{s(t,p)}]^2\} \quad (70)$$

respectively. Thus, if $L_1<L_4$, then R_1 overtakes S_1 first and the shocked and released projectile length is taken to be equal to L_1; if $L_1>L_4$, then R_4 is the first to overtake S_1 and the shocked and released projectile length is taken to be equal to L_4.

For multi-material projectiles, the location in the projectile where the rarefaction wave R4 overtakes shock wave S1 is determined using a technique derived from that used for ingle-material projectiles. Consider Figure 13, which is an extension of Figure 12 for a single material projectile to the case of a multi-material projectile. In Figure 13, the speeds of the waves R_4 and S_1, which are denoted by 'D' and 'E' subscripts, respectively, are seen to change as they move through the projectile material layers. In addition, the interface velocity, which is denoted by a 'C' subscript, is also seen to change from interface to interface due to the different material layer properties.

As before, we are interested in calculating the length L_4, which is the distance form the undisturbed leading edge of the projectile to the point within the projectile where the rarefaction wave R_4 overtakes the shock wave S_1 as it moves through the various projectile layers. This quantity is obtained by performing the following sequence of calculations. It is noted that as we proceed in the calculations that follow, the velocities V_A,V_B,V_C, etc. are presumed to be known for each successive layer. They are functions of the initial impact conditions an the impedance mismatches at the various projectile layers. Thus, the objective of the calculations that follow is to determine the various X and T quantities for the movement of the waves R_4 and S_1 through a multi-material projectile in X-T space as shown in Figure 13.

The first quantities that need to be determined are the time T_C and the position X_C at which the rarefaction wave R_4 intercepts the target/projectile interface. Referring to Figure

14 and following the procedure in [34], we have

$$X_C = t_s(V_{C1}/V_A)(V_B+V_A)/(V_B+V_{C1}) \quad (71)$$

$$T_C = X_C/V_{C1} = (t_s/V_A)(V_B+V_A)/(V_B+V_{C1}) \quad (72)$$

We now consider each projectile layer in sequence and determine whether or not R_4 will overtake S_1 within a given layer or at some point beyond it. Thus, for the first layer, referring again to Figure 14, we calculate

$$L_4^{(1)} = X_{ET} + X_{DT} \quad (73)$$

where

$$X_{ET} = X_C(V_{E1}/V_{C1})(V_{D1}+V_{C1})/(V_{D1}-V_{E1}) \quad (74)$$

$$T_{ET} = X_{ET}/V_{ET} = (X_C/V_{C1})(V_{D1}+V_{C1})/(V_{D1}-V_{E1}) \quad (75)$$

$$X_{DT} = X_{ET}(v_o/V_{E1}) \quad (76)$$

Thus, if $L_4^{(1)} < L_p^{(1)}$, R_4 overtakes S_1 within the first projectile layer; otherwise, it overtakes S_1 at some point beyond the first layer and the calculations proceed as follows.

Before moving on to the second layer, we must first determine the locations of the points in X-T space where R_4 and S_1 each intersect the moving interface between layers 1 and 2. These points correspond to points 4 and 5, respectively, in Figure 15. The coordinates of Point 5 are determined by calculating the quantities X_{E1} and T_{E1}. These are obtained from Figures 14 and 15 using simple geometric considerations with the following results:

$$X_{E1} = V_{E1}L_p^{(1)}/(V_{E1}+v_o) \quad (77)$$

$$T_{E1} = X_{E1}/V_{E1} = L_p^{(1)}/(V_{E1}+v_o) \quad (78a,b)$$

To determine the X-T coordinates of point 4, we again refer to Figure 15 and proceed as follows. First, noting that

$$T_4 = T_C + T_{D1} \quad (79)$$

we have

$$T_4 - T_C = T_C + T_{D1} - T_C = T_{D1} = (X_4 - X_C)/V_{D1} \quad (80)$$

so that

$$T_{D1} = (X_4 - X_C)/V_{D1} \quad (81)$$

Second,

$$T_4 - T_5 = (X_4 - X_5)/(-V_{C2}) \tag{82}$$

Substituting for T_4 according to equation (79) and substituting $T_5=T_{E1}$ and $X_5=X_{E1}$ allows equation (82) to be solved for X_4 as follows:

$$X_4 = X_{E1} - V_{C2}(T_C + T_{D1} - T_{E1}) \tag{83}$$

Equating this result to the expression for X_4 that is obtained from equation (81) yields

$$X_C + T_{D1}V_{D1} = X_{E1} - V_{C2}(T_C - T_{E1}) - V_{C2}T_{D1} \tag{84}$$

Using equation (83) to solve for T_{D1} yields:

$$T_{D1} = [X_{E1} + V_{C2}T_{E1} - (X_C + V_{C2}T_C)]/(V_{D1} + V_{C2}) \tag{85}$$

Since $X_C = -T_CV_{C1}$ we have

$$T_{D1} = [X_{E1} + V_{C2}T_{E1} + T_C(V_{C1}-V_{C2})]/(V_{D1} + V_{C2}) \tag{86}$$

Thus, since the X-coordinate of point 4 is given by

$$X_4 = X_C + T_{D1}V_{D1} \tag{87}$$

the position of point 4 is now also defined. We are now ready to the second projectile layer.

Referring to Figure 16 and proceeding as before, we have:

$$L_4^{(2)} = X_{E1} + X_{ET} + X_{DT} \tag{88}$$

$$X_{DT} = X_{DT}'(T_{E1}+T_{ET})/T_{ET} \tag{89a,b}$$

$$X_{DT}'/v_o = X_{ET}/V_{E2} \tag{90}$$

Substituting for X_{DT}' according to its definition in equation (89b) yields:

$$X_{DT} = X_{ET}(v_o/V_{E2})(T_{E1} + T_{ET})/T_{ET} \tag{91}$$

But also since $X_{ET}/T_{ET} = V_{E2}$, this equation simplifies to

$$X_{DT} = v_o(T_{E1} + T_{ET}) \tag{92}$$

Thus, substituting equation (92) into equation (88) yields

$$L_4^{(2)} = X_{E1} + X_{ET} + v_oT_{E1} + v_oT_{ET} \tag{93}$$

Since $v_oT_{E1} = X_{D1}$, this equation reduces to

$$L_4^{(2)} = X_{E1} + X_{D1} + X_{ET}(1 + v_o/V_{E2}) \tag{94}$$

Finally, since $X_{E1} + X_{D1} = L_p^{(1)}$, we have

$$L_4^{(2)} = L_p^{(1)} + X_{ET}(1 + v_o/V_{E2}) \quad (95)$$

To find X_{ET}, we note that

$$T_{E1} + T_{ET} = T_C + T_{D1} + T_{DT} \quad (96)$$

Since

$$T_{DT} = (X_{CT} + X_{ET})/V_{D2} \quad (97)$$

we have

$$T_{ET} = T_C + T_{D1} - T_{E1} + (X_{CT} + X_{ET})/V_{D2} \quad (98)$$

But since

$$X_{CT} = V_{C2}(T_C + T_{D1} - T_{E1}) \quad (99)$$

equation (98) can be written as

$$T_{ET} = T_C + T_{D1} - T_{E1} + [V_{C2}(T_C + T_{D1} - T_{E1}) + X_{ET}]/V_{D2} \quad (100)$$

Using the relationship $T_{ET} = X_{ET}/V_{E2}$, we obtain after simplification the following expression for X_{ET}:

$$X_{ET} = V_{E2}[(V_{D2} + V_{C2})/(V_{D2} - V_{E2})](T_C + T_{D1} - T_{E1}) \quad (101)$$

Substituting this expression into equation (95) completes the derivation of the expression of $L_4^{(2)}$. Thus, if $L_4^{(2)} < L_p^{(1)} + L_p^{(2)}$, R_4 overtakes S_1 within the second projectile layer; if not, we continue our calculations. As before, prior to moving on the third layer (assuming, of course, that it exists), we must first determine the locations of the points in X-T space where R_4 and S_1 each intersect the moving interface between layers 2 and 3. These points correspond to points 9 and 10, respectively, in Figure 17. From Figure 16 and 17, we obtain the following expressions for the coordinates for point 10:

$$X_{10} = X_{E1} + X_{E2} = X_{E1} + V_{E2}L_p^{(2)}/(V_{E2} + v_o) \quad (102a,b)$$

$$T_{10} = T_{E1} + T_{E2} = T_{E1} + X_{E2}/V_{E2} = T_{E1} + L_p^{(2)}/(V_{E2} + v_o) \quad (103a\text{-}c)$$

where X_{E1} and T_{E1} are given by equations (77) and (78), respectively. To determine the coordinates for point 9 in X-T space, we note that

$$T_9 - T_4 = (X_9 - X_4)/V_{D2} \quad (104a)$$

and

$$T_9 - T_{10} = (X_9 - X_{10})/(-V_{C3}) \qquad (104b)$$

Since

$$T_9 - T_4 = T_{D2} \qquad (105a)$$

we can substitute for T4 according to equation (79) and obtain

$$T_9 = T_C + T_{D1} + T_{D2} \qquad (105b)$$

Equations (104a,b) are then combined to yield:

$$X_9 = X_4 + T_{D2}V_{D2} = X_{10} - V_{C3}(T_9 - T_{10}) \qquad (106a,b)$$

Thus, to uniquely determine the position of point 9, all that remains is to find an expression for T_{D2}. Substituting equations (79), (87), (102a), (103a), and (105) into equations (106) and solving for T_{D2} yields

$$T_{D2} = (X_{E2} + V_{C3}T_{E2})/(V_{D2} + V_{C3}) + [(V_{C2} - V_{C3})/(V_{D2} - V_{C3})](T_C + T_{D1} - T_{E1}) \qquad (107)$$

Since X_4 is already known, equation (106a) can be used to obtain X_9. This completes the series of calculations required to define the position in X-T space of points 9 and 10.

The series of calculations presented for the first two projectile layers serves as the basis for the general forms of the equations that can be used for determining the location where R_4 overtakes S_1 in a multi-material projectile. These generalized equations, which are valid for material layers 2 through NPMAT-1 where NPMAT is the number of projectile layers, are derived as follows.

Referring to Figure 18 and 19, which are generalizations of Figures 16 and 17, respectively, we begin by writing the general form of $L_4^{(i)}$ as follows:

$$L_4^{(i)} = \sum_{j=1}^{i-1} X_{Ej} + X_{ET} + X_{DT} \qquad (108)$$

where the X_{Ej} are known for $1 \le j \le i-1$ (as are the accompanying T_{Ej}). Thus, the unknowns in equation (108) are X_{ET} and X_{DT}. To find expressions for these quantities, we refer to Figure 18 and write:

$$T_{ET} = X_{DT'}/v_o = X_{ET}/V_{Ei} \qquad (109a,b)$$

so that

$$X_{DT'} = X_{ET}(v_o/V_{Ei}) \qquad (110)$$

But also since

$$X_{DT'}/T_{ET} = X_{DT}/(\sum_{j=1}^{i-1} T_{Ej} + T_{ET}) \qquad (111)$$

we have

$$X_{DT} = X_{DT'}(\sum_{j=1}^{i-1} T_{Ej} + T_{ET})/T_{ET} \qquad (112)$$

Substituting for $X_{DT'}$ according to equation (110) and then replacing X_{ET}/T_{ET} with V_{Ei} yields the following expression for X_{DT}:

$$X_{DT} = v_o(\sum_{j=1}^{i-1} T_{Ej} + T_{ET})/T_{ET} \qquad (113)$$

It is noted that equation (113) is a simple generalization of equation (92). Substituting equation (113) into equation (108) yields, after replacing T_{ET} with X_{ET}/V_{Ei} and $v_o T_{Ej}$ with

$$X_{Dj'} = X_{Dj}T_{Ej}/\sum_{k=1}^{j-1} T_{Ek} \qquad (114)$$

the following expression for $L_4^{(i)}$:

$$L_4^{(i)} = \sum_{j=1}^{i-1} (X_{Ej} + X_{Dj}T_{Ej}/\sum_{k=1}^{j-1} T_{Ek}) + X_{ET}(1 + v_o/V_{Ei}) \qquad (115)$$

Having eliminated X_{DT} from the expression for $L_4^{(i)}$, all that remains is to find X_{ET}. To begin, we write

$$\sum_{j=1}^{i-1} T_{Ej} + T_{ET} = T_C + \sum_{j=1}^{i-1} T_{Dj} + T_{DT} \tag{116}$$

so that

$$T_{ET} = T_C + \sum_{j=1}^{i-1} (T_{Dj} - T_{Ej}) + (X_{CT} + X_{ET})/V_{Di} \tag{117}$$

Noting that

$$X_{CT} = V_{Ci}(T_C + \sum_{j=1}^{i-1} T_{Dj} - \sum_{j=1}^{i-1} T_{Ej}) \tag{118}$$

we have, after substituting equation (117) into equation (116) and simplifying, the following expression for X_{ET}:

$$X_{ET} = V_{Ei}[(V_{Di} + V_{Ci})/(V_{Di} - V_{Ei})][T_C + \sum_{j=1}^{i-1} (T_{Dj} - T_{Ej})] \tag{119}$$

Thus, if $L_4^{(i)} < L_p^{(1)} + L_p^{(2)} + \ldots + L_p^{(i)}$, then R_4 overtakes S_1 within layer 'i'; if not, then we must determine the coordinates of the points in X-T space where R_4 and S_1 intercept the moving interface between layers i and i+1. If we denote the coordinates of these points, which are labeled 'R' and 'S' in Figure 19, as (X_{R4},T_{R4}) and (X_{S1},T_{S1}), then we have

$$X_{S1} = \sum_{j=1}^{i-1} X_{Ej} + X_{Ei} \tag{120a}$$

and

$$T_{S1} = \sum_{j=1}^{i-1} T_{Ej} + T_{Ei} \tag{120b}$$

where

$$X_{Ei} = V_{Ei}L_p^{(i)}/(V_{Ei} + v_o) \tag{121a}$$

and

$$T_{Ei} = X_{Ei}/V_{Ei} \tag{121b}$$

Additionally,

$$T_{R4} = T_C + \sum_{j=1}^{i-1} T_{Dj} + T_{Di} \tag{122a}$$

$$X_{R4} = \sum_{j=1}^{i-1} X_{Ej} + X_{R4}' \tag{122b}$$

where the X_{Ej}, T_{Dj}, and T_{Ej} are known for $1 \le j \le i-1$, and the quantities T_{Di} and X_{R4}' are obtained by generalizing equations (106) and (107), respectively. Thus, we have

$$T_{Di} = (X_{Ei} + V_{C,i+1}T_{Ei})/(V_{Di} + V_{C,i+1}) + [(V_{C,i} - V_{C,i+1})/(V_{Di} - V_{C,i+1}][T_C + \sum_{j=1}^{i-1} (T_{Dj} - T_{Ej})]] \tag{123a}$$

and

$$X_{R4}' = X_{Ei} - V_{C,i+1}[T_C + \sum_{j=1}^{i} (T_{Dj} - T_{Ej})] \tag{123b}$$

At the last layer, i.e. when i=NPMAT, if $L_4^{(NPMAT)} > L_p$, then the entire projectile is shocked and released; if not, then R_4 overtakes S_1 in the final projectile material layer.

All that remains now is to relate the known quantities V_A, V_B, V_C, ..., etc. to physical quantities such as shock velocity, particle velocity, etc. Referring to [34], these relationships are readily obtained and are presented below.

$$V_A = u_{st} \qquad V_B = c_{st} - u_{pt}$$
$$V_{C1} = u_{pt} \qquad V_{D1} = c_{sp}(1) - u_{pt} \tag{124a-e}$$
$$V_{E1} = u_{sp}(1) - v_o$$

For $i \geq 2$,

V_{Ci} ... particle velocity at the interface between layers i-1 and i

$$V_{Di} = c_{sp}^{(i)} - V_{Ci} \qquad (125a\text{-}c)$$

V_{Ei} ... (shock velocity at the interface between layers i-1 and i) - v_o

It is noted that the quantity $c_{sp}^{(i)}$ is recalculated for each material layer based on the particle and shock velocities obtained for each layer using the impedance mismatch technique described in Section 3.5. Finally, if we substitute the definitions of V_A, V_B, V_{C1}, V_{D1}, and V_{E1} according to equations (124a-e) into equations (71-75) and simplify, we obtain equation (69), which is the equation obtained in [34] for single material projectiles.

Figure 20 shows the results obtained when this technique is applied to a 3-layer projectile impacting an aluminum plate at 6 km/sec. The projectile materials, their stacking sequence, and the geometry of the impact are also given in Figure 20. As can be seen from Figure 20, the original rarefaction wave emanating from the target rear surface overtakes the shock wave in the projectile at a distance of approximately 0.71 cm from the leading edge of the undisturbed projectile. This implies that at the impact velocity considered, the first two projectile layers (i.e. the aluminum and the steel) are completely shocked and released as is the first 0.202 cm of the third projectile layer (i.e. the tungsten).

It is the material through which both the shock wave and the release wave travel that is shocked and released and which is therefore either melted or vaporized, depending on the impact velocity. Any material beyond the point at which the rarefaction wave overtakes the shock wave is assumed, for the purposes of this study, not to be shocked and to remain in a solid matter state. If the point at which the release wave overtake the shock wave is beyond the thickness of the target plate or the length of the projectile, then all of the target and/or projectile material is shocked and released. Thus, according to the assumptions and definitions presented herein, the remaining 0.306 cm of the tungsten layer in the projectile corresponding to the impact depicted in Figure 20 is unshocked and unreleased.

In calculating the amount of target material subject to shock loading and release, it is assumed that the shocked target material comes from an area of the target equal to the presented area of the projectile [35]; the remaining material ejected from the target in the creation of the target plate hole is assumed to remain in a solid, albeit undoubtedly fragmented, state. This is due to the fact that if shear and viscous forces are neglected, there are no net forces acting on the projectile and target masses immediately after impact. This in turn implies that the force exerted by the projectile on the target equals the force exerted by the target on the projectile. Combining this result with equation (5) and noting that force is the product of pressure and area, the effective area of the target on which the impact pressure acts must, to an first-order approximation, equal the presented area of the projectile. This in turn implies that the shocked target material comes from an area of the target approximately equal to the presented area of the projectile.

Furthermore, it is also assumed that the depth of the shocked target material extends completely through the target thickness. Were this not the case, then other target failure modes, such as plugging, for example, might come into play. This in turn would seriously compromise the validity of the assumptions made in the development of this debris cloud model. A direct consequence of this assumption is that the model developed herein is not valid for "thick" target plates.

Once the projectile and target mass contributions to the debris cloud and the fractions of these masses that were shocked and released were obtained, the masses of the target and projectile materials in each of the three states of matter were computed by multiplying each matter state percentage by the appropriate total shocked and released mass. The mass of the solid shocked and released material (if any) was then added to the mass of the unshocked material (if any) to obtain the total mass of the solid component of the debris cloud material.

4.2.3 Summary and Comments

Thus, if we let L_o denote the length of the shocked and released portion of the projectile (original length L_p), then the mass distribution among the three matter states is

given by:

Target	Projectile	
$M_{st}=M_t-M_{tsr}+M_{st}'$	$M_{sp}=M_p-M_{psr}+M_{sp}'$	(126a,b)
$M_{st}'=P_{st}M_{tsr}$	$M_{sp}'=P_{sp}M_{psr}$	(127a,b)
$M_{lt}=P_{lt}M_{tsr}$	$M_{lp}=P_{lp}M_{psr}$	(128a,b)
$M_{vt}=P_{vt}M_{tsr}$	$M_{vp}=P_{vp}M_{psr}$	(129a,b)
$M_{tsr}=\pi d_p^2 t_s \rho_t/4$	$M_{psr}=(L_o/L_p)M_p$	(130a,b)
$M_t=\pi D^2 t_s \rho_t/4$	$M_p=\pi d_p^2 L_p \rho_p/4$	(131a,b)

where: M_{st},M_{sp}, M_{lt},M_{lp}, and M_{vt},M_{vp} are the total masses of the solid, liquid, and vapor components of the target and projectile contributions to the debris cloud, respectively; P_{st},P_{sp}, P_{lt},P_{lp}, and P_{vt},P_{vp} are the percentages of the solid, liquid, and vapor constituents of the shocked and released portions of the target, and projectile, respectively; M_{tsr}, and M_{psr} are the portions of the target and projectile that are shocked and released; ρ_t,ρ_p and M_t,M_p are the mass densities and total original mass contributions of the target and projectile to the debris cloud, respectively; and, M_{st}' and M_{sp}' are the masses of the shocked and released portions of the target and projectile that remain in a solid matter state upon release.

A limitation of this procedure is the assumption that no further projectile and/or target loading and unloading had occurred beyond the point where the release waves had overtaken the corresponding shock wave. This is not completely correct since the shock wave does not simply cease to exist once it is overtaken by a rarefaction wave. Rather, its magnitude decreases over a finite amount of time and a finite extent of material. Some additional projectile and target material will be heated and possibly melted until the strength of the shock wave diminishes to a point below which melt due to plastic deformation no longer occurs. However, the procedure set forth does allow the calculation of first-order accurate mass quantities for projectile and target materials in the three states of matter.

4.3 Debris Cloud Velocities

4.3.1 Introductory Comments

The equations developed in the subsequent section are presented in their most general form. They can be applied directly to a single-material projectile and adapted easily to apply to the impact of a multi-material projectile. In characterizing the velocities of the debris cloud created by a hypervelocity impact on a thin plate, there are two possibilities that need to be considered.

First, all of the projectile material is shocked and released. In this case, the debris cloud consists of the projectile and target material that is shocked and released and the additional fragmented target material that is ejected from the target plate during the perforation process but, according to the assumptions made herein, is not shocked and released. In the debris cloud model developed herein, all of this material is allowed to move axially and expand radially. The quantities of interest in this case are therefore the debris cloud leading edge, center-of-mass, trailing edge, and expansion velocities, that is, v_f, v_j, v_r, and v_{exp}, respectively.

Second, some of the projectile material remains, according to the assumptions employed herein, unshocked. While it would not be appropriate to call this unshocked projectile material a "residual projectile mass", it is reasonable to presume that this material is less severely stressed than that which is fully shocked and then released. Hence, it is also reasonable to presume that if there is any unshocked projectile material, then it does not significantly expand radially as it moves axially. In this case, the debris cloud consists of shocked and released target and projectile materials and the additional unshocked fragmented target material. The quantities of interest are the debris cloud leading edge, center-of-mass, and expansion velocities, that is, v_f, v_j, and v_{exp}, respectively, and the velocity of the remaining unshocked projectile material, v_{pr}. Note that due to the presence of the unshocked projectile mass, there is no debris cloud trailing edge for which to calculate a velocity.

4.3.2 Debris Cloud Velocity and Spread Calculations

Consider the impact of a projectile on a thin target and the debris cloud created by it as shown in Figure 21. As indicated in the Figure, the velocities of interest are v_f, v_i, v_{exp}, and v_r. As the initial shock wave created by the impact strikes the rear surface of the target, it creates a rarefaction wave that travels back into the target and eventually in some form into the projectile. This action and interaction of the shock wave and the free surface impacts a velocity u_{fst} to the target rear surface equal to the sum of the particle velocity in the target material due to the shock wave u_{pt} and the particle velocity due to the rarefaction wave u_{rt}, that is,

$$u_{fst} = u_{pt} + u_{rt} = u_{pt} + \int_0^{P_H} \sqrt{(-dV/dP)_{isen}}\,dP \qquad (132)$$

where the P-V curve used in the integration is the isentrope for the target material. Since $u_{rt} \approx u_{pt}$ [25], an alternative form for equation (132) is

$$u_{fst} = 2u_{pt} \qquad (133)$$

In both of the cases described in Section 4.3.1, the velocity of the leading edge of the debris cloud v_f is approximated with u_{fst} (see also [33]):

$$v_f = u_{fst} = u_{pt} + \int_0^{P_H} \sqrt{(-dV/dP)_{isen}}\,dP \qquad (134)$$

Also common to both cases is that the half-angle measuring the spread of the debris cloud materials is given by

$$\theta = \tan^{-1}(v_{exp}/v_i) \qquad (135)$$

What distinguishes the two types of debris clouds mathematically is the manner in which v_i, v_{exp}, and v_r or v_{pr} are calculated. When all of the projectile material is shocked and released, then:

$$v_r = v_o - u_{fsp}; \qquad (136)$$

v_i is obtained from momentum conservation before and after the impact event, that is,

$$v_i = m_p v_o / m_{dc}; \tag{137}$$

and, v_{exp} is obtained from the application of energy conservation before and after the impact event, that is,

$$m_p v_o^2/2 = E_{pr} + E_{tr} + m_{dc} v_i^2/2 + m_{dc} v_{exp}^2/2 \tag{138}$$

where $m_{dc} = m_p + m_t$ is the total debris cloud mass, m_p is the projectile mass, m_t is the total target hole-out mass, E_{pr} and E_{tr} are the internal projectile and target energies, respectively, that have gone into heating the projectile and target materials, and $u_{fsp} = u_{pp} + u_{rp}$ is the velocity of the rear free surface of the projectile. As in the case of u_{fst}, u_{fsp} is taken to be equal to the sum of the particle velocity in the projectile material due to the passage of the shock wave, u_{pp}, and the particle velocity due to the passage of the rarefaction wave in the projectile material, u_{rp}, created by the reflection of the shock wave from the projectile rear free surface.

In the event when not all of the projectile material is shocked and released, then v_i, v_{exp}, and v_{pr} are obtained through the solution of the following three simultaneous equations:

$$v_{exp} = v_f - v_i; \tag{139}$$

$$m_p v_o = m_{pr} v_{pr} + m_{dc} v_i; \tag{140}$$

$$m_p v_o^2/2 = E_{pr} + E_{tr} + m_{pr} v_{pr}^2/2 + m_{dc} v_i^2/2 + m_{dc} v_{exp}^2/2 \tag{141}$$

where in this case $m_{dc} = m_p + m_t - m_{pr}$ and m_{pr} is the mass of the unshocked projectile material. In this particular case, substituting for v_{exp} and v_{pr} into equation (141) using appropriate expressions obtained from equations (139) and (140) yields a quadratic equation for v_i. This equation is then solved to yield the following expression for v_i:

$$v_i = b/a - [(b/a)2 - (c/a)]^{1/2} \tag{142}$$

where

$$a = 2 + m_{dc}/m_{pr} \qquad b = v_f + (m_p/m_{pr})v_o \qquad (143a,b)$$

$$c = v_f^2 + (m_p/m_r - 1)(m_p/m_{dc})v_o^2 + 2(E_{pr}+E_{tr})/m_{dc} \qquad (143c)$$

The quantities v_{exp} and v_{pr} are then easily obtained from equations (139) and (140). If the solution of the above system of equations results in a situation where there is insufficient energy available for debris cloud expansion or motion of the unshocked portion of the projectile material, then the leading edge velocity is reduced until some kinetic energy does become available.

4.3.3 Comments

It is important to note that equation (136) can occasionally yield rear surface velocities that may be questionable. For example, for like-into-like impacts, $u_{fsp} \approx 2u_{pp} = 2(v_o/2) = v_o$ so that equation (136) yields $v_f = 0$. However, this may in fact be an acceptable result of one recalls the debris clouds in the x-ray photographs of lead-on-lead impacts, for example [24]. In these photographs, the debris cloud appears to remain attached to the target plate, thereby giving the impression that the rear end of the cloud does not move, i.e. that $v_f = 0$. In the copper-on-aluminum impacts in [33], the rear end of the copper projectile does in fact move through the aluminum target plate so that the rear end of the debris cloud does have a rather clear forward velocity component.

In addition, equation (136) may yield negative values in some cases where a less dense projectile impacted a more dense target plate. But even in this case, perhaps the negative velocity is that of the backsplash that would undoubtedly occur and which may be significant in such as case. Thus, caution should be exercised when using equation (136) to calculate the velocity of the rear surface of the debris cloud.

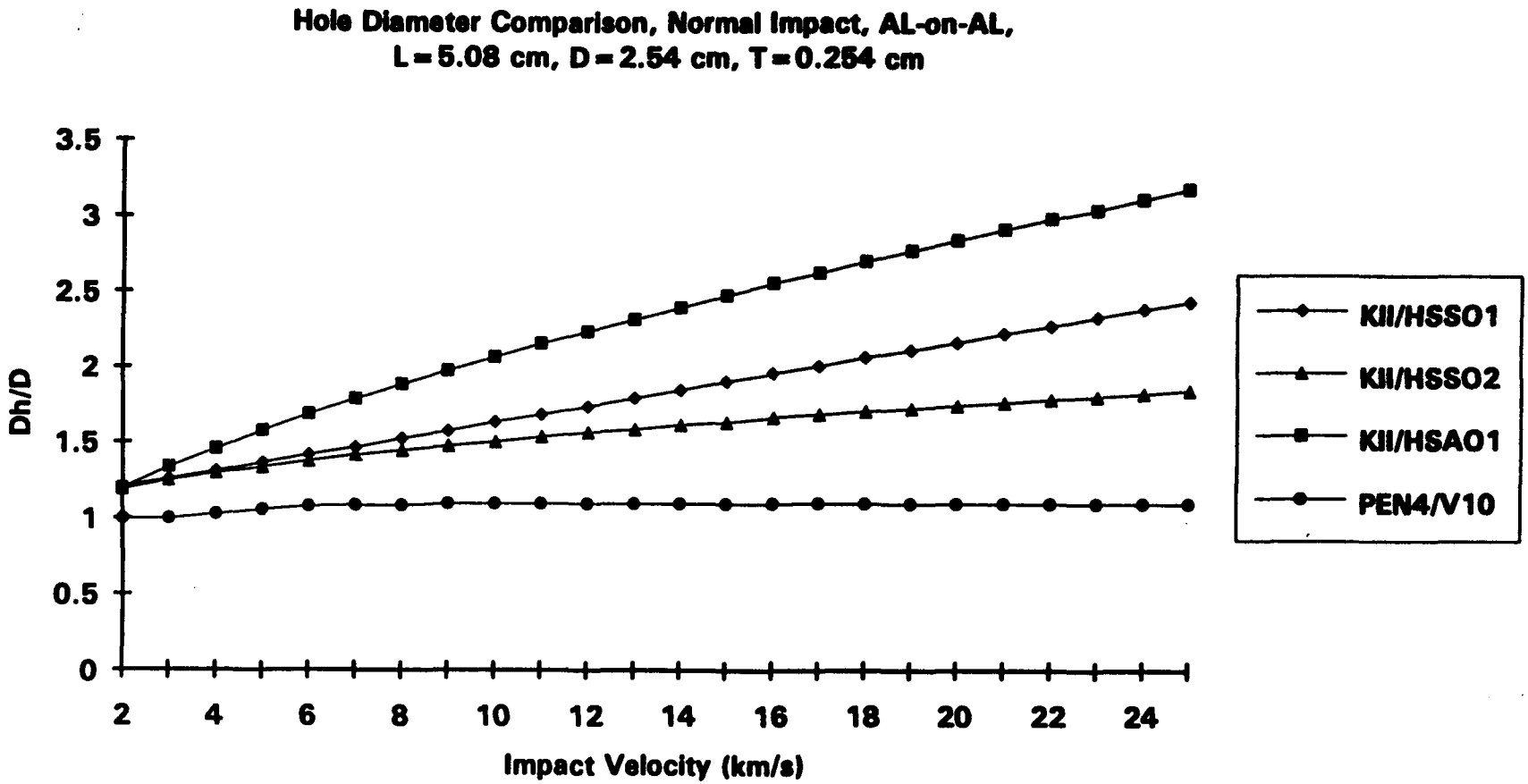

Figure 7. Target Hole Diameter Prediction Comparison, Aluminum-on-Aluminum Impact, L/D=2.0, T/D=0.1

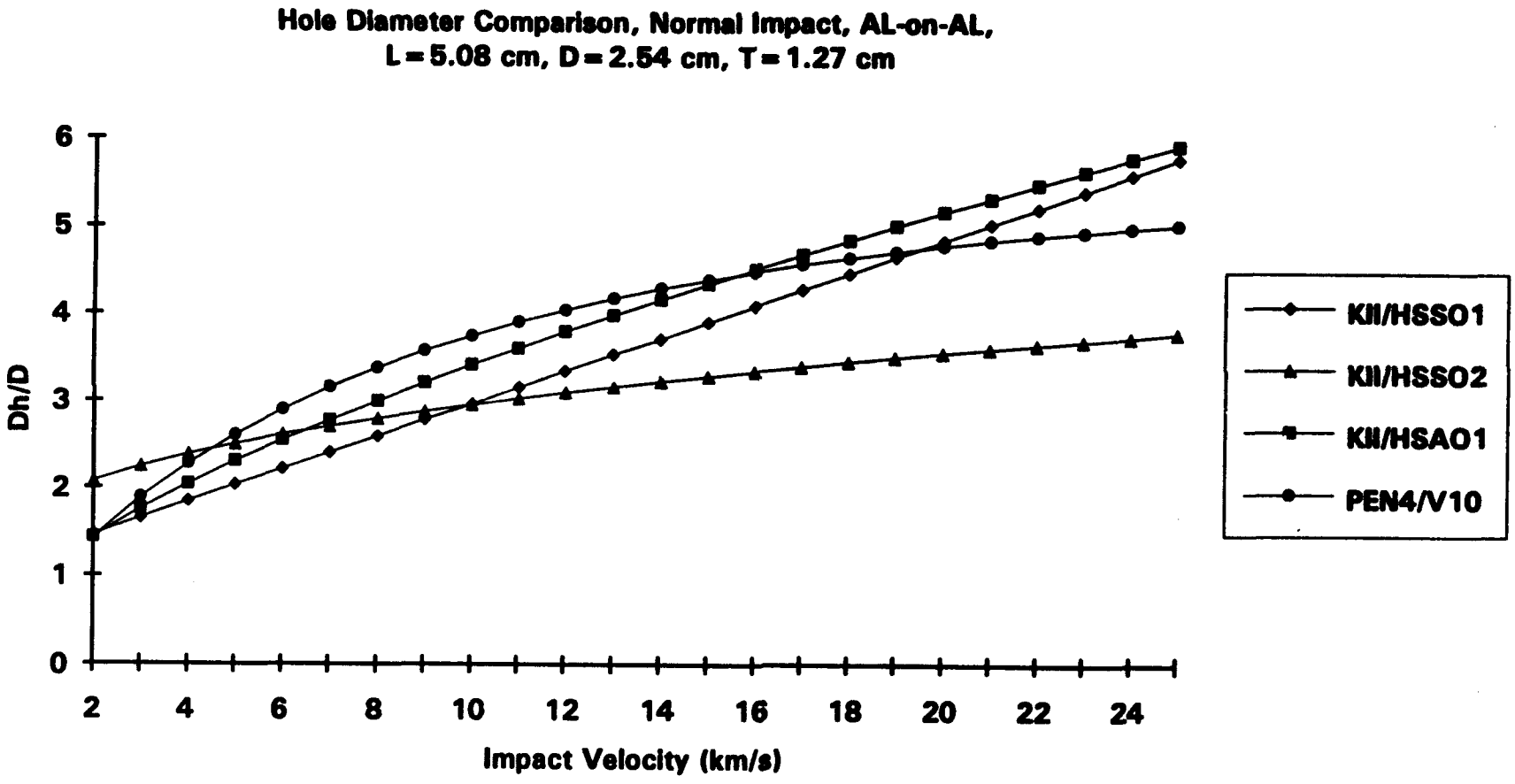

Figure 8. Target Hole Diameter Prediction Comparison, Aluminum-on-Aluminum Impact, L/D=2.0, T/D=0.5

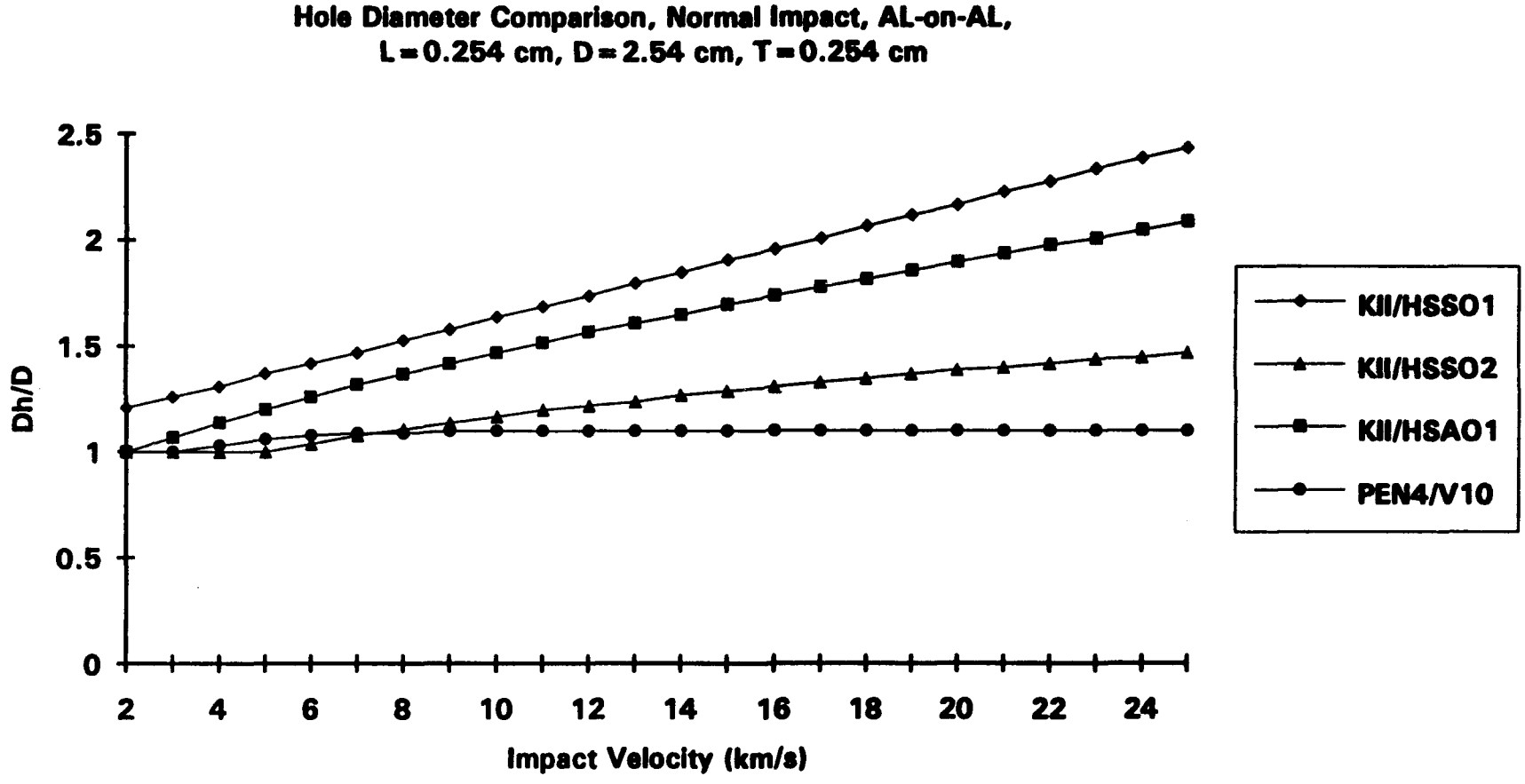

Figure 9. Target Hole Diameter Prediction Comparison, Aluminum-on-Aluminum Impact, L/D=0.1, T/D=0.1

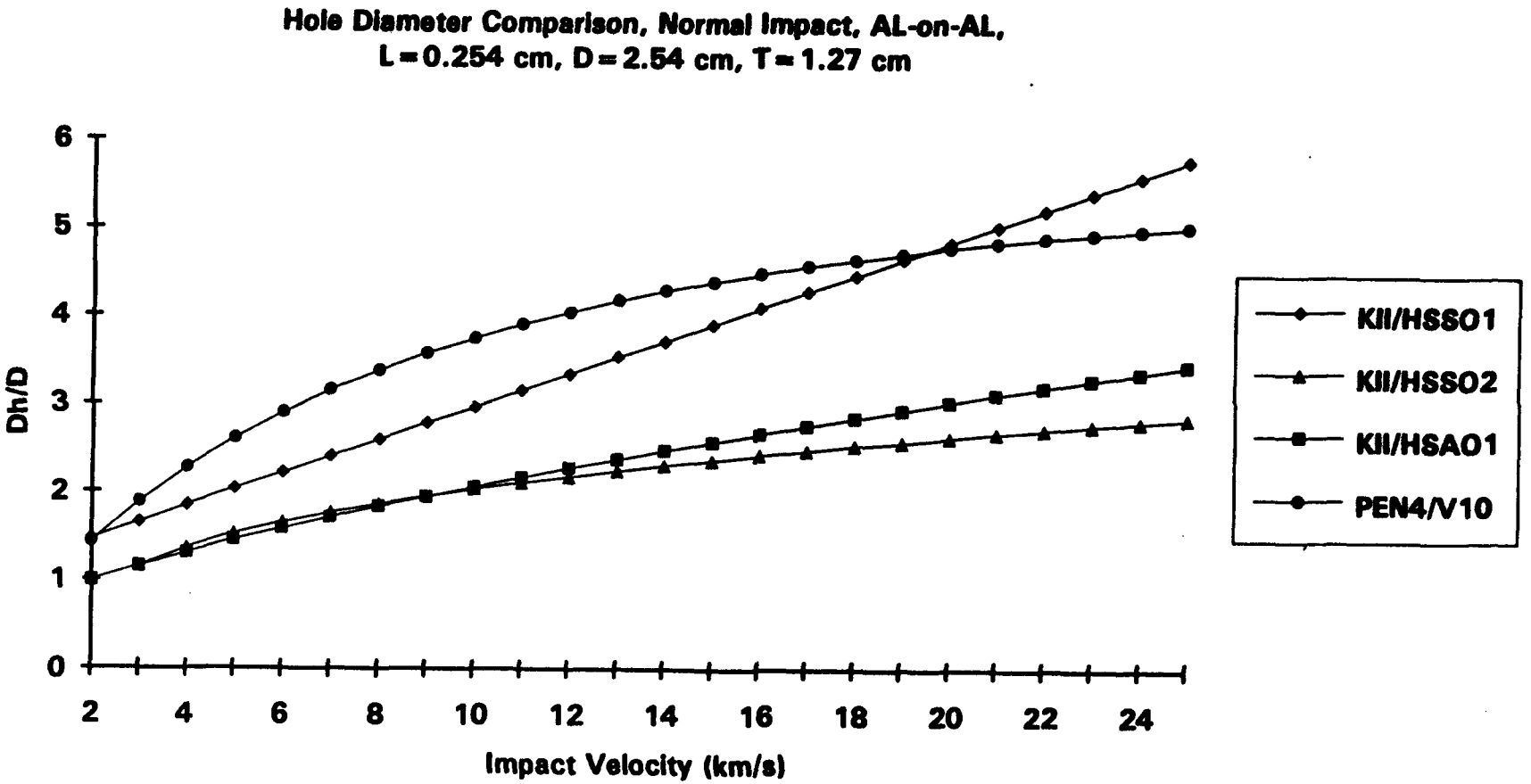

Figure 10. Target Hole Diameter Prediction Comparison, Aluminum-on-Aluminum Impact, L/D=0.1, T/D=0.5

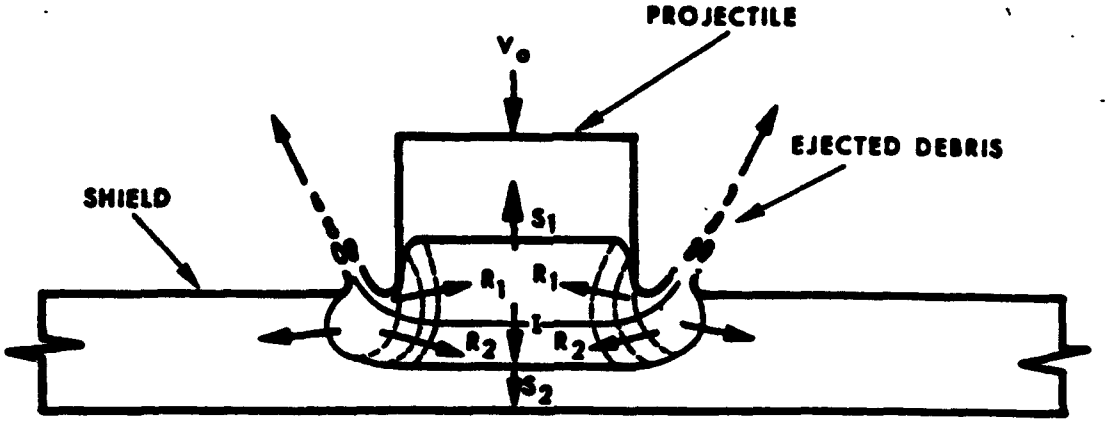

(a) In a Projectile and Shield Soon After Impact

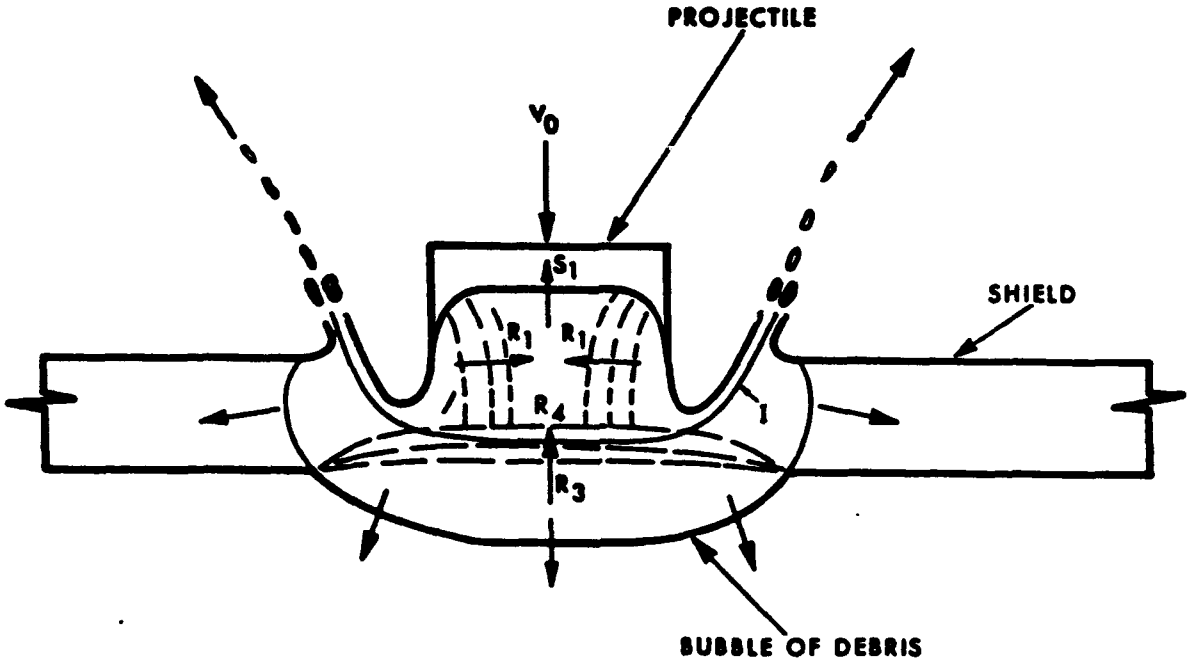

(b) After the Shock in the Shield Has Reflected From the Bottom Face of the Shield

Figure 11. Wave Patterns in a Projectile and an Impacted Target [34]

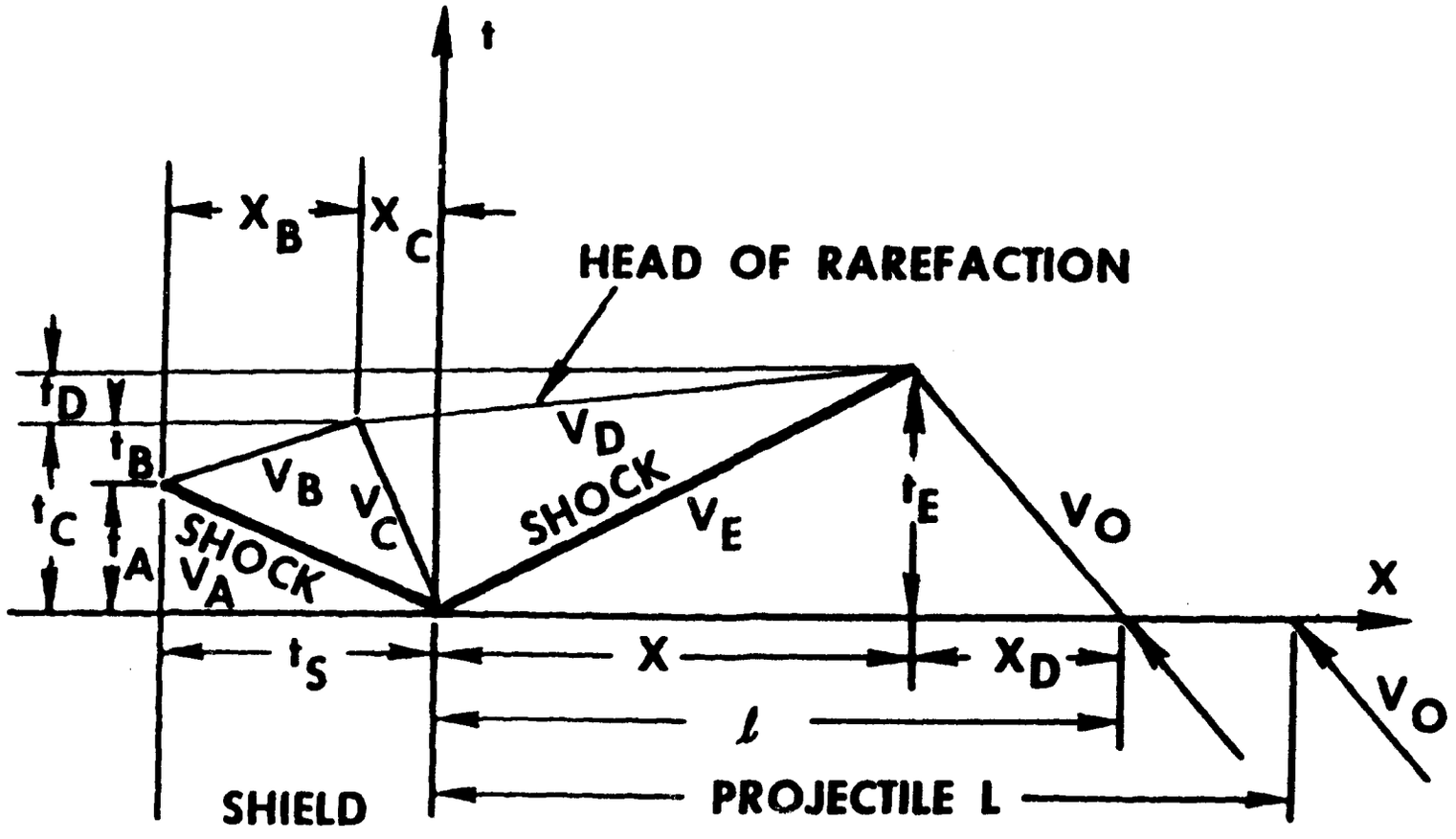

Figure 12. X-T Diagram Showing Where a Rarefaction Wave from the Rear Surface of a Target Plate Overtakes the Shock Wave in a Single-Material Projectile [34]

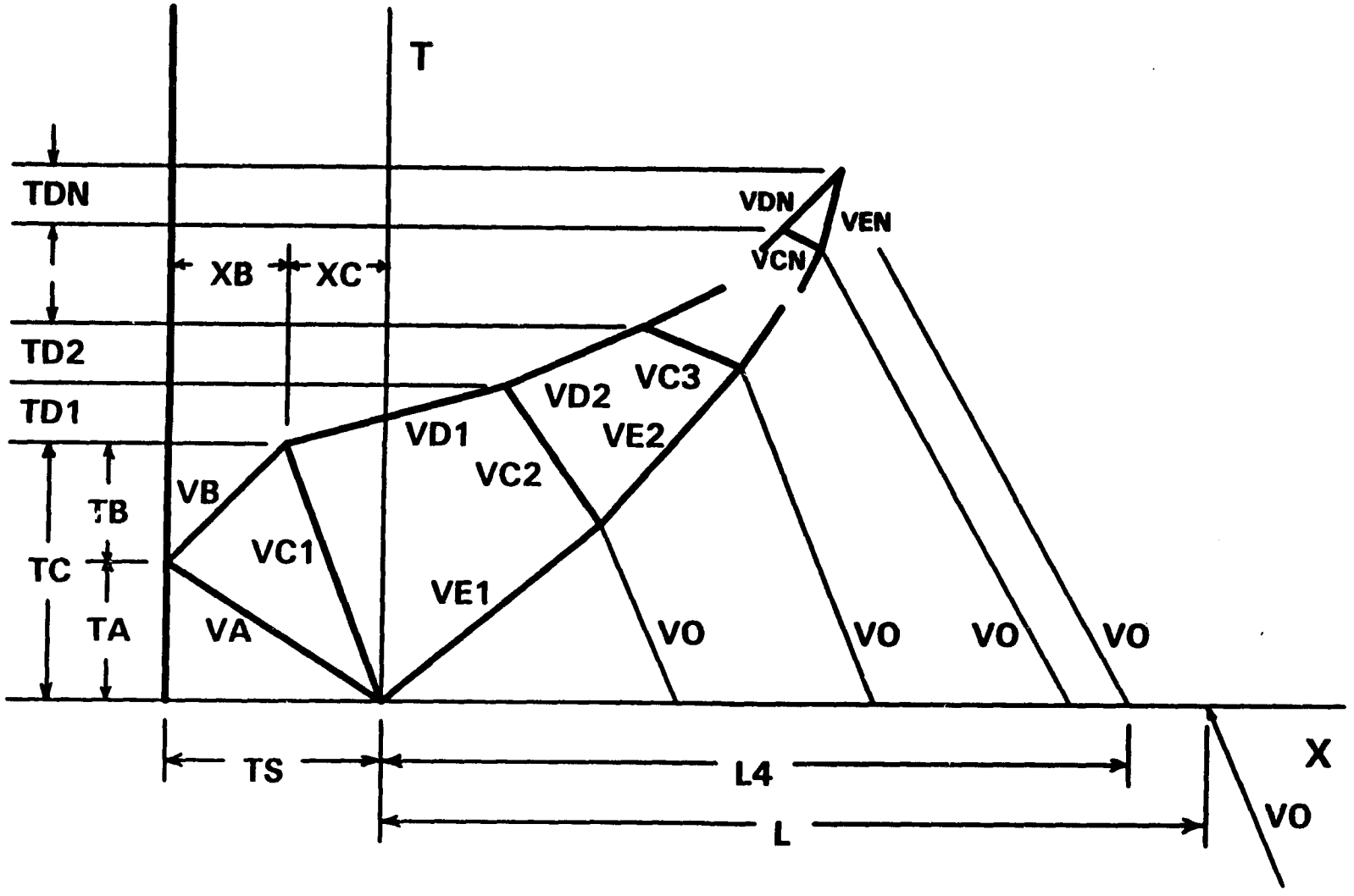

Figure 13. Extension of Figure 12 to Multi-Material Projectiles

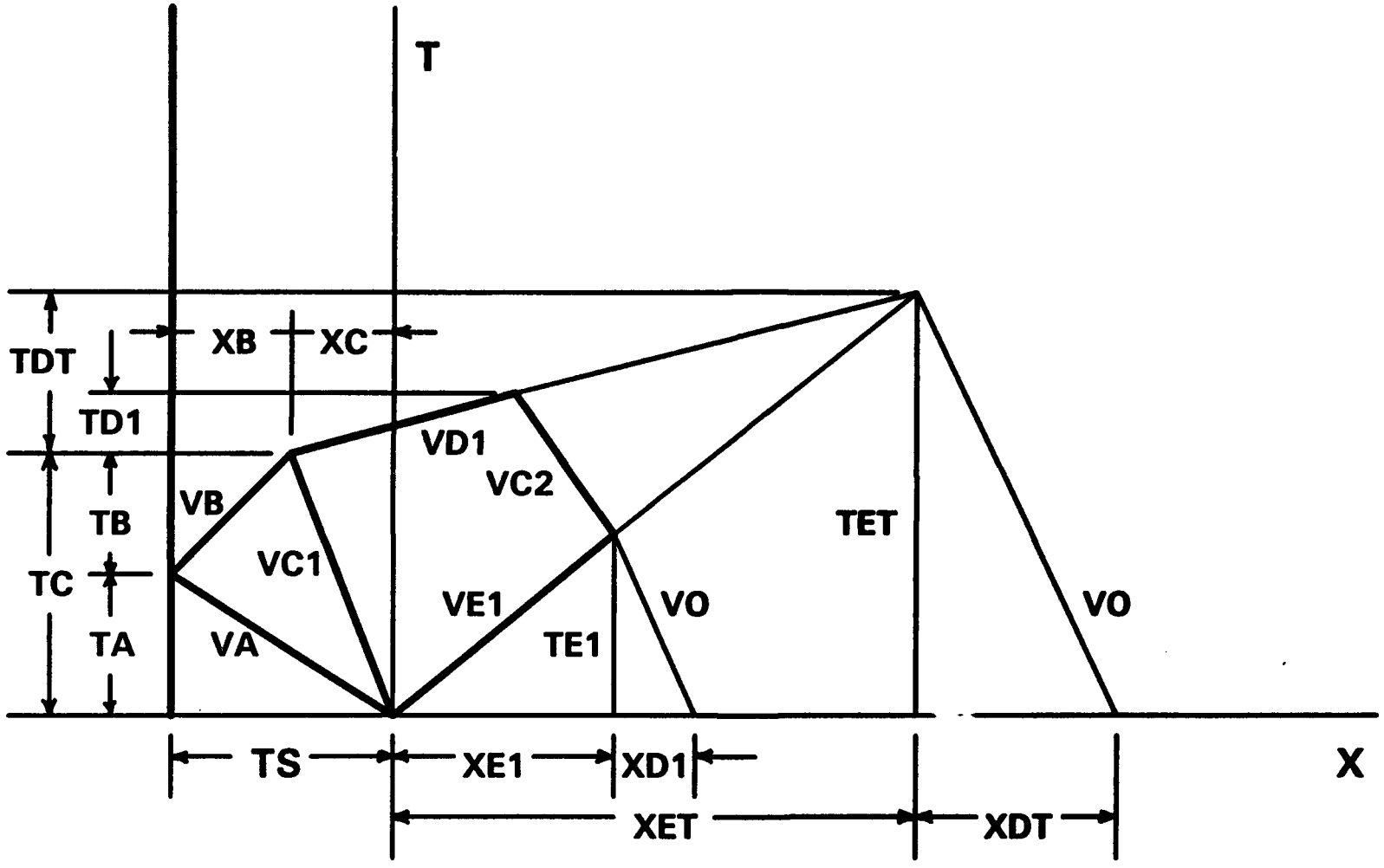

Figure 14. Movement of Rarefaction Wave R4 and Shock Wave S1 Through the First Projectile Layer

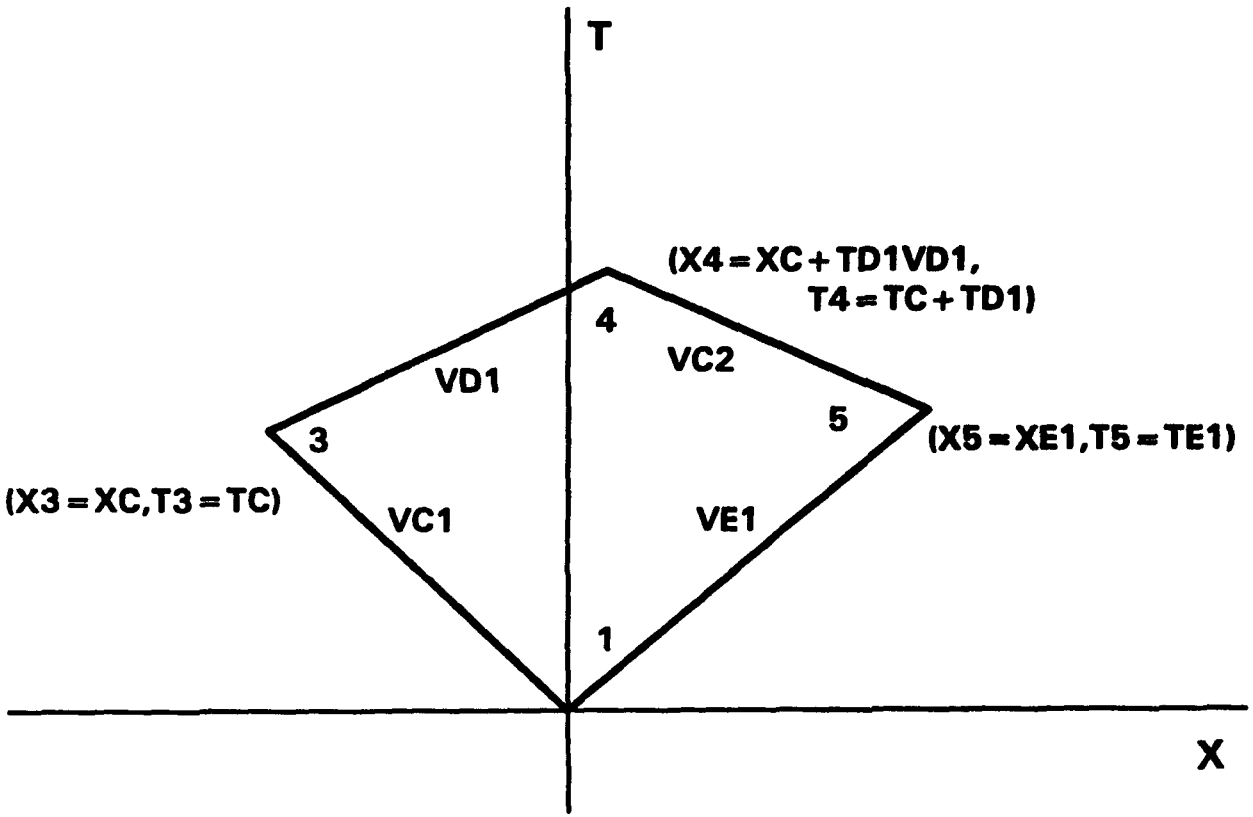

Figure 15. Final First Layer Calculations

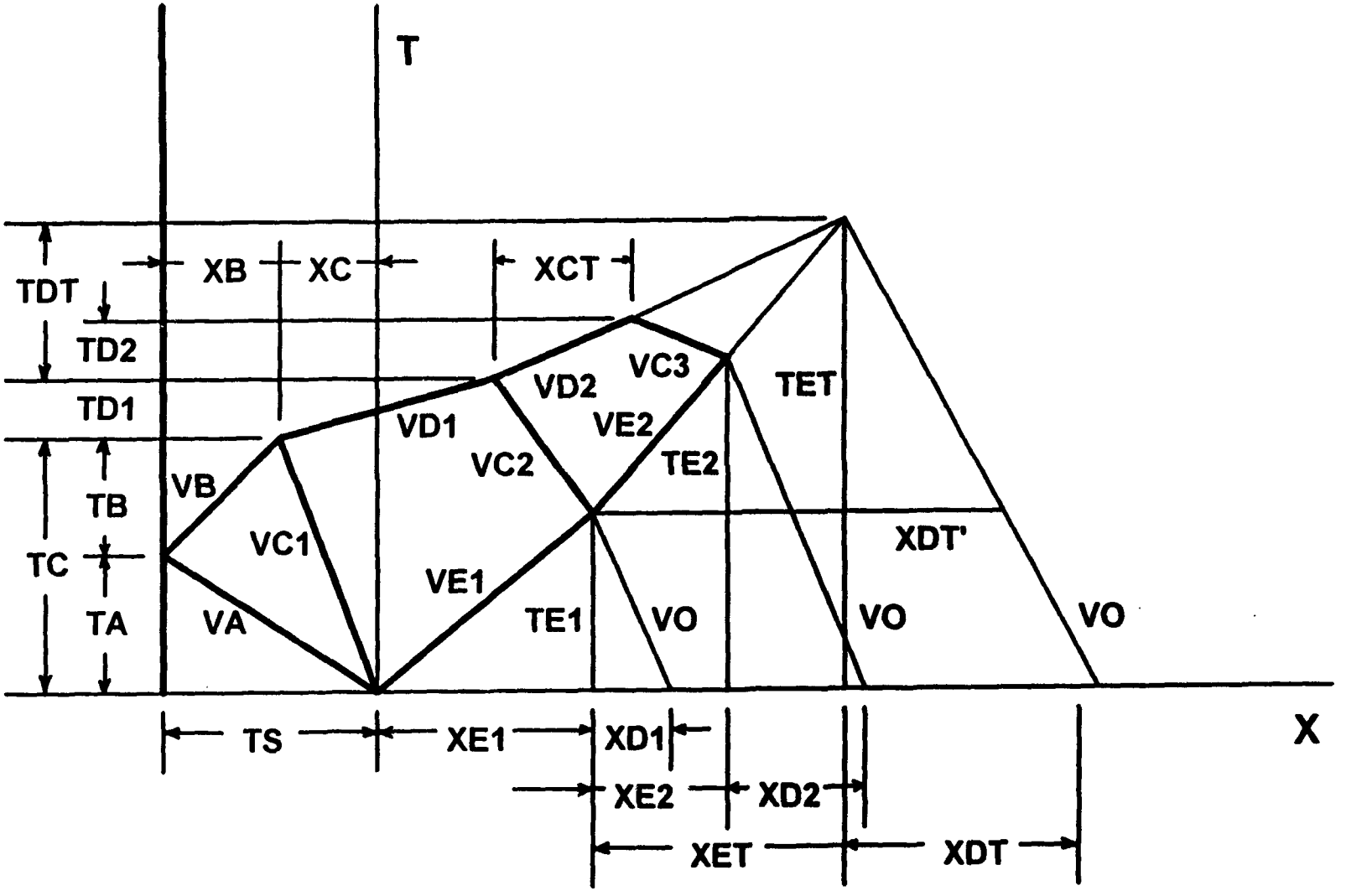

Figure 16. Movement of Rarefaction Wave R4 and Shock Wave S1 Through the Second Projectile Layer

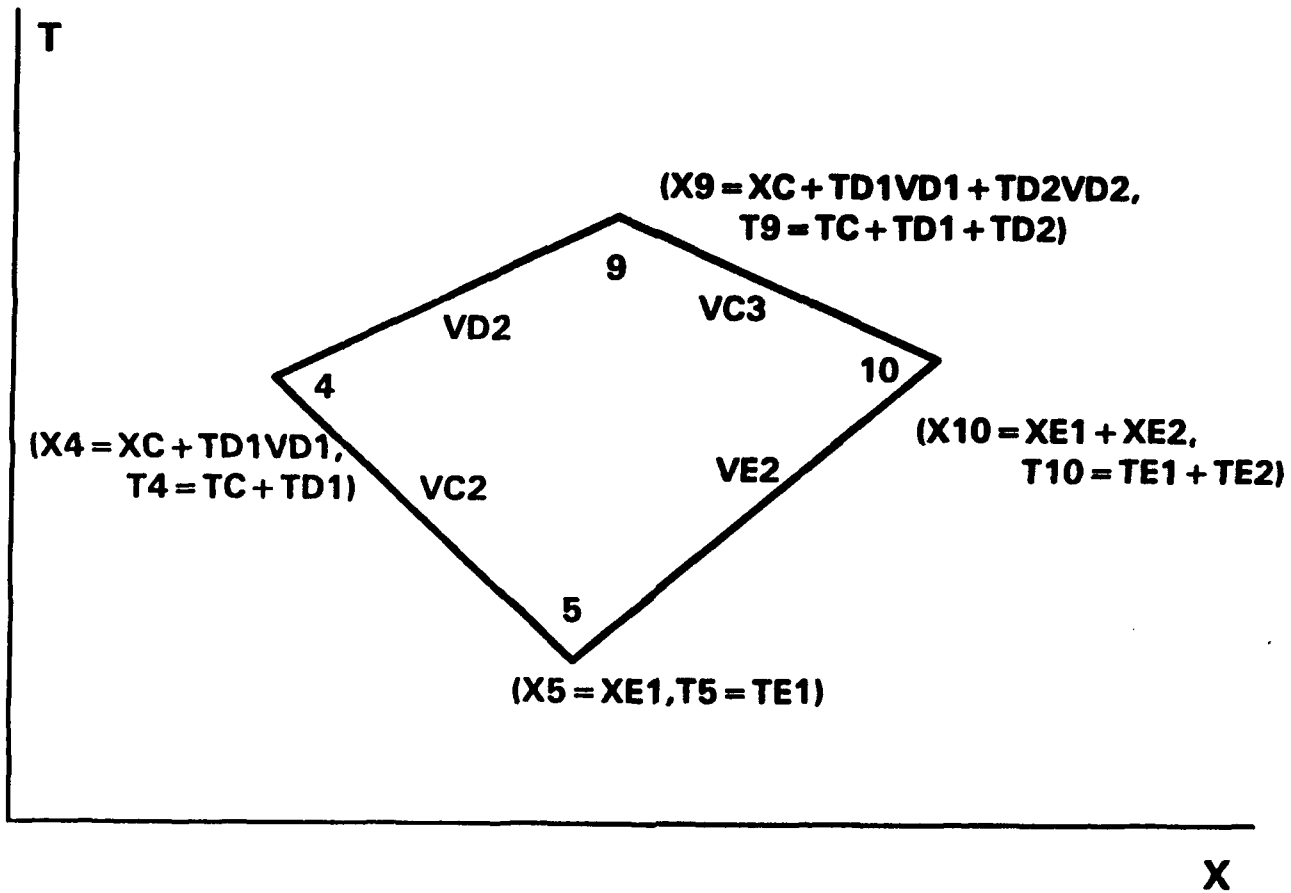

Figure 17. Final Second Layer Calculations

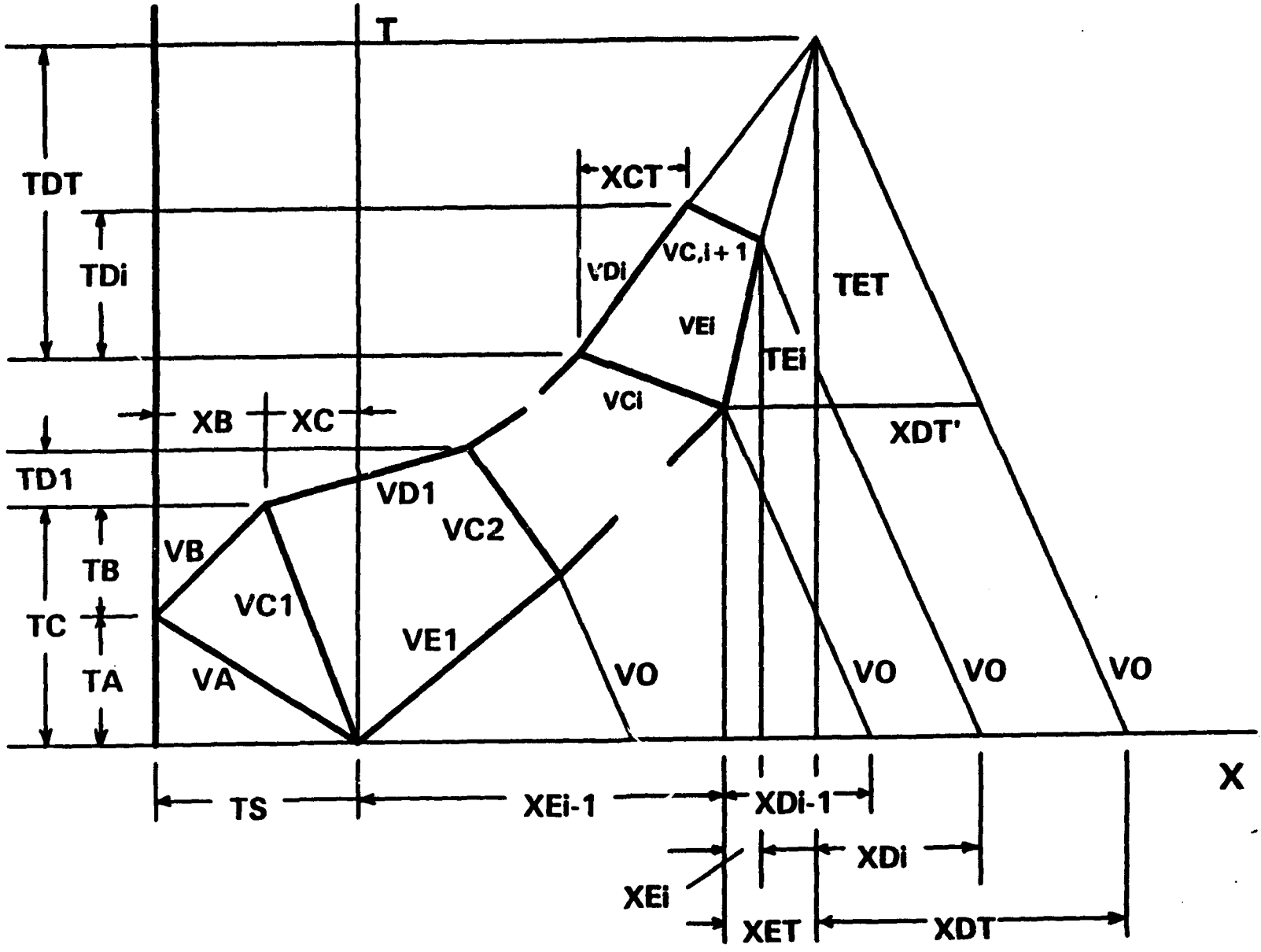

Figure 18. Movement of Rarefaction Wave R4 and Shock Wave S1 Through the i-th Projectile Layer

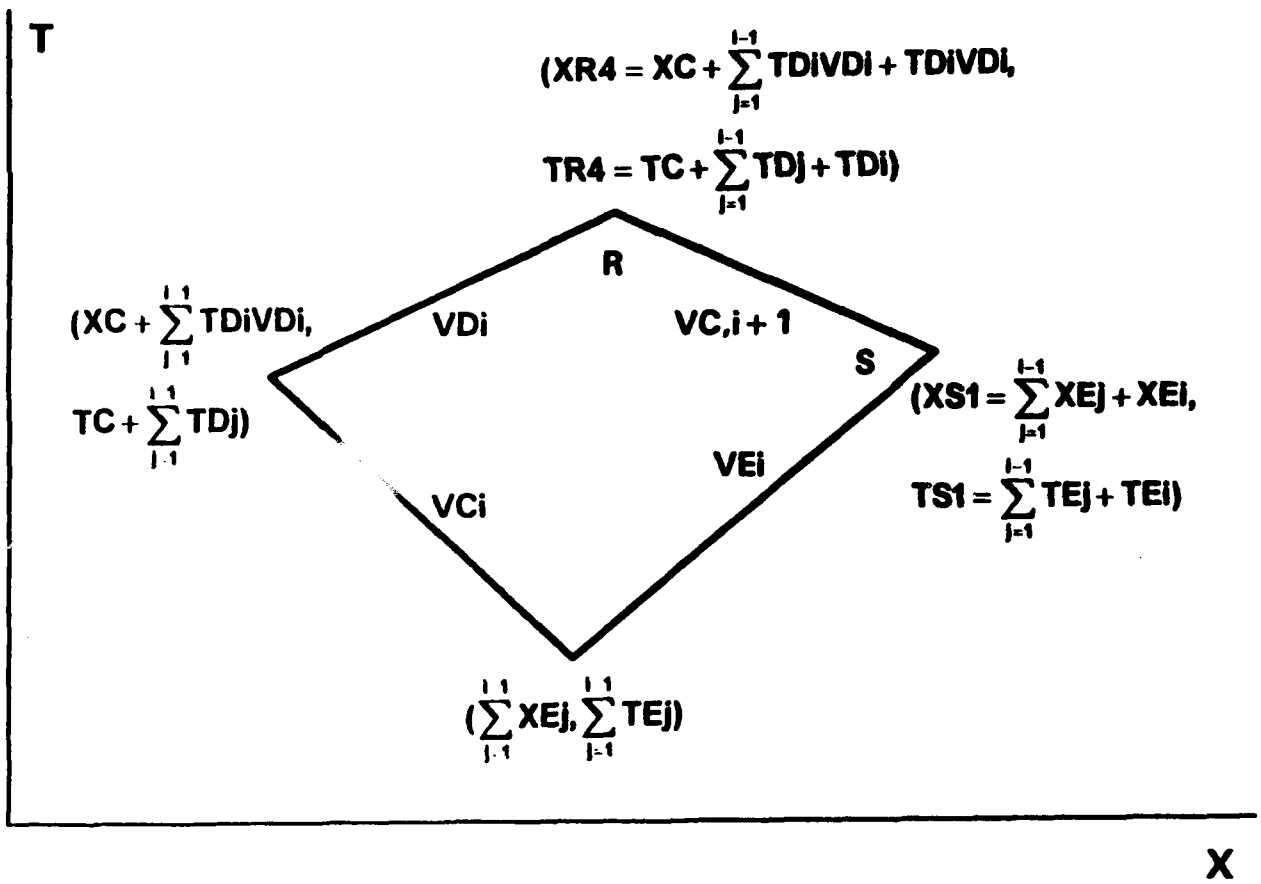

Figure 19. Final i-th Layer Calculations

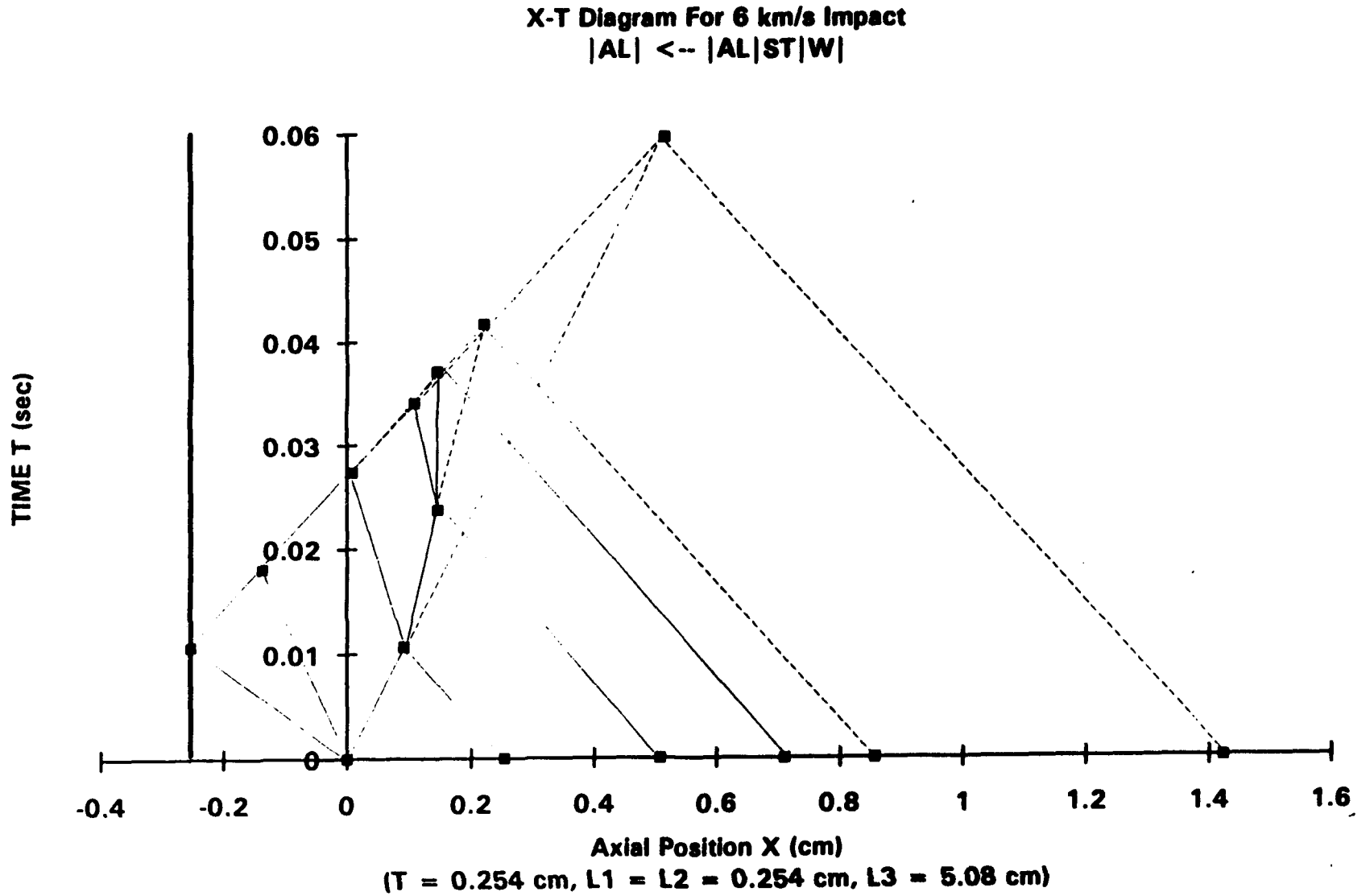

Figure 20. Movement of Rarefaction Wave R4 and Shock Wave S1 -- Specific Example

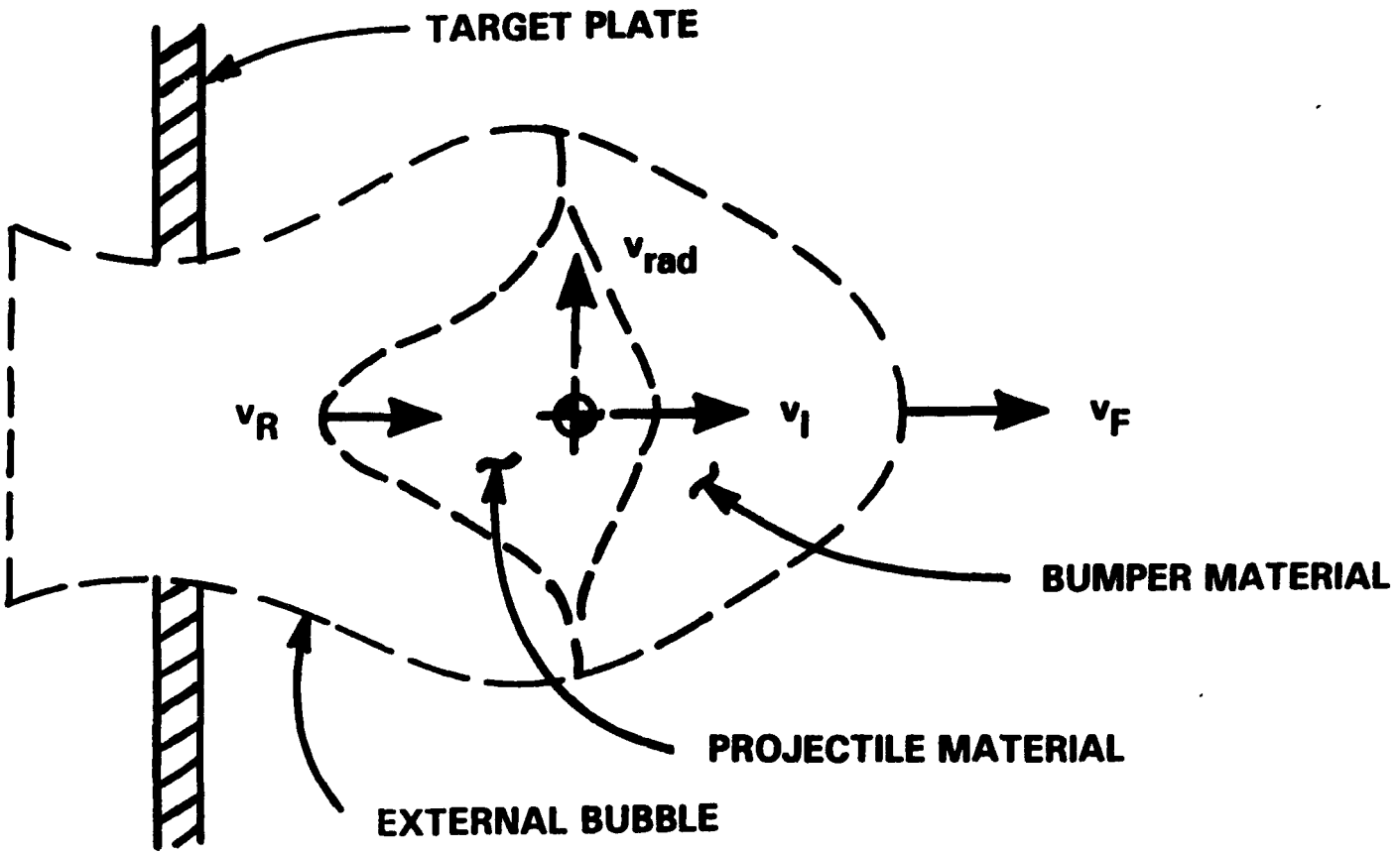

Figure 21. Debris Cloud Velocities

5.0 DEBRIS CLOUD CHARACTERIZATION SCHEME VERIFICATION

5.1 Introductory Comments

A FORTRAN program called DEBRIS3 was written to implement the various procedures described in Sections 3 and 4. The source code is given in Appendix A, with input and output files in Appendix B and C, respectively. DEBRIS3 is an interactive program that prompts the user for the following information: 1) number of projectile layers; 2) projectile material; 3) target material; 4) impact velocity; 5) target thickness; 6) projectile diameter; 7) lengths of projectile layers; 8) Tillotson EOS option; and, 9) hole diameter option. DEBRIS3 also requires the input file INDATA, which is a material library. INDATA also contains the choice of the dE=-PdV approximation, the Tillotson EOS parameters α and β, and the Tillotson EOS parameter ε which tells the program when to stop a release process in which the isentrope is asymptotic to the V-axis. The units for the data in the file INDATA are presented at the end of the sample file in Appendix B.

DEBRIS3 generates the output file IMPOUT, which contains a detailed summary of the following information: 1) projectile and target geometric and material properties; 2) impact conditions; 3) projectile and target material EOS parameters; 4) projectile and target material end-state calculation results, including the waste heat generated, the resulting temperature increase, the percent of solid, liquid, and vaporous material, and the masses of the solid, liquid, and vaporous components; and, 5) debris cloud velocities v_f,v_i, and v_r, and v_{exp}, as applicable. A sample of the output file IMPOUT generated by DEBRIS3 is given in Appendix C. A word of caution: while the Tillotson EOS is relatively straightforward to implement, its use requires a fair amount of familiarity with its peculiarities.

5.2 Single-Material Projectiles

5.2.1 Comparison with Experimental Results and 1-D Hydrocode Predictions

Debris cloud velocity values were calculated using DEBRIS3 and compared against experimental results and one-dimensional hydrocode predictions obtained from a previous study of debris cloud formation and growth using thin copper disks (L/D=0.3) impacting thin aluminum plates [33]. As can be seen in Table 5, the predictions of DEBRIS3 for v_ξ, v_i, and v_r were in excellent agreement with those of the 1-D hydrocode and the experimental results.

Table 5. Comparison of DEBRIS3 with Empirical Results and 1-D Hydrocode Predictions

			v_ξ/v_o			v_i/v_o			v_r/v_o			v_{exp}/v_o	
T (mm)	m_p (gms)	v_o (km/s)	(1)	(2)	(3)	(1)	(2)	(3)	(1)	(2)	(3)	(1)	(3)
Effect of Target Thickness													
1.0	1.0	6.39	1.44	1.41	1.40	0.91	0.89	0.89	0.36	0.34	0.34	0.24	0.27
1.5	1.0	6.36	1.44	1.41	1.40	0.88	0.83	0.84	0.36	0.34	0.34	0.24	0.32
2.0	1.0	6.38	1.42	1.41	1.40	0.83	0.79	0.79	0.35	0.34	0.33	0.27	0.36
2.5	1.0	6.53	1.46	1.41	1.40	0.79	0.76	0.75	0.35	0.34	0.33	0.27	0.38
Effect of Impact Velocity													
1.5	1.0	3.45	1.37	1.39	1.39	0.86	0.84	0.84	0.43	0.36	0.36	0.23	0.33
1.5	1.0	4.85	1.43	1.40	1.39	0.87	0.84	0.84	0.39	0.35	0.35	0.23	0.33
1.5	1.0	6.36	1.44	1.41	1.40	0.88	0.83	0.84	0.36	0.34	0.34	0.24	0.32
Effect of Projectile Mass													
2.0	1.0	6.38	1.41	1.41	1.40	0.83	0.79	0.79	0.35	0.34	0.34	0.27	0.36
2.9	3.0	5.66	1.44	1.40	1.40	0.82	0.80	0.79	---	0.34	0.34	0.23	0.36
4.4	10.0	5.12	1.40	1.40	1.39	0.83	0.80	0.79	0.36	0.35	0.35	0.22	0.37

(1) Experimental Results [33] (2) 1-D Hydrocode Predictions [33] (3) DEBRIS3 Predictions

Over all the cases considered, the average difference between the predictions of DEBRIS3 for v_ξ, v_i, and v_r and the corresponding experimental results was approximately 4% with a standard deviation of approximately 3%. However, the predictions of DEBRIS3 for v_{exp} exceeded the experimental results by an average of approximately 40% with a standard deviation of approximately 15%. This discrepancy may have been due to the fact that the expansion velocity measured in [33] was that of the heavier copper component of the debris cloud while the expansion velocity calculated by DEBRIS3 was based on both debris cloud materials.

5.2.2 Comparison with CTH and Lethality Assessment Scheme Predictions

Figure 22 presents a comparison of the predictions of DEBRIS3, the hydrocode CTH, and the semi-empirical code FATEPEN2 for debris cloud leading edge velocity v_f for steel cylinders (L/D=1) normally impacting thin aluminum target plates (T/D=0.125). As is evident in Figure 22, the predictions of DEBRIS3 compare favorably with those of FATEPEN2 in the velocity regime for which FATEPEN2 was designed to be used (i.e. less than approximately 5 to 6 km/sec). A quick calculation reveals that the difference between the DEBRIS3 predictions of leading edge velocity and those of FATEPEN2 was approximately 26% of the DEBRIS3 values with a standard deviation of approximately 4% for the impact velocities considered. One reason for this difference could be the fact that the mass of the impacting projectile considered (approximately 1555 grains ≅ 100 gms) exceeded the maximum value of projectile masses used to develop the FATEPEN2 equations.

The CTH values plotted in Figure 22 are average values of the velocities of three Lagrangian station points along the impact centerline within the aluminum target plate. These average values differed from the corresponding minimum and maximum values by approximately 0.5 km/sec at an impact speed of 2 km/sec and 3.0 km/sec at an impact speed of 14 km/sec. Inspection of Figure 22 also reveals that there is excellent agreement between the predictions of DEBRIS3 and CTH for debris cloud leading edge velocity. The average difference between the DEBRIS3 and CTH values was approximately 4% of the DEBRIS3 values with a standard deviation of approximately 3%.

Figure 23 presents a comparison of the predictions of DEBRIS3, CTH, FATEPEN2, PEN4, and KAPPII for debris cloud half-angle for steel cylinders (L/D=1.0) normally impacting thin aluminum target plates (T/D=0.125). In Figure 23, the average difference between the predictions of KAPP-II and DEBRIS3 was approximately 18% of the DEBRIS3 value with a standard deviation of approximately 10%; the average difference between PEN4 and DEBRIS3 was approximately 6% with a standard deviation of nearly 7%. Based on

these results, it may be argued that the predictions of DEBRIS3 agree fairly well with those of KAPP-II and PEN4. However, comparing the differences between DEBRIS3 and FATEPEN2 was somewhat more difficult because FATEPEN2 distinguishes between target debris spread and projectile debris spread while DEBRIS3 does not. In FATEPEN2, the target debris half-angle is fixed at 25^{o} while the projectile debris half-angle is based on material properties, impact conditions, etc.

It is interesting to note that unlike the smooth curve predictions of KAPP-II, FATEPEN2, and PEN4, the curve representing the growth of the debris cloud spread generated by DEBRIS3 contains numerous kinks. In particular, the impact velocities corresponding to the vertical lines in Figure 23 also correspond to impact velocities at which significant changes occur in the way the initial kinetic energy of the projectile is distributed to various competing mechanical and thermal processes during the impact event. These features of the curve predicted by DEBRIS3 are discussed in the following paragraph.

For the impact considered in Figure 23, between 2 and 5 km/sec, increasing the impact velocity resulted in a steady increase in debris cloud spread. However, at 5 km/sec, the target material began to melt. As a result, some of the additional kinetic energy of the initial impact provided as impact velocity increased beyond 5 km/sec was used up by the target material state change and was not available for debris cloud expansion. Thus, the rate of debris cloud expansion slowed, and the slope of the curve decreased as impact velocity increased beyond 5 km/sec. Between 8 and 9 km/sec, the projectile material began to melt and the target material began to vaporize. This further decreased the rate of debris cloud expansion. However, once the projectile was completely melted, the rate of debris cloud expansion increased. Near 12 km/sec, the projectile material began to experience vaporization. The rate of debris cloud expansion slowed down only slightly because by now the debris cloud consisted of a significant amount of hot vaporous material. By 15 km/sec, the debris cloud was nearly all vapor causing its rate of expansion to increase dramatically.

5.3 Multi-Material Projectiles

5.3.1 Introductory Comments

The validity of the multi-material modeling capability of DEBRIS3 was assessed by comparing the predictions of DEBRIS3 against experimental and numerical data. The experimental data and the results of one series of hydrocode simulations were obtained from a study that analyzed the effectiveness of layered projectiles against re-entry vehicle-type targets. The results of a second series of hydrocode runs were obtained using the CTH hydrocode specifically for the present investigation. The results of this validation exercise are presented in the next three sections.

5.3.2 Comparison with Experimental Results

Three high speed impact tests were performed at 4 km/sec using three different equal-weight projectiles [36]. The first was a solid 7.5 gm TA10W (i.e. a tantalum alloy with 10% tungsten) sphere, while the second and third projectiles were 7.5 gm layered spheres with a solid TA10W core surrounded by a steel shell. The outer shell of the second projectile was 1018 steel (i.e. mild strength steel) while that of the third projectile was 4340 steel (i.e. a high strength steel).

In simulating these three impact tests with DEBRIS3, the layered spheres were modeled as cylindrical projectiles with three layers. The middle layer corresponded to the spherical core while the first and third layers represented the outer shell material. The thicknesses of the first and third layer were set equal to the outer shell thickness. The thickness of the inner layer and the diameter of the cylindrical projectile were calculated by setting the inner layer thickness equal to the cylindrical projectile diameter and then solving for the diameter by equating the mass of the cylindrical projectile to the mass of the original layered sphere.

In addition to adapting the geometry of the original projectiles used in the test series to a projectile geometry that was compatible with DEBRIS3, some compromises were also made regarding the projectile and target materials. In the original test series, the target was a 2-D flat plate representation of a half-scale re-entry vehicle, i.e. a layer of silica phenolic bonded to a thin layer of aluminum. Since the current version of DEBRIS3 does not allow for multi-material targets, the targets used in the DEBRIS3 impact simulations did not have the outer layer of silica phenolic. In addition, while a witness block was placed behind the initial multi-layer target plate in the experimental tests to record the damage of the perforating projectile and target debris, DEBRIS3 was not developed to have a predictive capability for damage to subsequent witness blocks or plates. Finally, whereas one of the original projectile materials was a tantalum alloy with 10% tungsten, the corresponding material in the DEBRIS3 impact simulations was pure tantalum.

As expected, the simplifications described in the previous two paragraphs precluded any direct comparison of the predictions of DEBRIS3 and the experimental results. However, it was possible to make qualitative comparisons of the DEBRIS3 predictions and the actual test results because the simplifications maintained some similarity between the original test materials and configurations and the materials and geometries of the DEBRIS3 impact simulations. These qualitative comparisons became possible after the DEBRIS3 predictions were analyzed to infer the relative severity of the damage levels that could have been expected on subsequent witness plates had they been placed behind the initial target plate.

First, DEBRIS3 predicted that a significant portion of the target material would be melted when impacted by the solid tantalum sphere. Alternatively, when impacted by the layered projectiles, DEBRIS3 predicted that the target material would be shocked and released but would return to a solid state of matter. This indicates that the target material would probably be fragmented but not melted. Second, DEBRIS3 predicted that the kinetic energy of the remaining unshocked projectile material would be greatest for the layered

projectile with a tantalum core and a high-strength steel shell and would be least for the solid tantalum projectile. Taken together, these two features indicate that the cylindrical projectiles simulating the layered sphere projectiles would probably inflict more severe damage on a witness plate behind the target than would the cylindrical projectile simulating the solid TA10W projectile. This agrees with the actual test results, which state that among the three impact tests, the crater depth and volume in the witness block behind the target impacted by the projectile with a TA10W core and a 4340 steel shell were greatest and those in the block behind the target impacted by the solid TA10W projectile were least.

5.3.3 Comparison with Hydrocode Predictions -- First Series

The first series of numerical runs consisted of two sets of three high speed impacts at 11 km/sec using the SOIL hydrocode [36]. The projectiles used were similar in construction to those in the previously discussed experimental tests (i.e. one solid and two layered spheres in each test set). The major distinguishing feature between the two sets of impact simulations in this series is the mass of the projectiles: 45 gm projectiles were considered in the first set, while 5 gm projectiles were used in the second set. In both sets of simulations, the solid sphere was made out of tungsten as was the core in the layered spheres; the shells of the layered spheres were made out of different strength steels. In modeling the SOIL impact simulations with DEBRIS3, simplifications in the projectile and target geometries were made similar to those in the previous section. As a result, the following comparisons are again only qualitative in nature.

As in the DEBRIS3 simulations of the experimental tests, the DEBRIS3 simulations of the SOIL runs indicated that the solid projectiles would melt some of the target plate material whereas the layered projectiles would not. In addition, the kinetic energies of the unshocked projectile materials from the layered projectiles greatly exceeded those of the unshocked projectile materials from the solid projectiles. These two features again indicate that the

layered projectiles would inflict more severe damage on a witness plate behind the target than would an equal-weight solid projectile.

Interestingly enough, while the general trends observed in the DEBRIS3 impact simulations agreed with the hypothesis that motivated the layered projectile investigation, they disagree with the actual numerical results obtained as part of that investigation. The corresponding SOIL runs predicted that the witness block damage due to the impacts of the solid projectiles would be approximately the same as the damage caused by the layered projectiles. Apparently, either the impact and/or geometric parameters used in the SOIL runs masked subtle differences in damage levels resulting from the solid and layered projectile impacts and prevented them from being discernible, or the DEBRIS3 modeling of the projectile and target geometries over-emphasized some impact phenomenology that produced some differences in response that would otherwise have been negligible.

In any event, it is apparent that additional testing of multi-material projectile that are compatible with the modeling capabilities of DEBRIS3 are required to fully validate the predictive capabilities of DEBRIS3. As an intermediate step, several CTH runs were performed using projectile and target geometries that were ideally suited for and matched to the capabilities of DEBRIS3. The results of these runs and how they compared with the predictions of DEBRIS3 are discussed in the next section.

5.3.4 Comparison with Hydrocode Predictions -- Second Series

In the second series of hydrocode runs, four high speed impact simulations were performed at 10 km/sec using CTH with multi-material cylindrical projectiles. The projectile diameter and target plate thickness were kept constant at 2.54 cm and 0.3175 cm, respectively. In the first two runs, the layers were relatively "thin" (i.e. L/D=0.1 each), while in the second two runs, the projectile layers were relatively "thick" (i.e. L/D=1.0 each). In the first and third runs, an aluminum target plate was impacted by a projectile with an aluminum leading layer, a 4340 steel middle layer, and a tungsten rear layer. In the second and fourth

runs, the order of the projectile materials was reversed. A detailed description of the impact and geometric parameters are given in Table 6; the results of the DEBRIS3 impact simulations and the corresponding CTH results are given in Table 7. In Tables 6 and 7, a '1' in the first column refers to the leading layer of the projectile while a '3' refers to the rear-most projectile layer.

Table 6. Geometric and Impact Parameters for DEBRIS3 and CTH Comparison Runs

	Run No.			
	(1)	(2)	(3)	(4)
V (km/sec)	10.0	10.0	10.0	10.0
D (cm)	2.54	2 54	2.54	2.54
T (cm)	3.175	3.175	3.175	3.175
Target Material	Aluminum	Aluminum	Aluminum	Aluminum
Layer 1 Material	Aluminum	Tungsten	Aluminum	Tungsten
Layer 2 Material	4340 Steel	4340 Steel	4340 Steel	4340 Steel
Layer 3 Material	Tungsten	Aluminum	Tungsten	Aluminum
L_1 (cm)	0.254	0.254	2.54	2.54
L_2 (cm)	0.254	0.254	2.54	2.54
L_3 (cm)	0.254	0.254	2.54	2.54
L/D	0.3	0.3	3.0	3.0
Proj. Mass (gms)	38.24	38.24	382.40	382.40

The predictions of CTH and DEBRIS3 regarding the state of the target and projectile layer materials were compared quantitatively and qualitatively. To facilitate quantitative comparisons of material end-states, average densities were computed for each material layer using the DEBRIS3 and CTH results. The DEBRIS3 values were obtained by multiplying the mass of shocked and released material by its final density, adding to it the product of the density of the unshocked material and its mass, and then dividing by the total mass of the material layer under consideration. The CTH values are simply average values through the particular layer thickness and were obtained from density history plots along the centerline.

A feature common to all four impact simulations and evident in Table 7 is that the average target material densities predicted by DEBRIS3 were significantly higher than those predicted by CTH. However, the reason for this is that they include the solid component of target material not considered to be shocked and released by the impact (i.e. the remainder of the ejected target material not swept out by the projectile). The contributions of the solid material component to the average density of the target material are significant considering that they constitute approximately 90% of the target material in the debris cloud created by the impact. If the target hole diameter had been set equal to the projectile diameter (which is not an unreasonable assumption for the impact velocity and geometries considered), then there would not have been any unshocked target material and it is reasonable to presume that the average densities of the target material would have been much closer to the CTH values.

Table 7. Comparison of DEBRIS3 and CTH Impact Response Predictions

	Run No.							
	(1)		(2)		(3)		(4)	
	DEBRIS3	CTH	DEBRIS3	CTH	DEBRIS3	CTH	DEBRIS3	CTH
V_f (km/sec)	10.65	14.27	17.36	14.20	10.65	11.08	16.26	14.28
θ (deg)	36	32	34	27	48	37	21	22
ρ_{targ} (gm/cm^3)	2.56	0.21	2.36	~0.0	2.63	1.33	2.52	~0.0
ρ_1 (gm/cm^3)	2.02	~0.0	18.52	0.67	2.22	2.25	18.98	9.20
ρ_2 (gm/cm^3)	7.04	0.17	7.25	5.50	7.83	8.53	7.83	6.94
ρ_3 (gm/cm^3)	18.42	0.97	2.48	1.41	19.17	17.19	2.71	3.39

The differences between the DEBRIS3 predictions of debris cloud leading edge velocity and the corresponding CTH values in Runs No. 1-4 are 25.4%, 22.3%, 3.9%, and 13.9%, respectively, of the CTH values. The somewhat large differences in Runs No. 1 & 2 may be explained by the following considerations. In the characterization scheme employed

by DEBRIS3, the target shock loading and release analysis used to obtain the debris cloud leading edge velocity is truly one-dimensional. That is, it is performed using only the leading projectile layer and the target material; anything behind the first projectile material layer is ignored. In the case of thick projectile layers, the use of one-dimensional equations is appropriate because the rear layers of the projectile are sufficiently far from the impact site so as not to affect the magnitude of the velocity of the target rear free surface. However, in the case of the thin projectile layers, the second and third projectile layers are close enough to the projectile-target interface to influence the shock and release process in the target material and the resulting velocity of the target rear free surface. CTH, being a 3-D hydrocode, is apparently sensitive to these effects while DEBRIS3, being a first principles code, is not. As a result, the CTH and the DEBRIS3 predictions differ somewhat more in Runs No. 1 and 2 and are more in agreement in Runs No. 3 and 4.

The differences between the DEBRIS3 predictions of debris cloud leading edge velocity and the corresponding CTH values in Runs No. 1-4 are 11%, 26%, 23%, and 5%, respectively, of the DEBRIS3 values. The CTH predictions of debris cloud half-angle were obtained indirectly from debris cloud output plots. In some cases, the precise angles were difficult to determine from the CTH plots because not all of the debris cloud material was retained by CTH and subsequently plotted. If there is a very small fraction of a material in a cell in which more than one material is present, then it is possible for that small fraction of material to generate negative internal energies in that cell. CTH allows the user to set a flag that forces CTH to drop the cell from subsequent calculations in such cases. If this is not done, then in such cases the time-step becomes so small that the impact simulation will be forced to terminate prematurely. Apparently, in Runs No. 2 and 3, CTH dropped a fair amount of cells as the calculations proceeded which in turn produced rather sparse debris clouds. While the agreement between the DEBRIS3 predictions and the CTH values was in general fairly reasonable, this may explain in part why in Runs No. 2 and 3 the DEBRIS3

predictions of the debris cloud half-angle values were significantly higher than the CTH values.

For projectiles with thin layers, although Table 7 indicates that there were significant differences between the material densities predicted by DEBRIS3 and those obtained with CTH, closer examination of the DEBRIS3 and CTH predictions of material state did in fact reveal a qualitative agreement in the results. For example, the extremely low material densities for Run No. 1 predicted by CTH indicate that the material from the three projectile layers in both cases are in highly expanded states. However, the density of the rear-most portion of the third material layer in Run No. 1 (approximately the last 33%) was nearly 3.5 times that of the forward portion of that layer, indicating that the rear third of the final projectile layer was significantly more dense than the rest of the projectile material. Interestingly enough, for Run No. 1, DEBRIS3 predicted that the first two material layers would be in a liquid state, while the last 25% of the third layer would not be fully shocked. Thus, while the actual density values may have been different (which was not totally unexpected given the relatively simple nature of the physics employed by DEBRIS3), there was some agreement between CTH and DEBRIS3 with regard to the state of the projectile material following the initial impact.

With regard to the target material, CTH predicted that the target material would be in a highly expanded state in Run No. 1 and probably vaporized in Run No. 2; DEBRIS3 predicted that the target material would be completely melted in Run No. 1 while in Run No. 2 it would be partially vaporized as well. Thus, there was again some general agreement between CTH and DEBRIS3 regarding the state of the target material following a hypervelocity impact of a projectile whit thin material layers.

For projectiles with thick material layers, projectile material characterizations predicted by DEBRIS3 were again found to agree in a general sense with the post-impact material states predicted by CTH (Table 7). For example, DEBRIS3 predicted that in both

Run No. 3 and Run No. 4 that the second and third projectile layers would remain unshocked while part of the first layer would be shocked and released. The CTH results for Runs No. 3 & 4 clearly showed the third material layers to be relatively undisturbed and the second material layers to be only slightly deformed. These characteristics are also evident in Table 3 where the density values predicted by CTH for the second and third projectile material layers were near ambient values; the densities predicted by DEBRIS3 for the second and third layers were naturally exactly equal to the respective ambient values due to the assumptions within the DEBRIS3 model.

With regard to the first material layer, DEBRIS3 predicted that in Run No. 3 the entire shocked and released portion would be all liquid, whereas the shocked and released portion in Run No. 4 would be a mixture of liquid and solid material. The CTH results for both cases showed that the density of the leading edge of the first layer was approximately 30% of the ambient value, while the density of the rear portion of the leading layer approached the ambient value of the second layer material, indicating a significantly more compressed state than that of the leading edge.

Some interesting features are also evident in the CTH and DEBRIS3 predictions of the state of the target material. In Run No. 3, the average target material density as predicted by CTH is approximately 12% of ambient. This indicates a significant liquid, if not vaporous, component of the target material in the debris cloud. For Run No. 3, DEBRIS3 predicted that 100% of the shocked and released target material would be liquid and that the density of the shocked and released target material would be approximately 75% of ambient. The near-zero value of the target material density as predicted by CTH in Run No. 4 indicates a material state near complete vaporization for the ejected target material while DEBRIS3 predicted that approximately 24% of the shocked and released target material would be in a vapor state and that 76% would be liquid. The density of the shocked and released target material predicted by DEBRIS3 was 40% of the ambient value indicating a highly expanded material state.

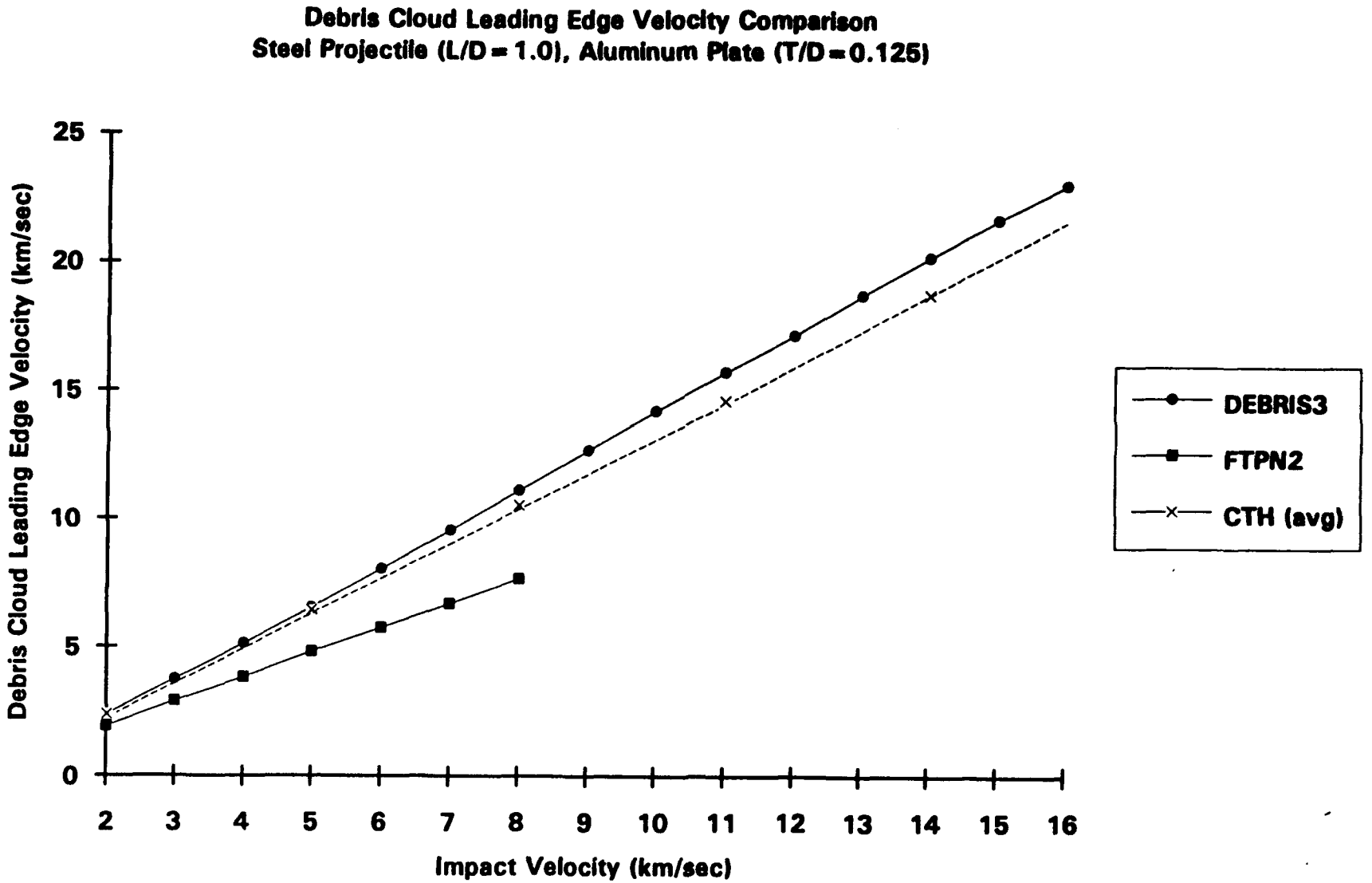

Figure 22. Debris Cloud Leading Edge Velocity Comparisons

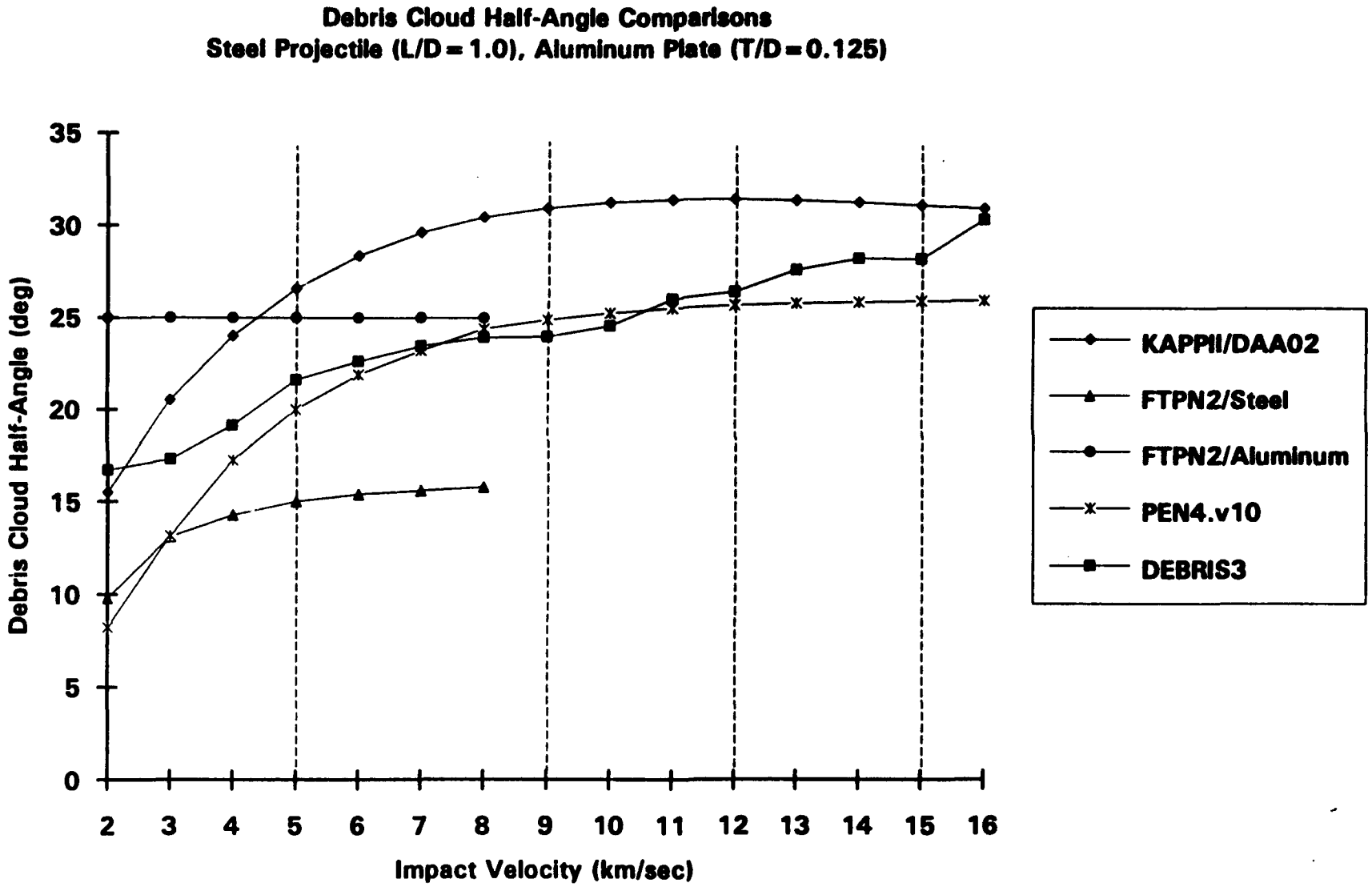

Figure 23. Debris Cloud Half-Angle Comparisons

6.0 ADDITIONAL RESULTS AND DISCUSSION

6.1 End State Calculations

Figures 24-27 compare the results of the release process for aluminum-on-aluminum impacts at three different energy levels using Mie-Gruneisen, Tillotson, Tillotson/SJC, and Tillotson/MPF equations-of-state. Figure 28 shows the differences in final specific volume obtained using the Mie-Gruneisen, Tillotson, and Tillotson/SJC equations-of-state.

In Figure 24, the release process as described by the Mie-Gruneisen EOS and the Tillotson EOS are nearly identical. This is to be expected for relatively low energy impact (i.e. those impacts in which the materials return to a solid matter state after release). Figure 25 shows the dramatic difference between using the Mie-Gruneisen EOS and the Tillotson EOS for very high energy impacts (i.e. those impacts in which the materials vaporize). The Mie-Gruneisen EOS cannot account for the expansion of the gaseous state and terminates the release process at a much lower specific volume than the Tillotson EOS.

Figure 26 highlights one of the difficulties in using the Tillotson EOS in its original formulation. This difficulty occurs under impact conditions that are not violent enough to vaporize the material, yet are strong enough to cause the material to melt and be in an energy state that is near incipient vaporization. Under these conditions, the jump in the release isentrope at $V=V_S$ generated by the original Tillotson EOS and the implementation of the Mixed Phase Formulation both result in a final volume that is artificially high. As stated previously, the final volume was considered to be artificially high because the jump at $V=V_S$ forced the release isentrope to follow a path as if complete vaporization of the material had occurred. Some vaporization will indeed occur if the internal energy at $V=V_S$ is greater than that required to initiate vaporization of the material. However, there is no need for the release isentrope to follow the path of complete vaporization unless the internal energy is greater than that required for complete vaporization.

Implementation of the jump correction given by equation (28) in this impact energy

regime caused the release processes to terminate at specific volume values that were much more reasonable. It is noted that this correction had no effect when the impact energy was relatively low or very high. Figure 27 shows the result of implementing the jump correction given by equation (28) for a 10 km/sec aluminum-on-aluminum impact. In a such a scenario, a fair amount of melting and expansion would be expected to occur. The Tillotson EOS release isentrope shown in Figure 27 after implementing the correction is more reasonable because it terminates at a specific volume that is greater than that predicted by the Mie-Gruneisen EOS which cannot account for greatly expanded states, yet is substantially less than that which would be obtained following the path of complete vaporization

Figure 28 illustrates the differences in the final specific volumes obtained in aluminum-on-aluminum impacts using the Tillotson, Tillotson/SJC, and Tillotson/MPF EOS formulations and contrasts these with the results obtained using the Mie-Gruneisen EOS. For impact velocities below approximately 9 km/sec, the results were, as expected, nearly identical. For impact velocities above approximately 24 km/sec, the final values predicted by the Tillotson EOS and the two alternative formulations of the Tillotson EOS overlap and significantly exceeded those predicted by the Mie-Gruneisen EOS due to the gaseous expansion of the released material at those impact velocities.

The odd behavior in the final values of specific volume due to the jump in the unmodified Tillotson EOS began for aluminum-on-aluminum impacts at an impact velocity of approximately 9 km/sec. However, the Tillotson/SJC formulation produced a smooth transition as the material changes from a solid state (below approximately 6 km/sec) to a liquid state (between approximately 6 and 11 km/sec) to a gaseous state (above approximately 11 km/sec). The specific volumes calculated by the Tillotson/MPF formulation closely followed those of the Mie-Gruneisen EOS until an impact velocity of approximately 18 km/sec beyond which they began to diverge rapidly. Apparently, the Tillotson/SJC formulation predicted a more expanded material end-state than did the Tillotson/MPF

formulation for impact velocities between 10 and 24 km/sec.

6.2 Debris Cloud Material Characterization

Figures 29-32 compare the effects of using the Mie-Gruneisen, Tillotson/SJC, and the Tillotson/MPF formulations, respectively, to calculate the percentages of the three matter states in debris clouds created by aluminum-on-aluminum impacts. While the results presented and discussed apply only to aluminum-on-aluminum impacts, the equations developed herein may be used to estimate the state of the material within a debris cloud created by the high speed impact of virtually any two materials for which the required material properties are available.

As can be seen in Figure 29, the Mie-Gruneisen equation-of-state predicted only a small amount of vaporized material at an impact velocity of 25 km/sec. However, Figures 30 through 32 reveal that the original formulation and both modified versions of the Tillotson equation-of-state predicted that aluminum was completely vaporized at an impact velocity between 20 and 25 km/sec. This difference is due to the fact that the Mie-Gruneisen equation-of-state did not account for the expansion of the material it neared vaporization and completed the release process with the material in a much lower energy state than did either of the two modified versions of the Tillotson equation-of-state.

Comparing Figures 30-32 reveals that the Tillotson, Tillotson/SJC, and the Tillotson/MPF formulations agreed in the percentages of the various states of matter at speeds below approx. 11 km/sec and above approximately 24 km/sec. Within the 11-24 km/sec impact velocity regime, the original formulation of the Tillotson EOS predicted a steady growth in the amount of vaporized material. Within the same impact velocity regime, the Tillotson/MPF formulation predicted vaporization to develop more rapidly than did the Tillotson/SJC formulation which predicted a more gradual transition to vaporized material. This appears to contradict the results shown in Figure 28 in which the Tillotson/MPF formulation initially predicted a more dense debris cloud than did the Tillotson/SJC

formulation. In fact, the question is raised as to how a more expanded material state can have less vapor than a less expanded state, especially since both Tillotson EOS formulations predicted approximately the same radial expansion of the debris cloud material!

The resolution of this apparent dilemma lies in the values of the leading and trailing edge velocities as predicted by the two alternative versions of the Tillotson EOS. In the 12 to 24 km/sec impact velocity regime, the Tillotson/SJC formulation predicted values of v_r and v_f that were smaller and larger, respectively, than the corresponding values predicted by the Tillotson/MPF formulation. Hence, in this impact velocity regime, the Tillotson/SJC formulation predicted the debris cloud to have a larger axial dimension than did the Tillotson/MPF EOS while the radial dimension in both cases was approximately the same. This naturally resulted in larger debris cloud volumes with the Tillotson/SJC formulation than with the Tillotson/MPF formulation, even though the vapor content predicted by the Tillotson/SJC formulation was less than that predicted by the Tillotson/MPF formulation.

6.3 Distribution of Solid, Liquid, and Gaseous Projectile and Target Materials

In Figure 33, the total projectile mass remained constant because the projectile length and diameter were fixed in all of the impact scenarios considered. The solid dark region represents the mass of the projectile that was unshocked and therefore was not subjected to melting and/or vaporization. This quantity increased with impact velocity because the speed of the rarefaction wave in the projectile increased at a faster rate than did the speed of the shock wave in the projectile. As the impact velocity increased, the rarefaction wave caught up with the shock wave within a shorter period of time. This in turn increased the amount of the projectile material that was not subject to melting and/or vaporization. The remaining shaded areas in Figure 33 show the amounts of the shocked and released projectile material in each of the three matter states as the impact velocity increased from 4 to 25 km/sec.

Figure 34 shows that the amount of target material in the debris cloud increased as impact velocity increased due to the growth in target hole size as impact velocity increased.

For the projectile and target geometries considered, all of the target material was shocked and released. Hence, there is no solid dark area, only the three lighter-shaded areas which show the amounts of shocked and released material in each of the three states of matter.

6.4 Debris Cloud Velocities

Figures 35 and 36 compare the differences in calculated debris cloud velocities for thin disk and long rod impacts, respectively. In the event of the disk impact, the quantities plotted were leading edge, trailing edge, center-of-mass, and expansion velocities relative to the initial impact velocity. In the case of the rod impact, the quantities plotted were leading edge, center-of-mass, expansion, and unshocked projectile mass velocities also relative to the initial impact velocity.

In the thin disk impact (Figure 35), the length of the disk was equal to the thickness of the target plate. In this case, all four normalized velocity components remained relatively constant, with minor increases and decreases, respectively, in the normalized leading edge and trailing edge velocities, respectively. This implies that the changes in the various components of the debris cloud velocity field in the event of a straight-on thin disk impact are directly proportional to changes in the initial impact velocity. Taken together, the slight increase in the leading edge velocity and the slight decrease in the trailing edge velocity (both relative to the impact velocity) indicate that the elongation of the debris cloud becomes more and more pronounced as the impact velocity is increased.

In the long rod impact, (Figure 36), the length of the rod was equal to four times the thickness of the target plate. In this case, all four normalized velocity components changed dramatically as the impact velocity was increased. As discussed in Section 5.2.2 for the same target/projectile combination, many of the changes evident in Figure 34 coincided with impact velocities at which changes occurred in the way in which the kinetic energy of the impacting projectile was distributed among the various competing mechanical and thermal processes during the impact event. Closer examination of Figure 36 reveals some additional features of interest. These are discussed in the following paragraph.

First, there is a significant decrease in the normalized velocity of the unshocked projectile material while the normalized leading edge velocity increases significantly as the impact velocity is increases beyond 5 km/sec. Taken together, this implies that the leading edge of the debris cloud, which contains the more molten and vaporous material, becomes increasingly separated from the trailing unshocked projectile material as the impact velocity is increased into the hydrodynamic regime. The accompanying rise in the normalized expansion velocity indicates that this leading non-solid material is also being spread out to a greater and greater extent as the impact velocity increases. Second, the normalized center-of-mass velocity remained relatively constant, with a value approximately equal to that in Figure 35 (i.e. in the case of a thin disk projectile). This was expected since the center-of-mass velocity is based on a conservation of momentum calculation which is relatively insensitive to changes in energy distribution among the competing processes during the impact event.

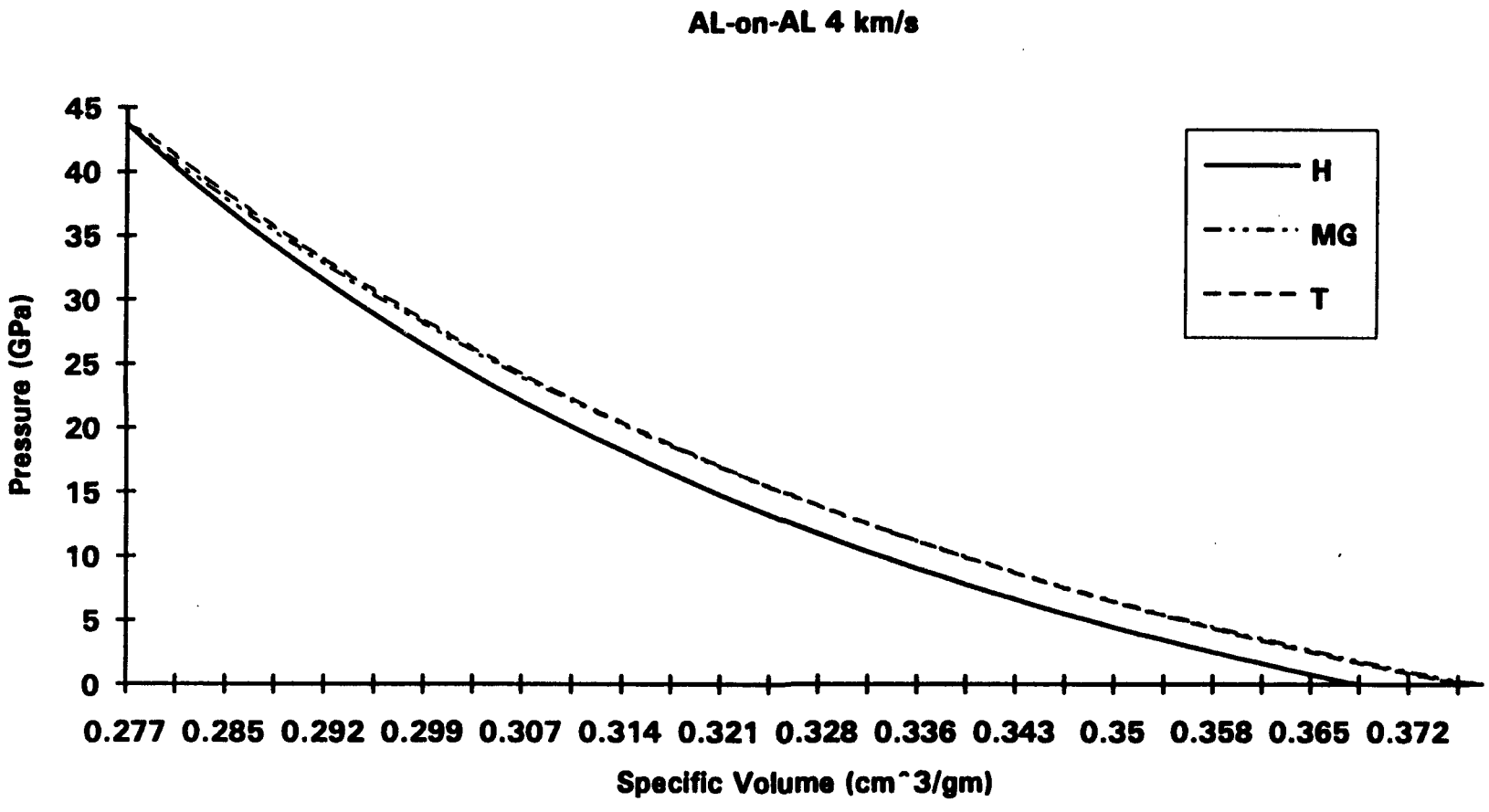

Figure 24. Low Energy Impact Shock Loading and Release Curves (H ... Hugoniot, MG ... Mie-Gruneisen EOS Release Isentrope, T ... Tillotson EOS Release Isentrope

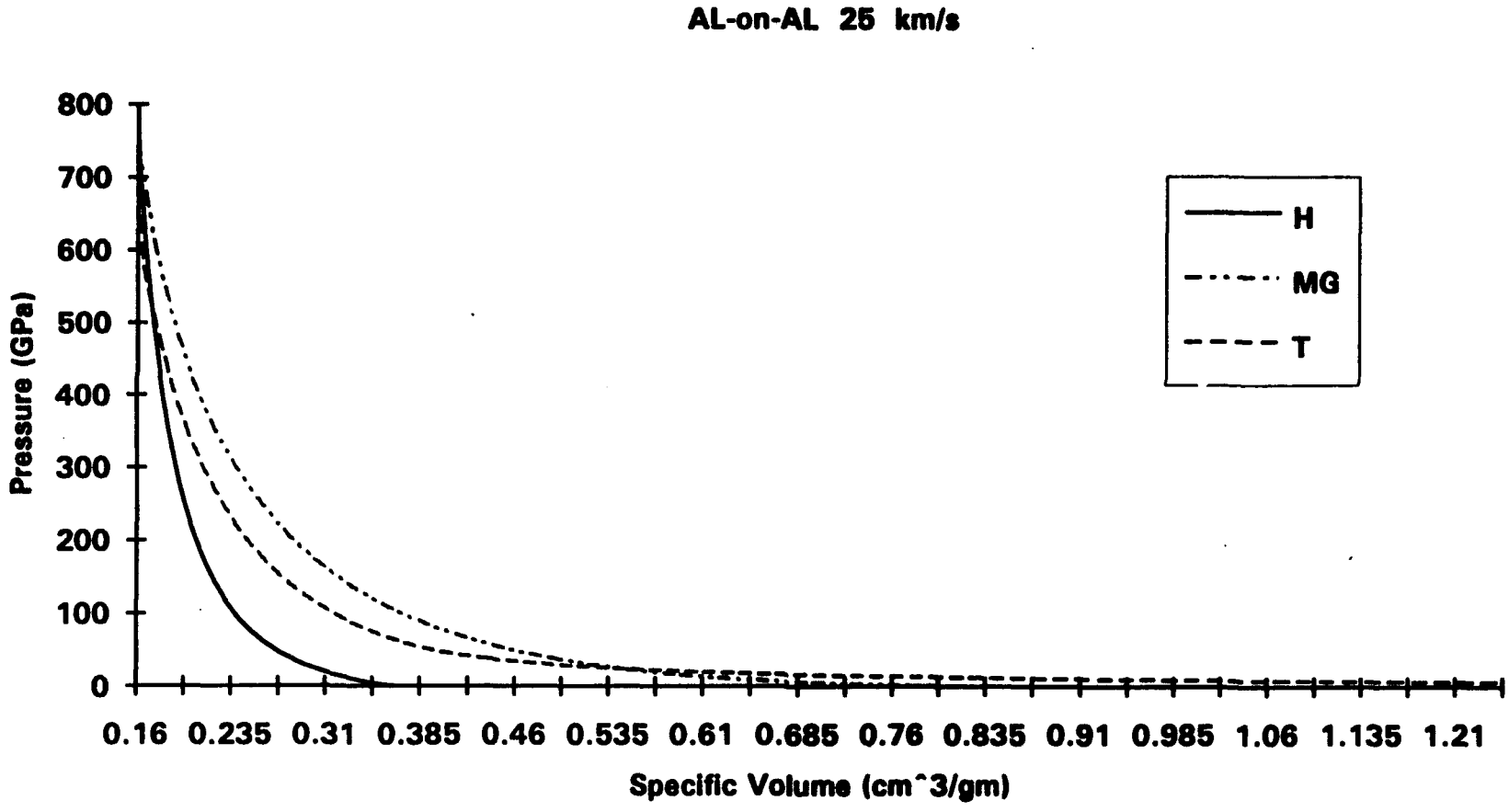

Figure 25. High Energy Impact Shock Loading and Release Curves (H ... Hugoniot, MG ... Mie-Gruneisen EOS Release Isentrope, T ... Tillotson EOS Release Isentrope)

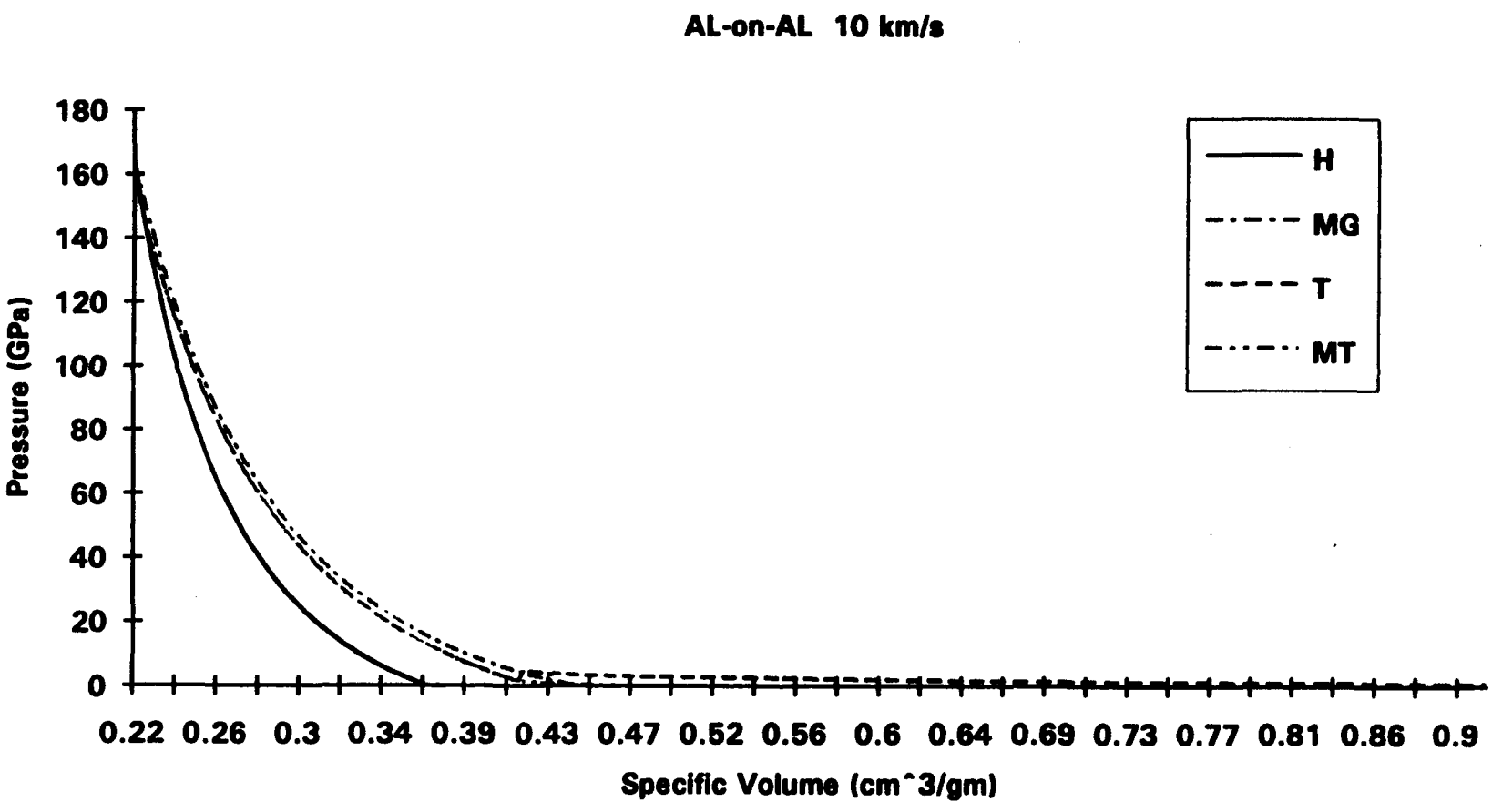

Figure 26. Moderate Energy Impact Shock Loading and Release Curves (H ... Hugoniot, MG ... Mie-Gruneisen EOS Release Isentrope, T ... Tillotson EOS Release Isentrope, MT ... Modified Tillotson EOS Release Isentrope)

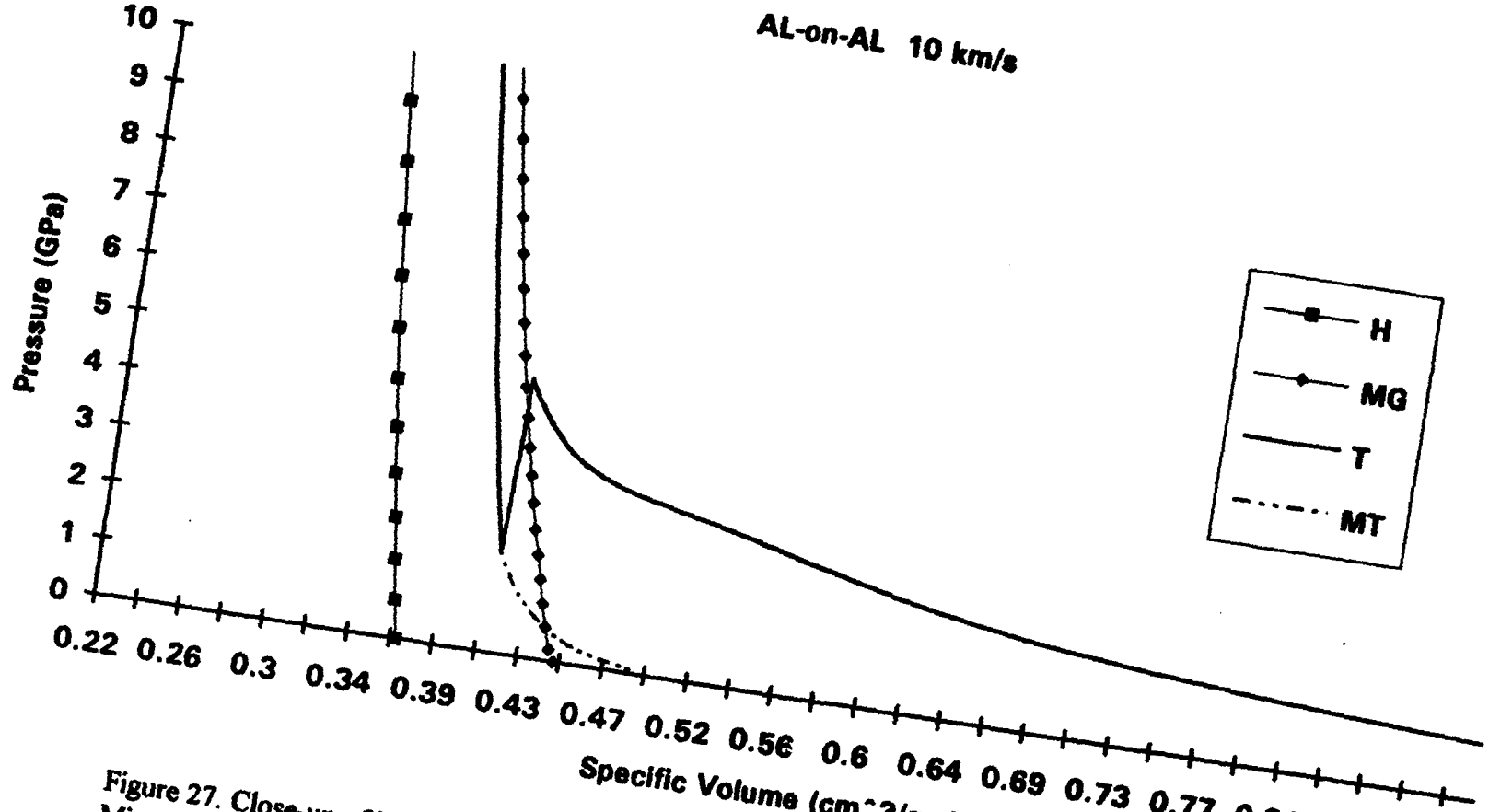

Figure 27. Close-up of Moderate Energy Impact Shock Loading and Release Curves (H ... Hugoniot, MG ... Mie-Gruneisen EOS Release Isentrope, T ... Tillotson EOS Release Isentrope, MT ... Modified Tillotson EOS Release Isentrope)

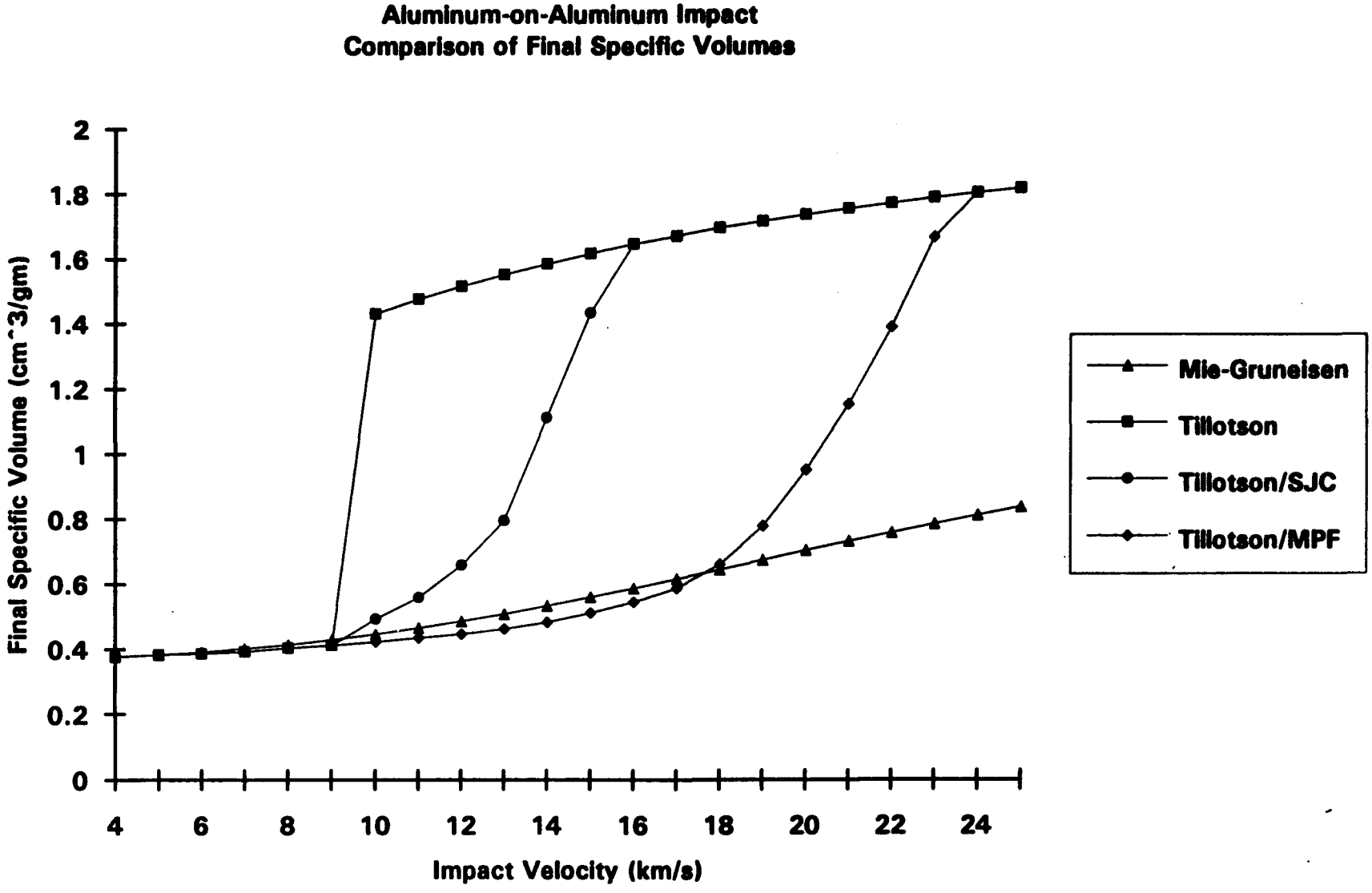

Figure 28. Final Specific Volume vs. Impact Velocity (MG ... Mie-Gruneisen EOS Values, T ... Tillotson EOS Values, MT ... Modified Tillotson EOS Values)

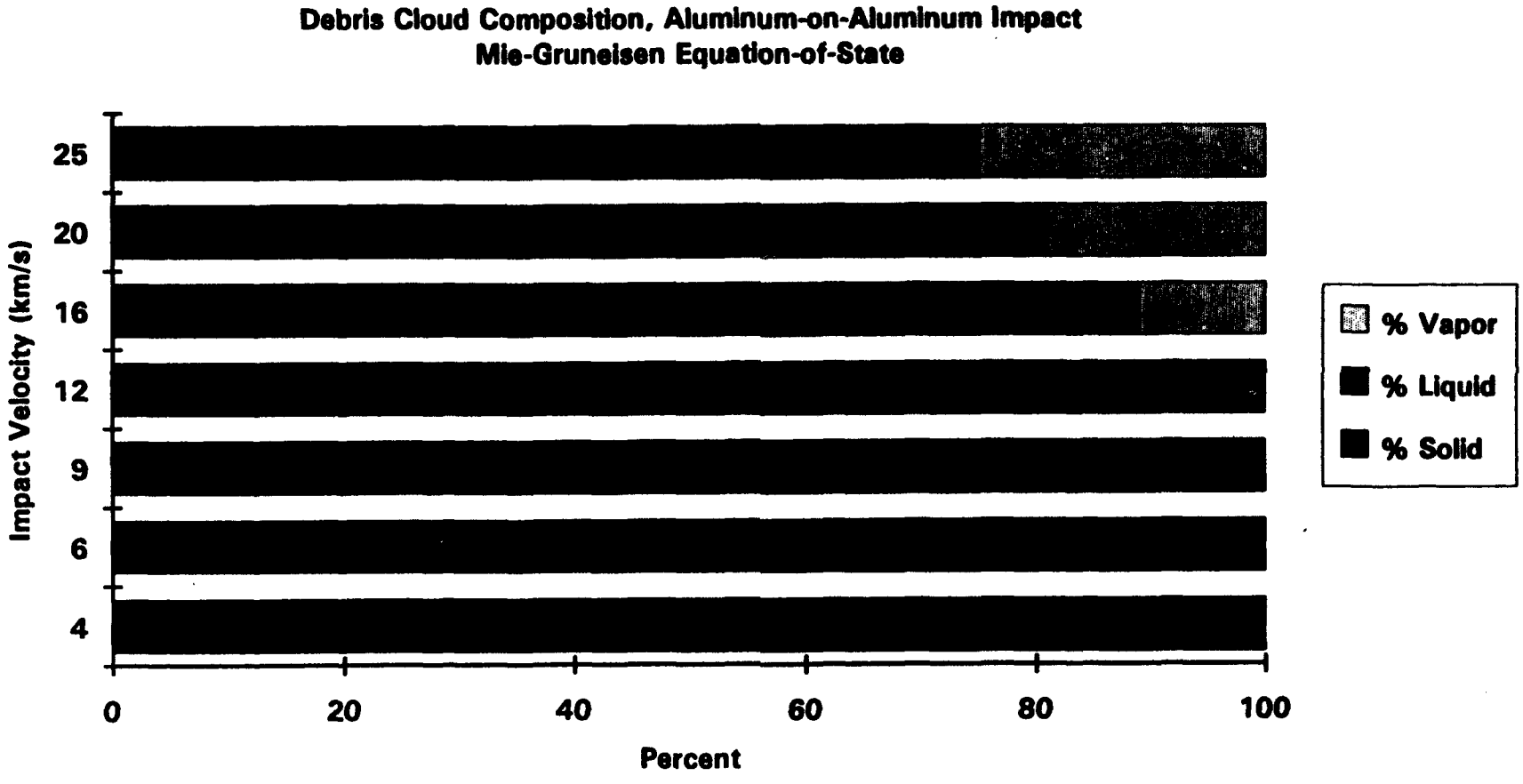

Figure 29. Debris Cloud Material Composition Using the Mie-Gruneisen EOS, Aluminum-on-Aluminum Impact

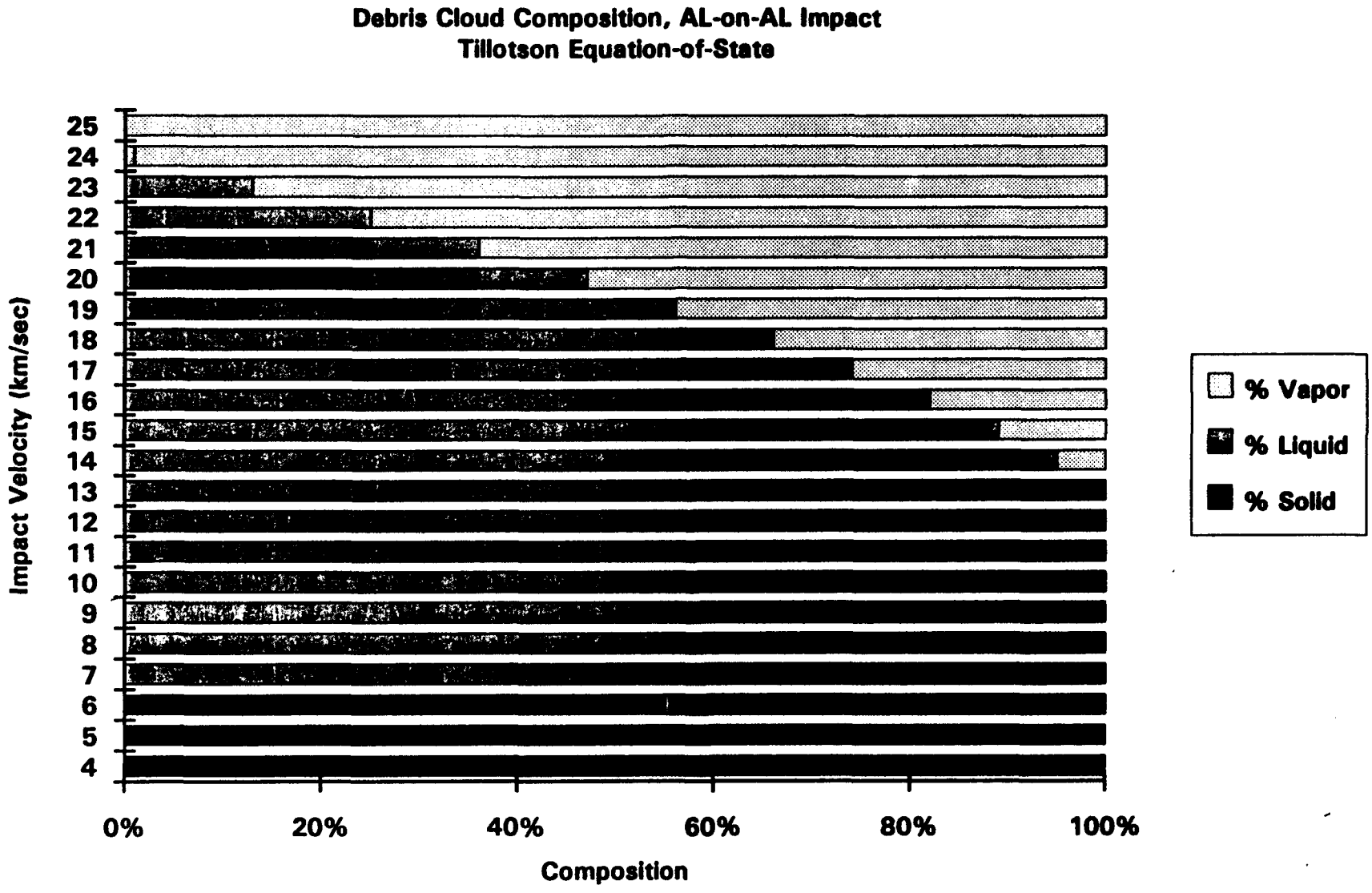

Figure 30. Debris Cloud Material Composition Using the Tillotson EOS, Aluminum-on-Aluminum Impact

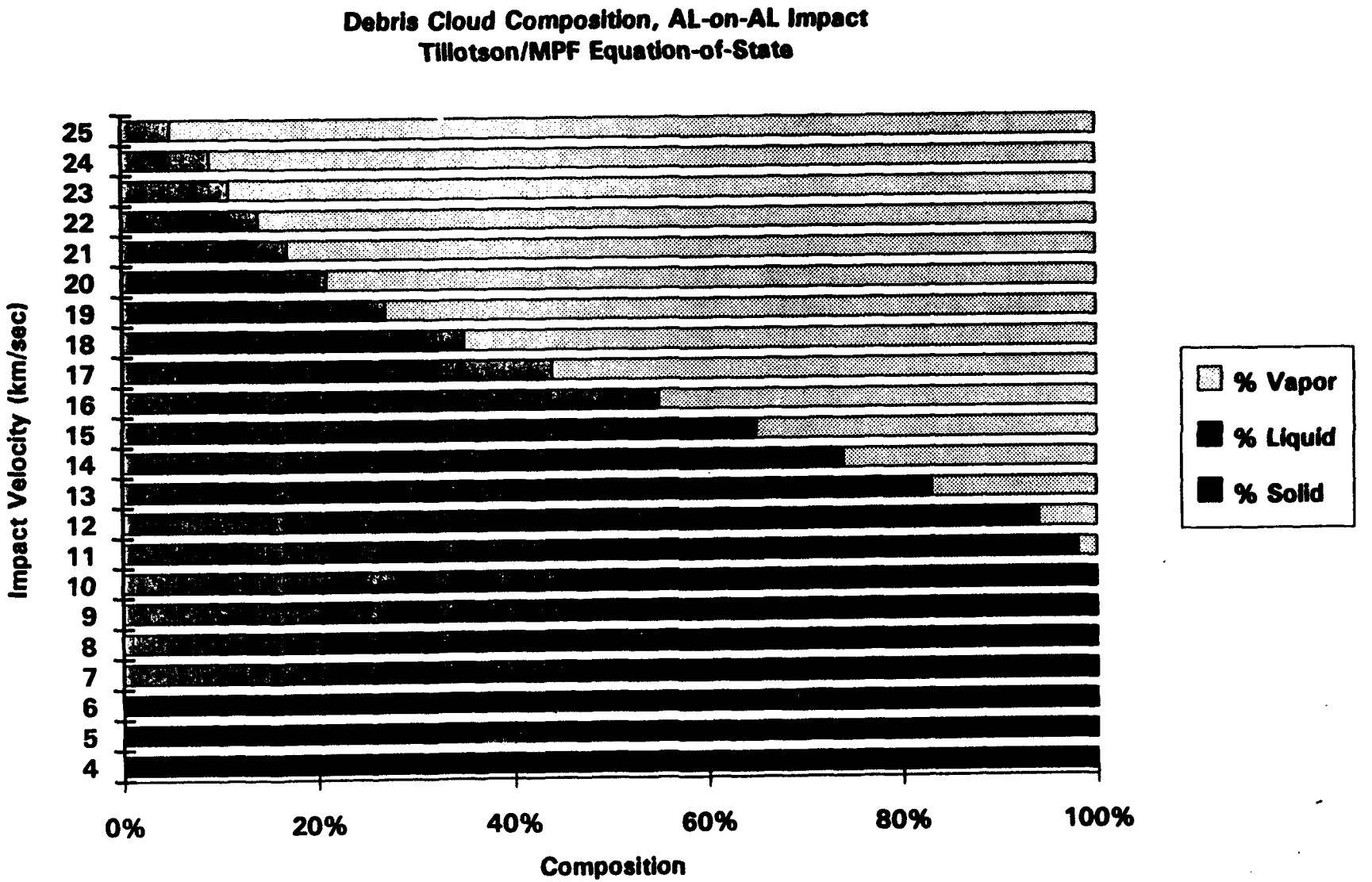

Figure 31. Debris Cloud Material Composition Using the Tillotson/SJC EOS, Aluminum-on-Aluminum Impact

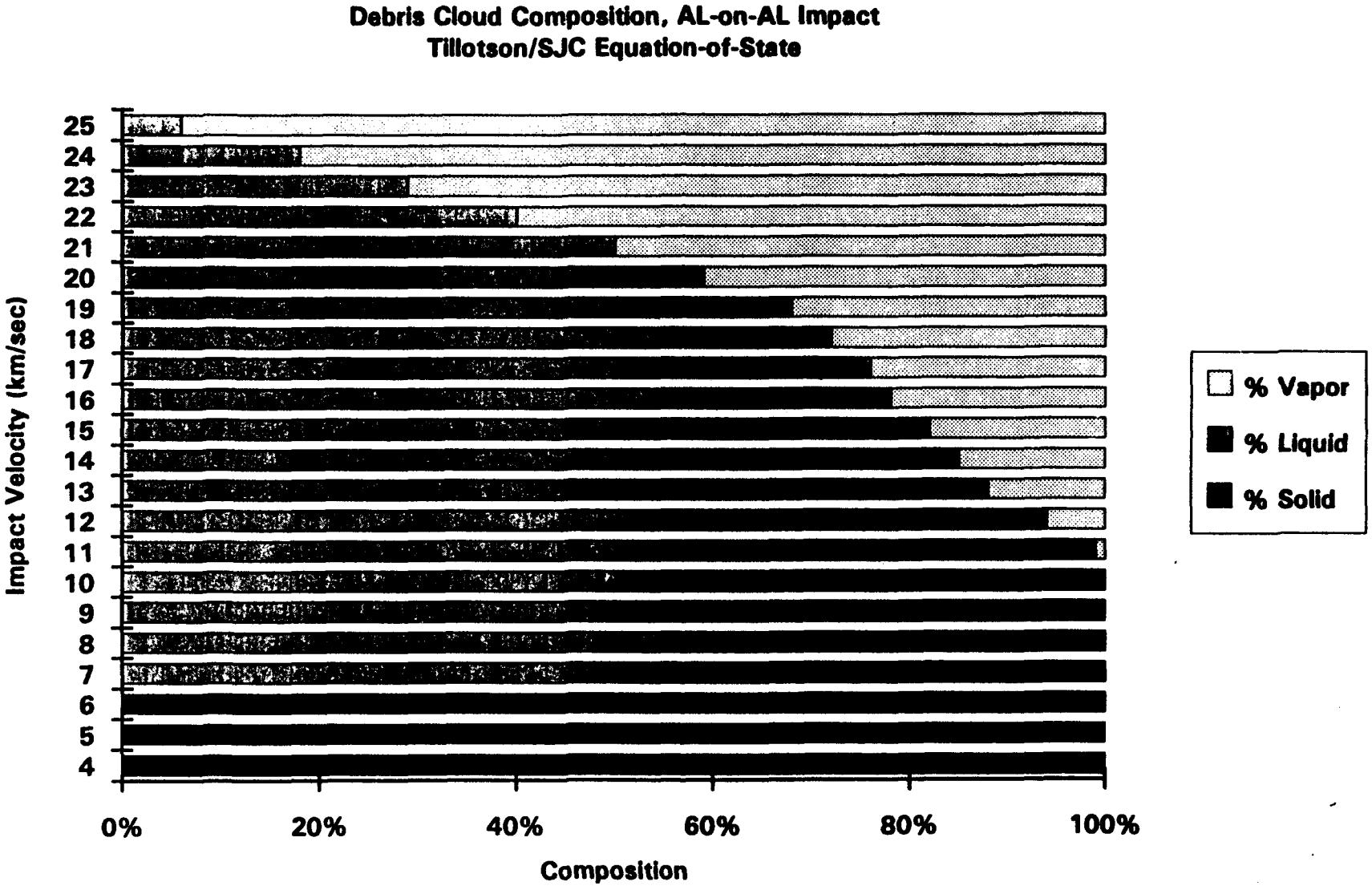

Figure 32. Debris Cloud Material Composition Using the Tillotson/MPF EOS, Aluminum-on-Aluminum Impact

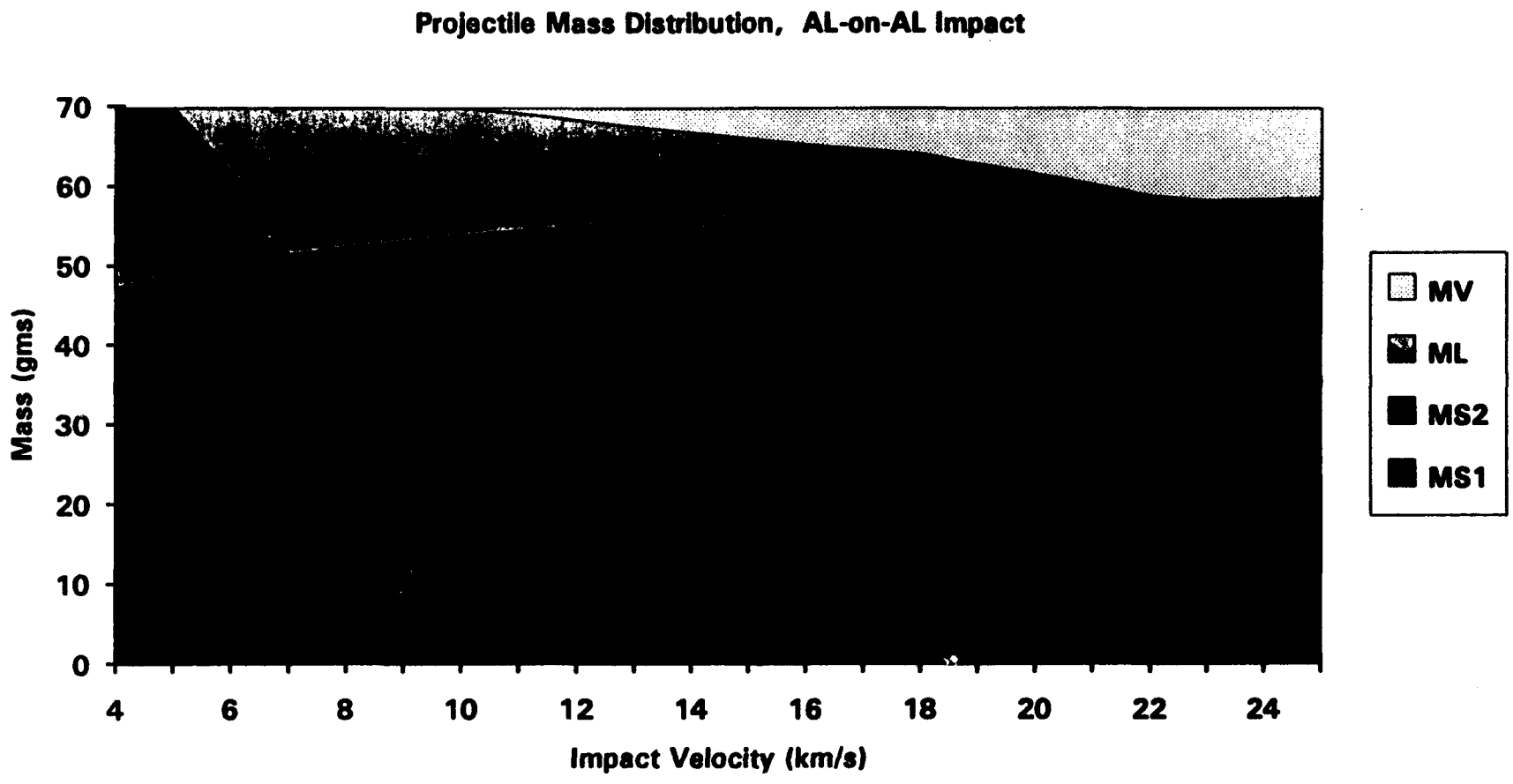

Figure 33. Projectile Material Mass Distribution, Aluminum-on-Aluminum Impact

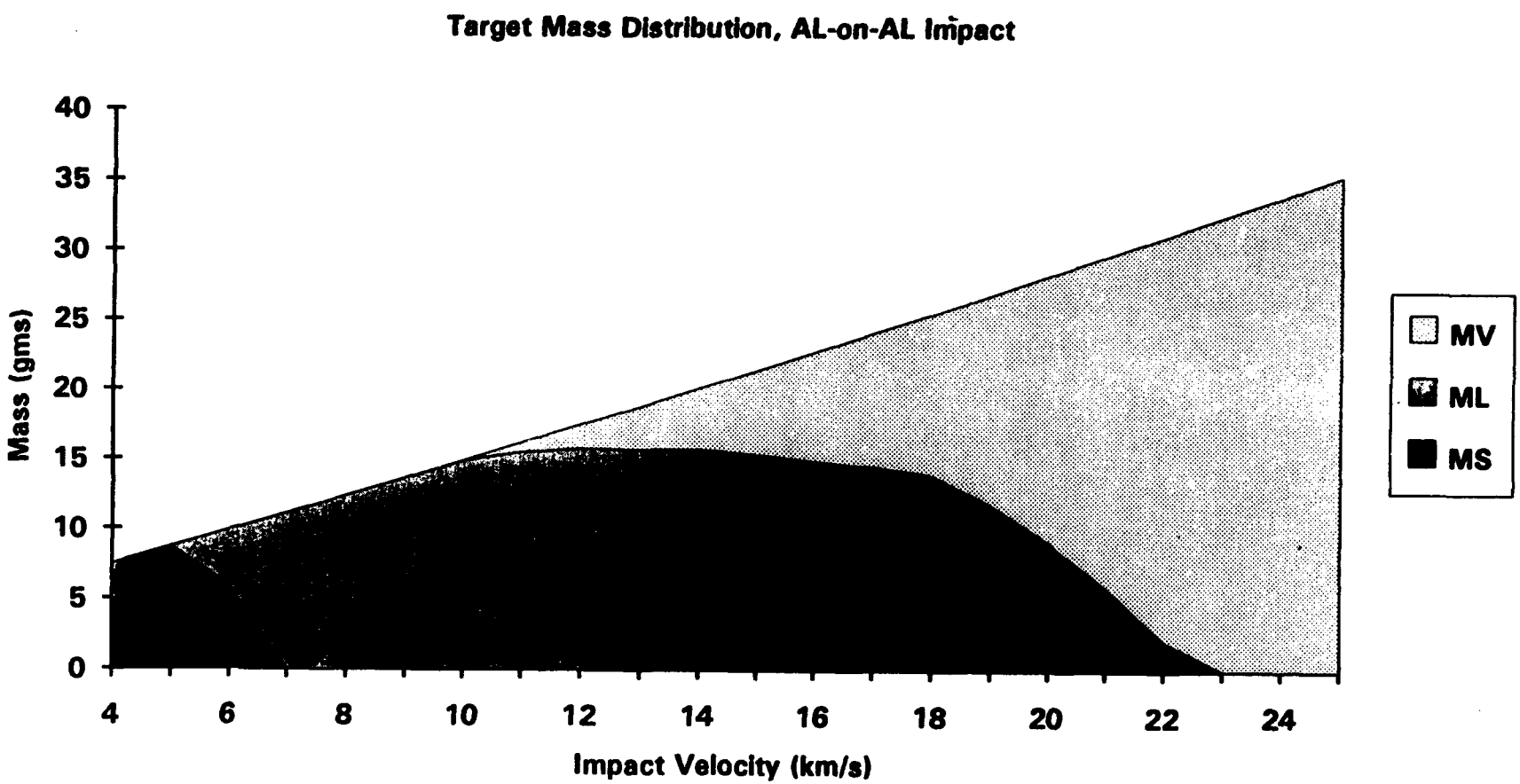

Figure 34. Target Material Mass Distribution, Aluminum-on-Aluminum Impact

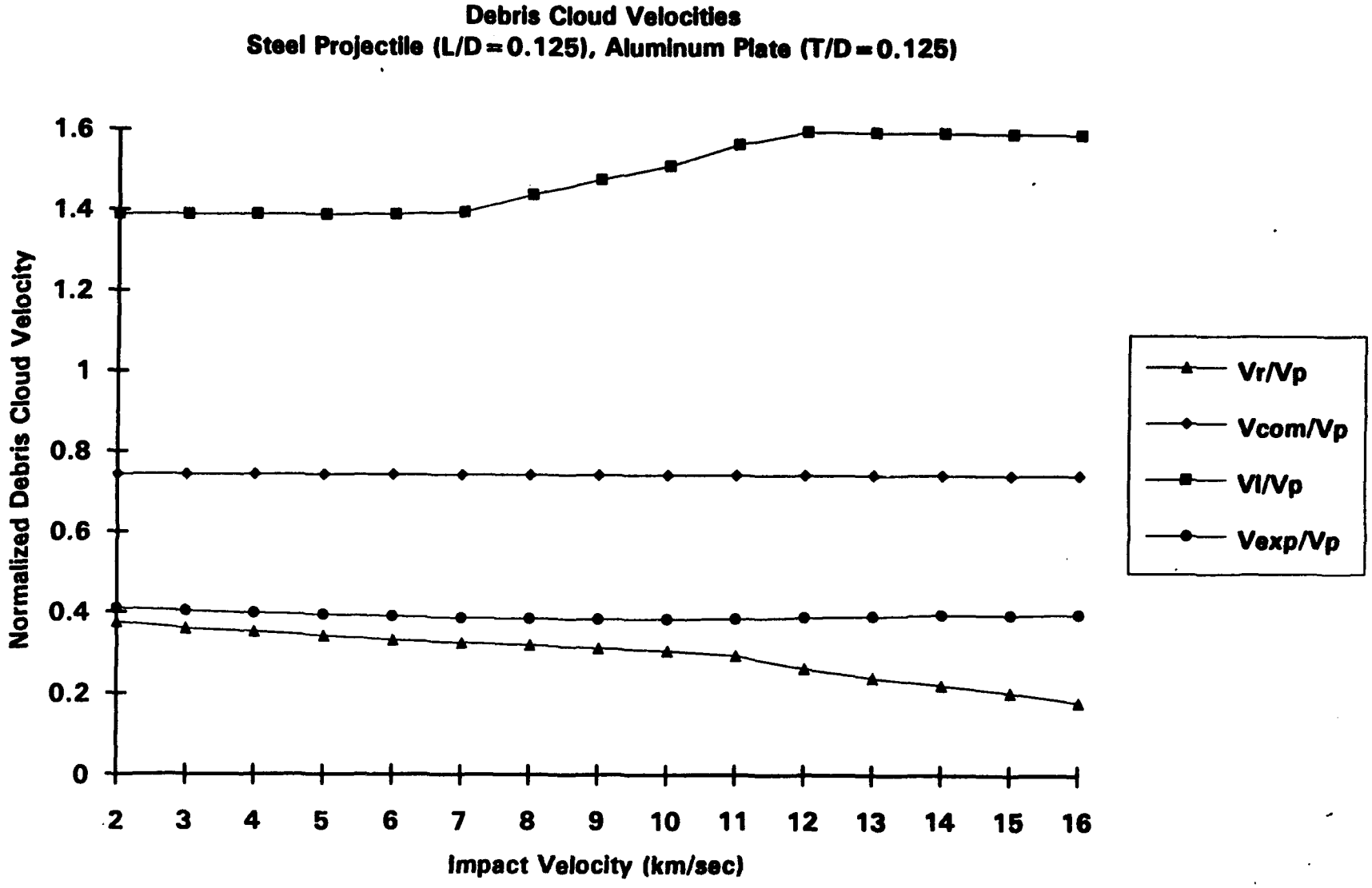

Figure 35. Debris Cloud Velocities, Thin Disk Impact, Steel-on-Aluminum

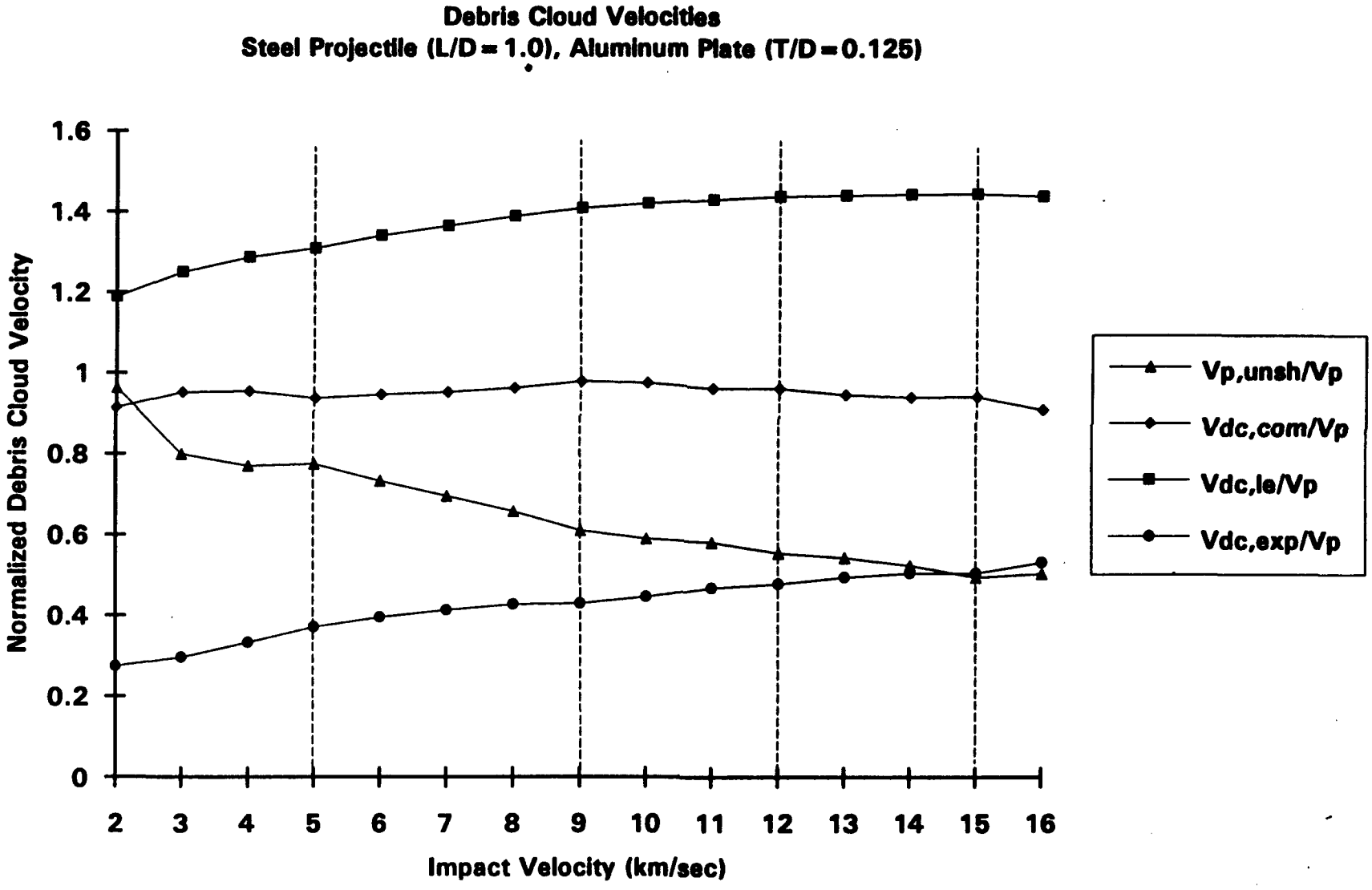

Figure 36. Debris Cloud Velocities, Long Rod Impact, Steel-on-Aluminum

7.0 SUMMARY AND RECOMMENDATIONS

7.1 Summary

A robust lethality assessment methodology must include the effects of discrete particle impacts as well as the response of the target to impulsive debris cloud loadings. A first-order accurate scheme has been implemented to determine the amount of material in each of the three states of matter in a debris cloud created by a hypervelocity impact on a thin target. A modified version of the Tillotson EOS was used to calculate the residual energy in the projectile and target materials upon release from their respective shocked states. Elementary thermodynamic principles were use to determine the percentages of shocked and released projectile and target materials that were melted and/or vaporized during the release process. Using assumed projectile and target geometries, these percentages were then used to calculate the mass of the projectile and target materials in solid, liquid, and gaseous form. Debris cloud velocities were calculated using the principles of momentum and energy conservation; the spread of the debris cloud material was then readily obtained.

The predictions of the debris cloud model were compared against experimental data, the predictions of three different empirically-based codes, and against the predictions of 1-D and 3-D hydrocodes. In general, the predictions of the characterization scheme developed herein compared favorably with the experimental results, the lethality assessment schemes' predictions, and the predictions of the hydrocodes. While some of the details in the debris cloud model differed from empirical evidence, it is noted that the debris cloud model presented herein was developed solely through the application of fundamental physical principles without any empirical 'adjustment' factors. In this light, the agreement between the elementary theory predictions and the experimental results is highly encouraging.

7.2 Recommendations

Based on the work completed thus far, the following recommendations are offered for

continuing the development of a lethality assessment model that would be applicable in impact scenarios where material melt and/or vaporization can be expected to occur.

The next step in the first-order characterization of the debris clouds created in a hypervelocity impact would be to determine the nature of the debris cloud solid fragment population. This includes calculating the number of projectile and target material fragments, as well as their sizes, speeds, and trajectories. In addition to the fragmentation models FATEPEN, PEN-4, and KAPP-II, the fragmentation models developed by Grady, et al. [37-39] can be used to predict the number of fragments that would result from a KEW impact. The predictions of the various fragmentation models can be compared against one another and against available experimental data to determine which fragmentation model is best suited for use in a lethality assessment methodology. Hypervelocity impact test results for a variety of target systems are available from a number of sources, including NASA [40], NSWC [41], NRL [42], BRL [43], and others [44-50].

After a satisfactory first-order accurate procedure that characterizes debris cloud composition is completed, the accuracy of the procedure needs to be improved. This includes modifying the methods presented herein to include a more appropriate hole diameter predictor equation, the impact of non-monolithic projectiles that are more representative of actual KEW geometries, and the impact of yawed and/or obliquely incident projectiles. Additional modifications to improve the accuracy of the debris cloud calculations are as follows.

First, the method of calculating the percentages of projectile and target material in the three states of matter should also be replaced with a more rigorous thermodynamic procedure. One method (see, e.g. [24]) would require calculating the entropy of the shocked state, that is, the entropy imparted to the material by shocking it to a given pressure. The material will retain that entropy during isentropic release to the final release pressure and specific volume. The calculation is completed by identifying the material state with that entropy at the final release pressure by consulting classical thermodynamic tables (see, e.g. [51,52]).

Second, a shock wave attenuation procedure [34,53,54] should be implemented to

obtain more accurate mass values for the material that is melted and/or vaporized in a high speed KEW impact. Such a procedure will result in a residual energy profile along the length of the projectile and through the thickness of the target. Energy levels at various positions can then be compared to energy levels necessary to begin material melt or vaporization. In addition, the assumption that the impact pressure acts on an area equal to the area of the hole created in the target plate needs to be reconsidered.

Third, in its present formulation, it is entirely possible that the value of the parameter E_0 in the Tillotson EOS can be different for different impact velocities even when the projectile and target materials are held constant. Since E_0 is part of an EOS and an EOS is a material property, the value of E_0 should be constant and should not depend on impact conditions. If E_0 were to change with a change in impact conditions, this would imply the existence of an EOS surface that also changes with impact conditions, which is not possible [55]. Thus, it is imperative to address the manner in which the value of E_0 is chosen in the application of the Tillotson EOS.

Subsequent to the development of a satisfactory debris cloud characterization scheme, an impulsive loading algorithm for the target should be developed to account for the effects of the non-solid debris cloud constituents as well as the solid non-perforating debris cloud fragments. This effort requires as input the masses and velocities of the non-solid debris cloud materials, the area of the inner wall over which the impulsive loading is applied, and the geometric and material properties of the inner wall, including the spacing between the outer and inner walls and the orientation of the inner wall with respect to that of the outer wall. Issues to be addressed include whether the impacts of the target and projectile debris cloud materials need to be considered separately or can be considered simultaneously, whether the effects of the molten and vaporous debris cloud components need to be considered separately or can be combined, and how to account for the decreasing time of the load application and the increasing area over which it is applied as the initial impact velocity increases.

The impulsive loading algorithm can be validated at velocities attainable using existing

hypervelocity launchers by comparing the predictions of the algorithm with available impact test data. The algorithm can be modified if necessary until a satisfactory level of accuracy is reached. It can then be combined with the debris cloud characterization scheme and a suitable fragmentation model to yield an improved, robust lethality assessment method for high speed KEW impacts.

8.0 REFERENCES

1. Anderson, C.E., Trucano, T.G., and Mullin, S.A., "Debris Cloud Dynamics", Int. J. Impact Engng., Vol. 9, No. 1, pp. 89-113, 1990.

2. Hopkins, A.K., Swift, H.F., and Lee, T.W., "Material Phase Transformations Effects Upon Performance of Spaced Bumper Systems", J. Spacecraft Rockets, Vol. 9, No. 5, pp. 342-345, 1972.

3. Yatteau, J.D., High Velocity Multiple Plate Penetration Model, NSWC-TR- 82-123, Dahlgren, Virginia, 1982.

4. Yatteau, J.D., Modifications to Program FATE_-_Fragment Residual Mass Calculations, Final Report, Denver Research Institute, University of Denver, Denver, Colorado, 1983.

5. Yatteau, J.D., Zernow, R.H., and Recht, R.F., Compact Fragment Multiple Plate Penetration Model, Volume_I: Model Description, NSWC-TR-91-399, Dahlgren, Virginia, 1991.

6. Yatteau, J.D., Zernow, R.H., and Recht, R.F., Compact Fragment Multiple Plate Penetration Model, Volume_II: Computer Code User's Manual, NSWC-TR-91- 399, Dahlgren, Virginia, 1991.

7. Henderson, B.J., and Zimmerschied, A.B., Very High Velocity Penetration Model, NSWC-TR-83-189, Dahlgren, Virginia, 1983.

8. Bjorkman, M.D., Geiger, J.D., and Wilhelm, E.E., Space Station Integrated Wall Design

and Penetration Damage Control, Task 3: Theoretical Analysis of Penetration Mechanics, Boeing Aerospace Corporation, Final Report, Contract NAS8-36426, Seattle, Washington, 1987.

9. Penetration Mechanics Handbook for Kinetic Energy Penetrators, 61- JTCG/ME-77-16-Rev-1, 1977.

10. Greer, R., and Hatz, M., KAPP-II user's Manual, Version 1.1, Kaman Sciences Corporation, K92-17U(R), Colorado Springs, Colorado, 1992.

11. Snow, P., KAPP - Kaman Analytical Penetration Program, Kaman Sciences Corporation, K85-7U(R), Colorado Springs, Colorado, 1985.

12. Cohen, L., Kaman New Analytical Penetration Program (KNAPP) Space-Based Interceptor Modelling Effort, AFATL-TR-90-02, Eglin AFB, Florida, 1990.

13. Schonberg, W.P., Toward a Characterization of the Debris Cloud Created in a Hypervelocity Impact on a Thin Plate, WL-TR-93-7028, Eglin AFB, Florida, 1993.

14. Idzorek, G.C., Keaton, P.W., Stradling, G.L., Callopy, M.T., Curling, H.L., and McColl, D.B., "Data Acquistion System for a Hypervelocity-Microparticle-Impacts Laboratory", Int. J. Impact Engng., Vol. 10, pp. 261-270, 1990.

15. Igiseder, H., and Idenbergs, E., "Crater Morphology at Impact Velocities Between 8 and 17 km/sec", Int. J. Impact Engng., Vol. 10, pp. 271-280, 1990.

16. Osher, J., Gathers, R., Chau, H., Lee, R., Pomykal, G., and Weingart, R., "Hypervelocity Acceleration and Impact Experiments with the LLNL Electric Guns", Int. J. Impact Engng., Vol. 10, pp. 439-452, 1990.

17. Lundeberg, J.F, Stern, P.H., Bristow, J.R., Meteoroid Protection for Spacecraft Structures, NASA-CR-54201, Washington, D.C., 1965.

18. Burch,. G.T., Multi-Plate Damage Study, AFATL-TR-67-116, Eglin AFB, Florida, 1967.

19. Swift, H.F., Bamford, R., and Chen, R., "Designing Space Vehicle Shields for Meteoroid Protection: A New Analysis", Adv. Space Research, Vol. 2, No. 12, 1983, pp 219-234.

20. Richardson, A.J., "Theoretical Penetration Mechanics of Multi-SHeet Structures Based on Discrete Debris Particle Modelling", J. Spacecraft, Vol. 7, No. 4, 1970, pp 486-489.

21. Swift, H.F., "On Predicting Projectile Breakup During Thin Plate Impact", Int. J. Impact Engng., Vol. 10, 1990, pp. 579-585.

22. Grady, D.E., and Passman, S.L., "Stability and Fragmentation of Ejecta in Hypervelocity Impact", Int. J. Impact Engng., Vol. 10, 1990, pp. 197-212.

23. Lawrence, R.J., "A Simple Model for the Optimization of Stand-Off Hypervelocity Particle Shields", Int. J. Impact Engng., Vol. 5, 1987, pp. 451-461.

24. Bjork, R.L., Vaporization and SDI Lethality, DNA-TR-89-28, Alexandria, Virginia, 1990.

25. Rice, M.H., McQueen, R.G., and Walsh, J.M, "Compression of Solids by Strong Shock

Waves", Solid State Physics, Vol. 6, Seitz, F. and Turnbull, D., eds., Academic Press, New York, 1958.

26. Tillotson, J.H., Metallic Equations of State for Hypervelocity Impact, General Dynamics, General Atomic Division, Report No. GA-3216, 1962.

27. Mullin, S.A., Littlefield, D.L., Anderson, C.A., Velocity Scaling for Lethality Applications, Southwest Research Institute, Final Report, Project No. 06-4438, 1992.

28. Allen, R.T., Equation of State of Rocks and Minerals, General Dynamics, General Atomic Division, Report No. GAMD-7834A, 1967.

29. Holian, K., and Burkett, M.W., "Sensitivity of Hypervelocity Impact Simulations to Eqns-of- State", Int. J. Impact Engng., Vol. 5, pp. 331-341, 1987.

30. Rinehart, J.S., Stress Transients in Solids, HyperDynamics, Santa Fe, New Mexico, 1975.

31. Goldsmith, W., Impact: The Theory and Physical Behaviour of Colliding Solids, Edward Arnold, London, 1960.

32. Zukas, J.A., et.al., High Velocity Impact Dynamics, John Wiley, New York, 1990.

33. Piekutowski, A.J., "A Simple Dynamic Model for the Formation of Debris Clouds", Int. J. Impact Engng., Vol. 10, 1990, pp. 453-471.

34. Maiden, C.J., Gehring, J.W., and McMillan, A.R., Investigation of Fundamental Mechanism of Damage to Thin Targets by Hypervelocity Projectiles, General Motors Defense Research Laboratory, TR-63-225, Santa Barbara, California, 1963.

35. Herrmann, W., and Wilbeck, J.S., "Review of Hypervelocity Impact Penetration Theories", Int. J. Impact Engng., Vol. 5, pp. 307-322, 1987.

36. Wilbeck, J.S., Scott, P.G., and Lew, T.M., Enhanced Fragment Lethality, AFATL-TR-88-105, Eglin Air Force Base, Florida, August, 1988.

37. Grady, D.E., "Local Inertial Effects in Dynamic Fragmentation", J. Appl. Phys., Vol. 53, No. 1, 1982, pp. 322-325.

38. Grady, D.E., "Fragmentation of Solids Under Impulsive Stress Loading", J. Geophys. Res., Vol. 86, No. B2, 1981, pp. 1047-1054.

39. Grady, D.E., and Kipp, M.E., "Geometric Statistics and Dynamic Fragmentation", J. Appl. Phys., Vol. 58, No. 3, 1985, pp. 1210-1222.

40. Schonberg, W.P., Bean, A.J., and Darzi, K., Hypervelocity Impact Physics, NASA-CR-4343, Washington, D.C., 1991.

41. Dickinson, D., Investigation of High Velocity Fragments Impacting Plate Arrays, NSWC-TR-79-66, 1979.

42. Williams, A.E., and Saravane, I., Debris Characterization Study, NRL Letter Report 4680-196, 1990.

43. Wenzel, A.B., and Dean, J.K., Behind Armor Spallation Tests, BRL-CR- 262, 1975.

44. Watson, R.W., "The Perforation of Thin Plates by High Velocity Fragments", Proceedings of the Fifth Hypervelocity Impact Symposium, Vol. 1, Pt. 2, Colorado School of Mines, Denver, Colorado, 1961, pp. 581-592.

45. Spells, K.E., "Velocities of Steel Fragments After Perforation of a Steel Plate", Proc. Phys. Soc. (London), Vol. B64, 1951, pp. 212-218.

46. Swift, H.F., Preonas, D.D., and Turpin, W.C., "Debris Clouds Behind Plates Impacted by Hypervelocity Pellets", J. Spacecraft, Vol. 7, No. 3, 1970, pp. 313-318.

47. Piekutowski, A.J., "Properties of Largest Fragment Produced by Hypervelocity Impact of Aluminum Spheres with Thin Aluminum Sheets", AIAA Space Programs and Technology Conference, Huntsville, Alabama, Paper No. 92-1588, 1992.

48. Stilp, A.J., Hohler, V., Schneider, E., and Weber, K., "Debris Cloud Expansion Studies", Int. J. Impact Engng., Vol. 10, 1990, pp. 543-553.

49. Klopp, R.W., Shockey, D.A., Osher, J.E., and Chau, H.H., "Characteristics of Hypervelocity Impact Debris Clouds", Int. J. Impact Engng., Vol. 10, 1990, pp. 323-335.

50. Finnegan, S.A., Schulz, J.C., and Heimdahl, O.E.R., "Spatial Fragment Mass and Velocity Distributions", Int. J. Impact Engng., Vol. 10, 1990, pp. 159-170.

51. Stull, D.R., and Prophet, H., JANAF Thermochemical Tables, Second Edition, U.S. Department of Commerce, National Bureau of Standards, Washington, D.C., 1971.

52. Stull, D.R., and Sinke, G.C., "Thermodynamic Properties of the Elements", in Advances in Chemistry, No. 18, American Chemical Society, Washington, D.C., 1956.

53. Fowles, G.R., "Attenutation of the Shock Wave Produced in a Solid by a Flying Plate", J. Appl. Phys., Vol. 31, No. 4, 1960, pp. 655-661.

54. Cohen, L., "Integrated Technology Support for Debris Cloud Material State Modelling", Science Applications International Corporation, Tech. Inf. Memo. WU4/TIM92-2, Shalimar, Florida, 1992.

55. Hoffman, M., Hypervelocity Impact Debris Cloud Characterization, Science Applications International Corporation, Tech. Memo. WU4/TM92-1, Shalimar, Florida, 1992.

56. Mullin, S.A., Private Communication, 1992.

APPENDIX A -- DEBRIS3 Source Code

```
$DEBUG
      PROGRAM DEBRIS3
C
C.....  THIS PROGRAM PERFORMS THE FOLLOWING TASKS:
C.....
C.....          1. IT CALCULATES THE RELEASE OF TARGET AND PROJECTILE
C.....  MATERIALS FROM SHOCKED CONDITIONS DUE TO A HYPERVELOCITY IMPACT
C.....  OF A MULTI-MATERIAL PROJECTILE ON A FLAT THIN TARGET PLATE
C.....  USING THE TILLOTSON EQUATION OF STATE TO CALCULATE THE RELEASE
C.....  ISENTROPE;
C.....
C.....          2. IT CALCULATES THE RESIDUAL MATERIAL TEMPERATURES FOR
C.....  THE TARGET AND PROJECTILE MATERIALS;
C.....
C.....          3. IT ESTIMATES THE PERCENTAGES OF THE TARGET AND PRO-
C.....  JECTILE MATERIALS IN EACH OF THE THREE MATTER STATES BASED ON
C.....  THE WASTE HEAT GENERATED BY THE RELEASE PROCESS;
C.....
C.....          4. IT CALCULATES THE AMOUNT OF SOLID, LIQUID, AND GAS-
C.....  EOUS MASS IN THE PROJECTILE AND TARGET MATERIAL CONTRIBUTIONS
C.....  TO THE DEBRIS CLOUD CREATED IN A HYPERVELOCITY IMPACT; AND,
C.....
C.....          5. IT CALCULATES THE DEBRIS CLOUD VELOCITIES AND THE
C.....  SPREAD OF THE DEBRIS CLOUD MATERIAL.
C.....
C.....  THE TILLOTSON EQUATION OF STATE USED BY THIS PROGRAM INCLUDES
C.....  THE MIXED PHASE EQUATIONS, THE CHECK AT V=VS, A CHOICE OF TWO
C.....  ADJUSTMENTS TO THE EQUATION OF STATE TO ELIMINATE THE DISCON-
C.....  TINUITY AT V=VS, A CHOICE OF WHICH HOLE DIAMETER EQUATION TO
C.....  USE, AND A CHOICE OF WHICH dE=-PdV APPROXIMATION TO USE.
C
       IMPLICIT DOUBLE PRECISION (A-H,O-Z)
       DOUBLE PRECISION IMEP,IVEP,IMET,IVET,KSP,KST,KP,KT,LO,LP,LPTOT,
      $NUP,NUT,MPROJ,MTARG,MUSTM,MTSR
       DOUBLE PRECISION COPA(10),RPA(10),KPA(10),EPA(10),ALPHPA(10),
      $CPSPA(10),CPLPA(10),TMPA(10),TVPA(10),GPIA(10),HFPA(10),HVPA(10),
      $BHNPA(10),ALFPA(10),LPA(10),BETPA(10),EPSPA(10),SYPA(10),SUPA(10),
      $NUPA(10),MUSPM(10),MPSR(10),FSRP(10),EXP(10),PMS(10),PML(10),
      $PMV(10),MPLYR(10),UFSP1(10),UFSP2(10),PMSSR(10),PMSSNR(10),
      $UPPA(10),UPSA(10),CSP(10),VE(10),VD(10),VC(10),TDSUM(10),XE(10),
      $TE(10),TD(10)
C
       INTEGER ROPT,ROPTPA(10),ROPTT,HCOPT
       CHARACTER*1 PGMSTP
       CHARACTER*2 PIDA(10),TID,PIDCHK,TIDCHK
       CHARACTER*10 PMATA(10),TMAT
       COMMON/TDATA/A,B,AA,BB,ALF,BET,EO,EOM,EOI,ROPT,JCOPT
       OPEN(1,FILE='INDATA')
       OPEN(2,FILE='IMPOUT')
C
C.....  READ PROJECTILE AND TARGET MATERIAL PROPERTIES.  THE PARAMETERS
C.....  MUST BE IN THE FOLLOWING UNITS:
C.....
C.....          PID,TID ....... PROJECTILE AND TARGET MATERIAL ID CODES
C.....          PMAT,TMAT ..... PROJECTILE AND TARGET MATERIALS
C.....          COP,COT ....... ADIABATIC BULK SOUND SPEED, KM/S
C.....          RP,RT ......... AMBIENT MATERIAL DENSITY, GM/CU.CM.
C.....          KP,KT ......... SLOPE OF US-UP LINE, DIMENSIONLESS
C.....          EP,ET.......... ELASTIC MODULUS, LBS/SQ.IN.
C.....          NUP,NUT ....... POISSON'S RATIO, DIMENSIONLESS
C.....          GP,GT ......... AMBIENT GRUNEISEN COEFF., DIMENSIONLESS
C.....          ALFAP,ALFAT ... LINEAR COEFF OF TERMAL EXP, 1/DEG-C
C.....          CPSP,CPST ..... SPECIFIC HEAT (SOLID), CAL/GM-DEG-C
C.....          CPLP,CPLT ..... SPECIFIC HEAT (LIQUID), CAL/GM/DEG-C
```

```
C.....          TMP,TMT ..... MELT TEMPERATURE, DEG-C
C.....          TVP,TVT ..... VAPORIZATION TEMPERATURE, DEG-C
C.....          HFP,HFT ..... LATENT HEAT OF FUSION, CAL/GM
C.....          HVP,HVT ..... LATENT HEAT OF VAPORIZATION, CAL/GM
C.....          BHNP,BHNT ..... BRINELL HARDNESS NUMBER, KG/SQ.MM
C.....          ALFP,ALFT ..... TILLOTSON EOS CONSTANTS
C.....          BETP,BETT ..... TILLOTSON EOS CONSTANTS
C.....          EPSP,EPST ..... TILLOTSON EOS CONSTANTS
C.....          SYP,SYT ..... TENSILE YIELD STRENGTH, MPA
C.....          SUP,SUT ..... ULTIMATE TENSILE STRENGTH, MPA
C.....          LP ..... PROJECTILE LAYER LENGTH, IN
C.....          DP ..... PROJECTILE DIAMETER, IN
C.....          TS ..... TARGET PLATE THICKNESS, IN
C.....          ROPTP,ROPTT ... TILLOTSON EOS RELEASE OPTION
C.....              ROPT=1 .... BACKWARD PRESSURE APPROXIMATION
C.....              ROPT=2 .... AVERAGE PRESSURE APPROXIMATION
C.....              ROPT=3 .... CURRENT PRESSURE APPROXIMATION
C.....          HCOPT ..... HOLE DIAMETER EQUATION OPTION
C.....              HCOPT=1 ... KAPPII/HSSO1
C.....              HCOPT=2 ... KAPPII/HSSO2
C.....              HCOPT=3 ... KAPPII/HSAO1
C.....              HCOPT=4 ... PEN4/V1O
C.....              HCOPT=5 ... HOLE DIA = PROJ DIA
C
      WRITE(*,1)
    1 FORMAT(' ENTER NUMBER OF PROJECTILE MATERIAL LAYERS (I2) AND HIT R
     $ETURN')
      READ(*,6) NPMAT
    6 FORMAT(I2)
      DO 79 I=1,NPMAT
      WRITE(*,3) I
    3 FORMAT(' ENTER PROJ MATL ID CODE FOR LAYER NO. ',I2,' (A2) AND HIT
     $ RETURN')
      READ(*,5) PIDA(I)
    5 FORMAT(A2)
   79 CONTINUE
      WRITE(*,7)
    7 FORMAT(' ENTER TARGET MATERIAL ID CODE (A2) AND HIT RETURN')
      READ(*,9) TID
    9 FORMAT(A2)
C
      DO 88 I=1,NPMAT
      REWIND 1
      READ(1,4)
    4 FORMAT(/////)
   99 READ(1,8) PIDCHK
    8 FORMAT(A2)
      IF (PIDA(I).EQ.PIDCHK) THEN
      READ(1,10) PMATA(I),COPA(I),KPA(I),RPA(I),GPIA(I),BHNPA(I)
   10 FORMAT(A10,5F10.5)
      READ(1,100) EPA(I),NUPA(I),ALPHPA(I),CPSPA(I),CPLPA(I),
     $              EPSPA(I)
  100 FORMAT(2(E10.3,F10.5),2(F10.5))
      READ(1,102) TMPA(I),TVPA(I),HFPA(I),HVPA(I),ALFPA(I),BETPA(I)
  102 FORMAT(6F10.5)
      READ(1,104) SYPA(I),SUPA(I),ROPTPA(I)
  104 FORMAT(2F10.5,I1)
      ENDIF
      IF (PIDA(I).NE.PIDCHK) THEN
      IF (PIDCHK.EQ.'XX') THEN
      WRITE (*,17) I
   17 FORMAT(' PROJ MATL FOR LAYER NO. ',I2,' NOT FOUND IN MATERIAL LIBR
     $ARY.',/,' PLEASE CHECK PROJ MATL ID CODES AND BEGIN AGAIN.')
      STOP
```

```
      ENDIF
      IF (PIDCHK.NE.'XX') THEN
      READ (1,2)
    2 FORMAT(////)
      GOTO 99
      ENDIF
      ENDIF
   88 CONTINUE
C
      REWIND 1
      READ(1,4)
  999 READ(1,8) TIDCHK
      IF (TID.EQ.TIDCHK) THEN
      READ(1,10) TMAT,COT,KT,RT,GTI,BHNT
      READ(1,100) ET,NUT,ALPHAT,CPST,CPLT,EPST
      READ(1,102) TMT,TVT,HFT,HVT,ALFT,BETT
      READ(1,104) SYT,SUT,ROPTT
      ENDIF
      IF (TID.NE.TIDCHK) THEN
      IF (TIDCHK.EQ.'XX') THEN
      WRITE (*,117)
  117 FORMAT(' TARGET MATERIAL NOT FOUND IN MATERIAL LIBRARY.',/,
     $' PLEASE CHECK TARGET MATERIAL ID CODE AND BEGIN AGAIN.')
      STOP
      ENDIF
      IF (TIDCHK.NE.'XX') THEN
      READ (1,2)
      GOTO 999
      ENDIF
      ENDIF
C
C.....  READ IMPACT VELOCITY IN KM/S
C
      WRITE(*,29)
   29 FORMAT(' INPUT IMPACT VELOCITY IN KM/SEC (F5.2) AND HIT RETURN')
      READ(*,30) V
   30 FORMAT(F5.2)
C
C.....  READ TARGET THICKNESS AND PROJECTILE DIAMETER
C
      WRITE(*,13)
   13 FORMAT(' ENTER TS AND DP VALUES IN INCHES (F10.5,/,F10.5) AND HIT
     $RETURN');
      READ(*,11) TS,DP
   11 FORMAT(F10.5,/,F10.5)
C
C.....  READ PROJECTILE LAYER THICKNESSES
C
      DO 66 I=1,NPMAT
      WRITE(*,44) I
   44 FORMAT(' ENTER LP VALUES IN INCHES (F10.5) FOR LAYER NO. ',I2,
     $' AND HIT RETURN')
      READ(*,33) LPA(I)
   33 FORMAT(F10.5)
   66 CONTINUE
C
C.....  READ TARGET HOLE DIAMETER EQUATION OPTION
C
      WRITE(*,16)
   16 FORMAT(' INPUT HOLE DIAMETER EQUATION OPTION (I1) AND HIT RETURN',
     $/,5X,'HCOPT=1 ... KAPPII/HSSO1',/,5X,'HCOPT=2 ... KAPPII/HSSO2',/,
     $5X,'HCOPT=3 ... KAPPII/HSAO1',/,5X,'HCOPT=4 ... PEN4/V10',/,5X,
     $'HCOPT=5 ... DH=DP')
      READ(*,18) HCOPT
```

```
   18 FORMAT(I1)
C
C.....  READ TILLOTSON EOS DISCONTINUITY ADJUSTMENT OPTION
C
      WRITE(*,21)
   21 FORMAT(' INPUT EOS DISCONTINUITY ADJUSTMENT OPTION (I1) AND HIT RE
     $TURN',/,5X,'JCOPT=1 ... SCHONBERG JUMP CORRECTION',/,5X,'JCOPT=2 .
     $.. MIXED-PHASE FORMULATION')
      READ(*,23) JCOPT
   23 FORMAT(I1)
C
C.....  SOME PRELIMINARY CALCULATIONS ...
C
      PI=4.0*ATAN(1.0)
      RPAVG=0.0
      LPTOT=0.0
      MPROJ=0.0
      DO 242 I=1,NPMAT
      RPAVG=RPAVG+LPA(I)*RPA(I)
      LPTOT=LPTOT+LPA(I)
      MPROJ=MPROJ+LPA(I)*RPA(I)
  242 CONTINUE
      RPAVG=RPAVG/LPTOT
      MPROJ=PI*MPROJ*(DP/2.0)*(DP/2.0)*(2.54*2.54*2.54)
C
      REWIND 2
      WRITE(2,40) MPROJ,TMAT,V
   40 FORMAT('HYPERVELOCITY IMPACT OF A ',F8.3,' GM MULTI-MATERIAL PROJE
     $CTILE ON A',/,A10,' TARGET AT A ',F5.2,' KM/SEC IMPACT VELOCITY')
C
      WRITE(2,50) TMAT,COT,KT,RT,TS*2.54,DP*2.54
   50 FORMAT(/,'TARGET MATERIAL PROPERTIES ...',//,3X,'MAT = ',A10,/,3X,
     $'CO  = ',F7.3,' KM/S',/,3X,'K   = ',F7.3,/,3X,'RHO = ',F7.3,
     $' GM/CU.CM.',/,3X,'TS  = ',F7.3,' CM',//,'PROJECTILE MATERIAL PROP
     $ERTIES (DP = ',F7.3,' CM) ...')
      DO 53 I=1,NPMAT
      WRITE(2,51) I,PMATA(I),COPA(I),KPA(I),RPA(I),LPA(I)*2.54
   51 FORMAT(/,3X,'MAT ',I2,' = ',A10,/,3X,'CO     = ',F7.3,' KM/S',/,
     $3X,'K      = ',F7.3,/,3X,'RHO    = ',F7.3,' GM/CU.CM.',/,3X,
     $'LP     = ',F7.3,' CM')
   53 CONTINUE
C
C.....  CALCULATE TARGET MATERIAL AND 1ST PROJECTILE LAYER MATERIAL
C.....  PARTICLE AND SHOCK WAVE VELOCITIES AND INTERFACE HUGONIOT IMPACT
C.....  PRESSURE.  THIS INFORMATION IS REQUIRED TO DETERMINE THE DEPTH
C.....  TO WHICH THE TARGET MATERIAL IS SHOCKED AND TO RELEASE THE
C.....  TARGET MATERIAL FROM ITS SHOCKED STATE.
C
      IF (TMAT.EQ.PMATA(1)) GOTO 35
      A=KPA(1)-KT*(RT/RPA(1))
      B=2.0*KPA(1)*V+COPA(1)+COT*(RT/RPA(1))
      C=COPA(1)*V+KPA(1)*V*V
      D=B*B-4.0*A*C
      UTP=(B-SQRT(D))/(2.0*A)
      GOTO 38
   35 UTP=V/2.0
   38 UPPA(1)=V-UTP
      UTS=COT+KT*UTP
      UPSA(1)=COPA(1)+KPA(1)*UPPA(1)
      PT=RT*UTS*UTP
C
C.....  CALCULATE SHOCK WAVE AND PARTICLE VELOCITIES IN SUBSEQUENT
C.....  PROJECTILE LAYER MATERIALS
C
```

```
      IF (NPMAT.GE.2) THEN
      DO 55 I=2,NPMAT
      CALL UPPCAL(RPA(I-1),RPA(I),KPA(I-1),KPA(I),COPA(I-1),COPA(I),
     $              UPPA(I-1),UPPA(I))
      UPSA(I)=COPA(I)+KPA(I)*UPPA(I)
   55 CONTINUE
      ENDIF
C
C.....  CALCULATE LOCATION IN PROJECTILE WHERE ORIGINAL TARGET
C.....  RAREFACTION WAVE OVERTAKES PROJECTILE SHOCK WAVE
C
      CALL RSINT(NPMAT,UTS,UTP,UPSA,UPPA,LPA,DP,TS,V,LO)
C
C.....  TARGET MATERIAL RELEASE CALCULATION PHASE
C
      WRITE(2,599)
  599 FORMAT(/,'***** TARGET MATERIAL RELEASE CALCULATION *****')
C
      VTO=1.0/RT
      VT1=RT*UTS/(UTS-UTP)
      VT1=1.0/VT1
      PH=PT*1.0E09
      EHT=0.5*PH*(VTO-VT1)/1000.0
      PHMB=PH/101.3E+09
C
      WRITE(2,60) UTP,UTS,PT,PHMB,EHT,VTO,VT1
   60 FORMAT(/,'INITIAL CONDITIONS FOR TARGET MATERIAL ...',/,3X,'PARTIC
     $LE VELOCITY ..... UP = ',F8.3,' KM/S',/,3X,'SHOCK WAVE SPEED
     $ ..... US = ',F8.3,' KM/S',/,3X,'HUGONIOT IMPACT PRESSURE .
     $... PH = ',F8.3,' GPA = ',F6.3,' MBAR',/,3X,'HUGONIOT IMPACT ENERG
     $Y ..... EH = ',E10.4,' JOULES/KG',/,3X,'SPECIFIC VOLUME AT REST .
     $.... VO = ',F10.3,' CU.CM./GM',/,3X,'SPECIFIC VOLUME AT IMPACT ...
     $ V1 = ',F10.3,' CU.CM./GM')
C
C.....  CALCULATE AMBIENT GRUNEISEN COEFFICIENT AND GAMMA/SP.VOL. RATIO
C.....  FOR TARGET MATERIAL
C
      ET=ET*68947.0
      BETAT=3.0*ALPHAT
      IF (NUT.LT.0.5) THEN
      KST=ET/3.0/(1.0-2.0*NUT)
      COTC=DSQRT((KST/10.0)/(RT*1000.0))/1000.0
      ENDIF
      IF (NUT.EQ.0.5) THEN
      KST=-1.0
      COTC=-1.0
      ENDIF
      IF (NUT.LT.0.5) GT=2.3885E-08*KST*BETAT/CPST/RT
      IF (NUT.EQ.0.5) GT=GTI
C
      WRITE(2,75) ET/10.0,NUT,KST/10.0,ALPHAT,CPST,CPLT
   75 FORMAT(/,'PARAMETERS REQUIRED FOR CALCULATING TARGET MATERIAL RELE
     $ASE FROM SHOCKED',/,'STATE USING THE TILLOTSON EQUATION OF STATE:'
     $,/,3X,'TARG MATL ELASTIC MODULUS ..... E    =',E10.4,
     $' N/SQ.M.',/,3X,'TARG MATL POISSON RATIO ..... NU   =',
     $F10.3,/,3X,'TARG MATL BULK MODULUS ..... K    =',E10.4,
     $' N/SQ.M.',/,3X,'TARG MATL LIN. COEF. OF THERM. EXP. ... ALFA =',
     $E10.4,' /DEG-C',/,3X,'TARG MATL SP HEAT (SOLID) ..... CPS
     $ =',F10.3,' CAL/GM/DEG-C',/,3X,'TARG MATL SP HEAT (LIQUID) .....
     $..... CPL  =',F10.3,' CAL/GM/DEG-C')
      WRITE(2,80) GT,GTI,SYT,SUT,BHNT,TMT,TVT,HFT,HVT
   80 FORMAT(3X,'TARG MATL AMB M-GRUN COEF (CAL,INP) ... GAM0 =',F10.3,
     $',',F6.3,/,3X,'TARG MATL YIELD STRENGTH ..... SY   =',
     $F10.3,' MPA',/,3X,'TARG MATL ULT STRENGTH ..... SU   ='
```

```
     $,F10.3,' MPA',/,3X,'TARG MATL BRN HDNS NO ..................... BHN  =
     $',F10.3,/,3X,'TARG MATL MELT TEMPERATURE ..............., TM   =',F10.
     $2,' DEG-C',/,3X,'TARG MATL VAPOR TEMPERATURE ........... TV   =',
     $F10.2,' DEG-C',/,3X,'TARG MATL HEAT OF FUSION ............... HF
     $=',F10.2,' CAL/GM',/,3X,'TARG MATL HEAT OF VAPORIZATION ........ H
     $V   =',F10.2,' CAL/GM')
C
      SHST=CPST*4186.
      SHLT=CPLT*4186.
      HFT=HFT*4186.
      HVT=HVT*4186.
      IMET=TMT*SHST
      IVET=IMET+HFT+(TVT-TMT)*SHLT
C
      WRITE (2,76) IMET,IVET
   76 FORMAT(3X,'TARG MATL INICPIENT MELT ENERGY ....... IME  =',
     $E10.4, ' JOULES/KG',/,3X,'TARG MATL INCIPIENT VAPOR ENERGY ......
     $IVE  =',E10.4,' JOULES/KG')
C
      WRITE (*,230)
  230 FORMAT(/,1X,'ENTER EO MULTIPLIER VALUE FOR TARGET MATERIAL (F4.2)
     $AND HIT RETURN')
      READ (*,240) EOM
  240 FORMAT(F4.2)
C
      ALP=ALFT
      BET=BETT
      ROPT=ROPTT
      CALL TCONST(VTO,COT,KT,GT,TMT,TVT,HFT,HVT,IVET)
      CALL TRELS1(VTO,VT1,PH,EXT,UTP,URT,UFST1,UFST2,IVET,HVT,COT,KT,
     $            EPST)
      CALL TINC(SHST,SHLT,TMT,TVT,HFT,HVT,EXT,IMET,IVET,PS,PL,PV,TRT)
C
      WRITE(2,87) UFST1,UFST2
   87 FORMAT(/,'FREE SURF VEL (UP+UR) .........',F7.3,' KM/SEC',/,'FREE S
     $URF VEL (2.0*UP) .......',F7.3,' KM/SEC')
C
      CALL TMCALC(V,PS,PL,PV,RPAVG,RT,TRT,TMT,TVT,TS,LPTOT,DP,BHNT,
     $TSOLT,TMS,TML,TMV,MTARG,HCOPT,SYT,SUT,UTS,UPSA(1),UTP,UPPA(1),
     $MUSTM,MTSR)
C
C.....  PROJECTILE MATERIALS RELEASE CALCULATIONS PHASE
C
      CHKL=0.0
      DO 9999 I=1,NPMAT
C
      WRITE(2,89) I
   89 FORMAT(/,'***** PROJECTILE MATERIAL RELEASE CALCULATIONS, LAYER NO
     $.',I2,' *****')
C
C.....  READ MATERIAL PARAMETERS FOR CURRENT PROJECTILE LAYER MATERIAL
C
      COP=COPA(I)
      RP=RPA(I)
      KP=KPA(I)
      EP=EPA(I)
      ALPHAP=ALPHPA(I)
      CPSP=CPSPA(I)
      CPLP=CPLPA(I)
      TMP=TMPA(I)
      TVP=TVPA(I)
      GPI=GPIA(I)
      HFP=HFPA(I)
      HVP=HVPA(I)
```

```
      BHNP=BHNPA(I)
      ALFP=ALFPA(I)
      LP=LPA(I)
      BETP=BETPA(I)
      EPSP=EPSPA(I)
      SYP=SYPA(I)
      SUP=SUPA(I)
      NUP=NUPA(I)
      ROPTP=ROPTPA(I)
      PMAT=PMATA(I)
      UPP=UPPA(I)
      UPS=UPSA(I)
      CHKL=CHKL+LPA(I)*2.54
C
C.....  CALCULATE SHOCKED STATE QUANTITIES FOR PROJECTILE LAYER MATERIAL
C
      PP=RP*UPS*UPP
      PH=PP*1.0E+09
      PHMB=PH/101.3E+09
      VPO=1.0/RP
      VP1=RP*UPS/(UPS-UPP)
      VP1=1.0/VP1
      EHP=0.5*PH*(VPO-VP1)/1000.0
C
      WRITE(2,93) I,UPP,UPS,PP,PHMB,EHP,VPO,VP1
   93 FORMAT(/,'INITIAL CONDITIONS FOR PROJECTILE LAYER NO. ',I2,' MATER
     $IAL ...',/,3X,'PARTICLE VELOCITY ..... UP = ',F8.3,' KM/S',/
     $,3X,'SHOCK WAVE SPEED ..... US = ',F8.3,' KM/S',/,3X,'SHOCK
     $ PRESSURE ..... PH = ',F8.3,' GPA = 'F6.3,' MBAR',/,3X,
     $'SHOCK ENERGY ..... EH = ',E10.4,' JOULES/KG',/,3X,
     $'SPECIFIC VOLUME (AT REST) ... V0 = ',F10.3,' CU.CM./GM',/,3X,
     $'SPECIFIC VOLUME (SHOCKED) ... V1 = ',F10.3,' CU.CM./GM')
C
C.....  CALCULATE AMBIENT GRUNEISEN COEFFICIENT AND GAMMA/SP.VOL. RATIO
C.....  FOR PROJECTILE MATERIAL.
C
      EP=EP*68947.0
      BETAP=3.0*ALPHAP
      IF (NUP.LT.0.5) THEN
      KSP=EP/3.0/(1.0-2.0*NUP)
      COPC=DSQRT((KSP/10.0)/(RP*1000.0))/1000.0
      ENDIF
      IF (NUP.EQ.0.5) THEN
      KSP=-1.0
      COPC=-1.0
      ENDIF
      IF (NUP.LT.0.5) GP=2.3885E-08*KSP*BETAP/CPSP/RP
      IF (NUP.EQ.0.5) GP=GPI
C
      WRITE(2,105) I,EP/10.0,NUP,KSP/10.0,ALPHAP,CPSP,CPLP
  105 FORMAT(/,'PARAMETERS REQUIRED FOR CALCULATING RELEASE OF PROJ LAYE
     $R NO. ',I2,' MATERIAL FROM',/,'SHOCKED STATE USING THE TILLOTSON E
     $QUATION OF STATE:',/,3X,'MATL ELASTIC MODULUS ..... E    =
     $',E10.4,' N/SQ.M.',/,3X,'MATL POISSON RATIO ..... NU   =
     $',F10.3,/,3X,'MATL BULK MODULUS ..... K    =',E10.4,
     $' N/SQ.M.',/,3X,'MATL LIN. COEF. OF THERM. EXP. ... ALFA =',E10.4,
     $' /DEG-C',/,3X,'MATL SP HEAT (SOLID) ..... CPS  =',F10.3,
     $' CAL/GM/DEG-C',/,3X,'MATL SP HEAT (LIQUID) ..... CPL  =',
     $F10.3,' CAL/GM/DEG-C')
      WRITE(2,110) GP,GPI,SYP,SUP,BHNP,TMP,TVP,HFP,HVP
  110 FORMAT(3X,'MATL AMB M-GRUN COEF (CAL,INP) ... GAM0 =',F10.3,',',
     $F6.3,/,3X,'MATL YIELD STRENGTH ..... SY   =',F10.3,' MPA'
     $,/,3X,'MATL ULT STRENGTH ..... SU   =',F10.3,' MPA',/,
     $3X,'MATL BRN HDNS NO ..... BHN  =',F10.3,/,3X,'MATL ME
```

```
     $LT TEMPERATURE ..... TM   =',F10.2,' DEG-C',/,3X,'MATL VAPO
     $R TEMPERATURE ..... TV   =',F10.2,' DEG-C',/,3X,'MATL HEAT O
     $F FUSION ..... HF   =',F10.2,' CAL/GM',/,3X,'MATL HEAT OF
     $ VAPORIZATION ..... HV   =',F10.2,' CAL/GM')
C
      SHSP=CPSP*4186.
      SHLP=CPLP*4186.
      HFP=HFP*4186.
      HVP=HVP*4186.
      IMEP=TMP*SHSP
      IVEP=IMEP+HFP+(TVP-TMP)*SHLP
C
      WRITE (2,77) IMEP,IVEP
   77 FORMAT(3X,'MATL INICPIENT MELT ENERGY ..... IME  =',E10.4, ' JOU
     $LES/KG',/,3X,'MATL INCIPIENT VAPOR ENERGY ..... IVE  =',E10.4,' J
     $OULES/KG')
C
      WRITE (*,231) I
  231 FORMAT(/,1X,'ENTER EO MULTIPLIER VALUE FOR PROJECTILE LAYER NO. ',
     $I2,' MATERIAL (F4.2)',/,1X,'AND HIT RETURN')
      READ (*,241) EOM
  241 FORMAT(F4.2)
C
      ALF=ALFP
      BET=BETP
      ROPT=ROPTP
      CALL TCONST(VPO,COP,KP,GP,TMP,TVP,HFP,HVP,IVEP)
      CALL TRELS1(VPO,VP1,PH,EXP(I),UPP,URP,UFSP1(I),UFSP2(I),IVEP,
     $              HVP,COP,KP,EPSP)
      CALL TINC(SHSP,SHLP,TMP,TVP,HFP,HVP,EXP(I),IMEP,IVEP,PS,PL,PV,
     $            TRP)
      CALL PMCALC(I,UPS,UTS,UPP,UTP,RP,PS,PL,PV,TS,LP,DP,PMS(I),
     $              PMSSR(I),PML(I),PMV(I),MPLYR(I),MUSPM(I),MPSR(I),
     $              FSRP(I),PGMSTP,ISTOP,LO,CHKL)
      PMSSNR(I)=0.0
C
      IF (PGMSTP.EQ.'Y') GOTO 498
C
 9999 CONTINUE
C
  498   WRITE (2,499)
  499 FORMAT(//,'MASS DISTRIBUTION SUMMARY ...')
      DO 501 I=1,NPMAT
      IF (PGMSTP.EQ.'Y'.AND.I.GT.ISTOP) THEN
      PMS(I)=PI*(DP/2.0)*(DP/2.0)*(LPA(I)*2.54)*RPA(I)
      PML(I)=0.0
      PMV(I)=0.0
      MUSPM(I)=PMS(I)
      PMSSR(I)=0.0
      PMSSNR(I)=0.0
      MPSR(I)=0.0
      FSRP(I)=0.0
      ENDIF
      WRITE (2,500) I,PMS(I),MUSPM(I),PMSSNR(I),PMSSR(I),PML(I),PMV(I)
  500 FORMAT(3X,'PROJECTILE LAYER NO. ',I2,' ... SOLID .... ',F7.2,
     $' GMS',/,32X,'UNSH .... ',F7.2,' GMS',/,32X,'SNR ..... ',F7.2,
     $' GMS',/,32X,'S&R ..... ',F7.2,' GMS',/,31X,'LIQUID ... ',F7.2,
     $' GMS',/,31X,'VAPOR .... ',F7.2,' GMS')
  501 CONTINUE
      TMFRAG=MTARG-MTSR
      WRITE (2,502) TSOLT,TMFRAG,TMS,TML,TMV
  502 FORMAT(3X,'TARGET MATERIAL ..... SOLID .... ',F7.2,' GMS',/,
     $32X,'FRAG .... ',F7.2,' GMS',/,32X,'S&R ..... ',F7.2,' GMS',/,31X,
     $'LIQUID ... ',F7.2,' GMS',/,31X,'VAPOR .... ',F7.2,' GMS')
```

```
C
C....   COMPUTE DEBRIS CLOUD VELOCITIES
C
      CALL DCVEL(UFST1,UFSP1,V,MTARG,MPROJ,MPLYR,MTSR,MPSR,MUSTM,
     $              MUSPM,PMSSNR,EXT,EXP,FSRP,NPMAT)
C
      CLOSE(1)
      CLOSE(2)
      CLOSE(3)
      STOP
      END
C
      SUBROUTINE TCONST(VO,CO,K,G,TM,TV,HF,HV,ES)
      IMPLICIT DOUBLE PRECISION (A-H,O-Z)
      DOUBLE PRECISION K
      INTEGER ROPT
      COMMON/TDATA/A,B,AA,BB,ALF,BET,EO,EOM,EOI,ROPT,JCOPT
C
C.....  THIS SUBROUTINE CALCULATES THE VALUES OF THE CONSTANTS
C.....  REQUIRED BY THE TILLOTSON EQUATION OF STATE (SwRI FINAL
C.....  REPORT FOR PROJ. NO. 06-4438).
C
      AA=(1000.0/VO)*(CO*1000.0)*(CO*1000.0)
      BB=AA*(2.0*K-1.0-0.5*G)
      A=0.5
      B=G-0.5
      R1=TM/TV
      R2=HF/HV
      EOI=EXP(-0.199)*(K**6.5939)*(R2**0.5720)/(G**0.7680)
     $      /(R1**0.0210)
      EOI=EOI*(ES+HV)
      EO=EOM*EOI
C
      WRITE (2,10) AA,BB,A,B,ALF,BET,EOI,EOM,EO
   10 FORMAT(/,'ADDITIONAL PARAMETERS REQUIRED FOR CALCULATING MATERIAL
     $RELEASE FROM',/,'SHOCKED STATE USING THE TILLOTSON EQUATION OF STA
     $TE:',/,3X,'AA  = ',E11.4,' M/SQ.M.',/,3X,'BB  = ',E11.4,' M/SQ.M.'
     $,/,3X,'A   = ',F7.4,/,3X,'B   = ',F7.4,/,3X,'ALF = ',F7.4,/,3X,
     $'BET = ',F7.4,/,3X,'EOI = ',E11.4,' JOULES/KG',/,3X,'EOM = ',F7.4,
     $,/,3X,'EO  = ',E11.4,' JOULES/KG')
C
      RETURN
      END
C
      SUBROUTINE TRELS1(VO,V1,PHO,EX,UP,UR,UFS1,UFS2,IVE,HV,CO,K,EPS)
      IMPLICIT DOUBLE PRECISION (A-H,O-Z)
      DOUBLE PRECISION Q(401),MU(401),V(401),E(401),P(401),R(401)
      DOUBLE PRECISION RP(401),U(401),S(401),PH(401),IVE,K
      INTEGER ROPT
      COMMON/TDATA/A,B,AA,BB,ALF,BET,EO,EOM,EOI,ROPT,JCOPT
C
C.....  THIS SUBROUTINE, TOGETHER WITH THE SUBROUTINE PCALC, CALCULATE
C.....  THE RELEASE OF THE PROJECTILE AND TARGET MATERIALS USING THE
C.....  TILLOTSON EQUATION OF STATE. IT IS ASSUMED THAT FOR MOST METALS
C.....  THE SPECIFIC VOLUME VS IS APPROX. 13.1% GREATER THAN THE AMBIENT
C.....  SPECIFIC VOLUME VO.
C
      ESP=IVE+HV
      VS=1.131*VO
C
      WRITE (2,5) IVE,HV,ESP,VS,EPS
    5 FORMAT(3X,'ES  = ',E11.4,' JOULES/KG',/,3X,'HV  = ',E11.4,
     $' JOULES/KG',/,3X,'ESP = ',E11.4,' JOULES/KG',/,3X,'VS  = ',
     $F7.4,' CU.CM./GM',/,3X,'EPS = ',F7.4)
```

```
C
      PH(1)=PHO
      V(1)=V1
      P(1)=PHO
      E(1)=0.5*P(1)*(VO-V1)/1000.0
      DELV=(VO-V1)/50.0
      MU(1)=VO/V(1)-1.0
      Q(1)=AA*MU(1)+BB*MU(1)*MU(1)
      R(1)=EO*(VO/1000.0)*(VO/1000.0)
      RP(1)=B*R(1)
C
C ....  NOTE: MU(1),Q(1),R(1),RP(1) ARE INITIALIZED BUT NOT USED
C
      PEQ2=0.0
      DELP=0.0
      DE=0.0
      UR=0.0
      II=0
      DO 10 I=2,401
      V(I)=V(I-1)+DELV
      PH(I)=CO**2*(1000.0/VO)*(1.0-V(I)/VO)/(1.0-K*(1.0-V(I)/VO))**2
      PH(I)=PH(I)*1.0E06
      MU(I)=VO/V(I)-1.0
      R(I)=E(I-1)*(V(I)/1000.0)*(V(I)/1000.0)
     $       +EO*(VO/1000.0)*(VO/1000.0)
C
      IF (V(I).LT.VO) THEN
      Q(I)=AA*MU(I)+BB*MU(I)*MU(I)
      RP(I)=A*E(I-1)*(V(I)/1000.0)*(V(I)/1000.0)
     $        +B*EO*(VO/1000.0)*(VO/1000.0)
      CALL PCALC(E(I-1),P(I-1),V(I),Q(I),R(I),RP(I),VO,DELV,P(I))
      ENDIF
C
      IF (JCOPT.EQ.1.AND.V(I).GE.VO) THEN
C
C.....  IMPLEMENTATION OF SCHONBERG JUMP CORRECTION (WL-TR-93-7028)
C.....  TOGETHER WITH MIXED PHASE FORMULATION
C
      IF (V(I).LT.VS) THEN
C
      IF (E(I-1).LT.IVE) THEN
      Q(I)=AA*MU(I)+BB*MU(I)*MU(I)
      RP(I)=A*E(I-1)*(V(I)/1000.0)*(V(I)/1000.0)
     $        +B*EO*(VO/1000.0)*(VO/1000.0)
      CALL PCALC(E(I-1),P(I-1),V(I),Q(I),R(I),RP(I),VO,DELV,P(I))
      ENDIF
C
      IF (E(I-1).GE.IVE.AND.E(I-1).LT.ESP) THEN
      Q(I)=AA*MU(I)+BB*MU(I)*MU(I)
      RP(I)=A*E(I-1)*(V(I)/1000.0)*(V(I)/1000.0)
     $        +B*EO*(VO/1000.0)*(VO/1000.0)
      CALL PCALC(E(I-1),P(I-1),V(I),Q(I),R(I),RP(I),VO,DELV,PC)
      C=V(I)/VO-1.0
      U(I)=DEXP(-ALF*C*C)
      S(I)=AA*MU(I)*DEXP(-BET*C)
      B=B*U(I)
      Q(I)=U(I)*S(I)
      RP(I)=A*E(I-1)*(V(I)/1000.0)*(V(I)/1000.0)
     $        +B*EO*(VO/1000.0)*(VO/1000.0)
      CALL PCALC(E(I-1),P(I-1),V(I),Q(I),R(I),RP(I),VO,DELV,PE)
      B=B/U(I)
      T1=PE*(E(I-1)-IVE)
      T2=PC*(ESP-E(I-1))
      DEN=ESP-IVE
```

```
      P(I)=(T1+T2)/DEN
      ENDIF
C
      IF (E(I-1).GE.ESP) THEN
      C=V(I)/VO-1.0
      U(I)=DEXP(-ALF*C*C)
      S(I)=AA*MU(I)*DEXP(-BET*C)
      B=B*U(I)
      Q(I)=U(I)*S(I)
      RP(I)=A*E(I-1)*(V(I)/1000.0)*(V(I)/1000.0)
     $        +B*EO*(VO/1000.0)*(VO/1000.0)
      CALL PCALC(E(I-1),P(I-1),V(I),Q(I),R(I),RP(I),VO,DELV,P(I))
      B=B/U(I)
      ENDIF
C
      DELVS=VS-V(I)
      IF (DELVS.LT.DELV) THEN
      C=V(I)/VO-1.0
      U(I)=DEXP(-ALF*C*C)
      S(I)=AA*MU(I)*DEXP(-BET*C)
      B=B*U(I)
      Q(I)=U(I)*S(I)
      RP(I)=A*E(I-1)*(V(I)/1000.0)*(V(I)/1000.0)
     $        +B*EO*(VO/1000.0)*(VO/1000.0)
      CALL PCALC(E(I-1),P(I-1),V(I),Q(I),R(I),RP(I),VO,DELV,PEQ2VS)
      B=B/U(I)
      DELP=PEQ2VS-P(I)
      ENDIF
C
      ENDIF
C
      IF (V(I).GE.VS) THEN
      C=V(I)/VO-1.0
      U(I)=DEXP(-ALF*C*C)
      S(I)=AA*MU(I)*DEXP(-BET*C)
      B=B*U(I)
      Q(I)=U(I)*S(I)
      RP(I)=A*E(I-1)*(V(I)/1000.0)*(V(I)/1000.0)
     $        +B*EO*(VO/1000.0)*(VO/1000.0)
      CALL PCALC(E(I-1),P(I-1),V(I),Q(I),R(I),RP(I),VO,DELV,PEQ2)
      B=B/U(I)
      P(I)=PEQ2-DELP
      ENDIF
C
      ENDIF
C
      IF (JCOPT.EQ.2.AND.V(I).GE.VO) THEN
C
C.....  IMPLEMENTATION OF PURE MIXED PHASE FORMULATION
C
      IF (E(I-1).LT.IVE) THEN
      Q(I)=AA*MU(I)+BB*MU(I)*MU(I)
      RP(I)=A*E(I-1)*(V(I)/1000.0)*(V(I)/1000.0)
     $        +B*EO*(VO/1000.0)*(VO/1000.0)
      CALL PCALC(E(I-1),P(I-1),V(I),Q(I),R(I),RP(I),VO,DELV,P(I))
      ENDIF
C
      IF (E(I-1).GE.IVE.AND.E(I-1).LT.ESP) THEN
      Q(I)=AA*MU(I)+BB*MU(I)*MU(I)
      RP(I)=A*E(I-1)*(V(I)/1000.0)*(V(I)/1000.0)
     $        +B*EO*(VO/1000.0)*(VO/1000.0)
      CALL PCALC(E(I-1),P(I-1),V(I),Q(I),R(I),RP(I),VO,DELV,PC)
      C=V(I)/VO-1.0
      U(I)=DEXP(-ALF*C*C)
```

```
      S(I)=AA*MU(I)*DEXP(-BET*C)
      B=B*U(I)
      Q(I)=U(I)*S(I)
      RP(I)=A*E(I-1)*(V(I)/1000.0)*(V(I)/1000.0)
     $         +B*EO*(VO/1000.0)*(VO/1000.0)
      CALL PCALC(E(I-1),P(I-1),V(I),Q(I),R(I),RP(I),VO,DELV,PE)
      B=B/U(I)
      T1=PE*(E(I-1)-IVE)
      T2=PC*(ESP-E(I-1))
      DEN=ESP-IVE
      P(I)=(T1+T2)/DEN
      ENDIF
C
      IF (E(I-1).GE.ESP) THEN
      C=V(I)/VO-1.0
      U(I)=DEXP(-ALF*C*C)
      S(I)=AA*MU(I)*DEXP(-BET*C)
      B=B*U(I)
      Q(I)=U(I)*S(I)
      RP(I)=A*E(I-1)*(V(I)/1000.0)*(V(I)/1000.0)
     $         +B*EO*(VO/1000.0)*(VO/1000.0)
      CALL PCALC(E(I-1),P(I-1),V(I),Q(I),R(I),RP(I),VO,DELV,P(I))
      B=B/U(I)
      ENDIF
C
      ENDIF
C
C.....  CALCULATE ENERGIES BASED ON RELEASE APPROXIMATION OPTION
C
      IF (ROPT.EQ.1) THEN
      E(I)=E(I-1)-P(I-1)*DELV/1000.0
      ENDIF
      IF (ROPT.EQ.2) THEN
      E(I)=E(I-1)-0.5*(P(I-1)+P(I))*DELV/1000.0
      ENDIF
      IF (ROPT.EQ.3) THEN
      E(I)=E(I-1)-P(I)*DELV/1000.0
      ENDIF
C
      DP=P(I)-P(I-1)
      IF (DP.GE.0.0) THEN
      WRITE (2,11) I
   11 FORMAT('*** AN ERROR HAS OCCURRED IN RELEASE PROCESS AT THE ',I3,
     $'-TH ITERATION ***')
      STOP
      ENDIF
      DUR=DSQRT(-DP*(DELV/1000.0))
      UR=UR+DUR/1000.0
      II=II+1
      IF (P(I).GE.0.0) THEN
      IF (ROPT.EQ.1) DE=DE+P(I-1)*DELV/1000.0
      IF (ROPT.EQ.2) DE=DE+0.5*(P(I)+P(I-1))*DELV/1000.0
      IF (ROPT.EQ.3) DE=DE+P(I)*DELV/1000.0
      ADP=DABS(DP)
      DPR=ADP/(P(I-1)+DELP)
      IF (DPR.LT.EPS) GOTO 15
      ENDIF
      IF (P(I).LT.0.0) GOTO 15
   10 CONTINUE
C
   15 EX=E(1)-DE
      VF=V(II)
      UFS1=UP+UR
      UFS2=2.0*UP
```

```
C
      WRITE(2,20) VF,E(1),DE,EX
   20 FORMAT(/,'END-STATE CALCULATION RESULTS USING THE TILLOTSON EOS ..
     $.',/,'MATERIAL FIN SP VOL (VF) ..... ',F10.3,' CU.CM./GM',/,
     $'MATERIAL SHOCK ENERGY ..... ',E10.4,' JOULES/KG',/,'MATERIAL E
     $NERGY RECOVERED .... ',E10.4,' JOULES/KG',/,'WASTE HEAT GENERATED
     $..... ',E10.4,' JOULES/KG')
C
      RETURN
      END
C
      SUBROUTINE PCALC(E,P,V,Q,R,RP,VO,DELV,PI)
      IMPLICIT DOUBLE PRECISION (A-H,O-Z)
      INTEGER ROPT
      COMMON/TDATA/A,B,AA,BB,ALF,BET,EO,EOM,EOI,ROPT,JCOPT
C
C.....  CALCULATE PRESSURES BASED ON RELEASE APPROXIMATION OPTION
C
      IF (ROPT.EQ.1) THEN
      T1=E-P*DELV/1000.0
      DT1=T1/EO
      DEN=DT1*(V/VO)*(V/VO)+1
      PI=(A+B/DEN)*(T1/(V/1000.0))+Q
      ENDIF
C
      C2P=0.0
      C3P=0.0
      IF (ROPT.EQ.2) THEN
      DELV=DELV/2.0
      C2P=P*(DELV/1000.0)*(V/1000.0)*(V/1000.0)*(1.0+A*(2.0*DELV/V))
      C3P1=(1.0+A)*E*(V/1000.0)*(V/1000.0)
     $       +(1.0+B)*EO*(VO/1000.0)*(VO/1000.0)
     $       +Q*(V/1000.0)*(V/1000.0)*(V/1000.0)
      C3P=P*(DELV/1000.0)*C3P1
     $      -(P*(DELV/1000))*(P*(DELV/1000.0))*(V/1000.0)*(V/1000.0)
      ENDIF
C
      IF (ROPT.EQ.2.OR.ROPT.EQ.3) THEN
      C1=(V/1000.0)*(DELV/1000.0)*(1.0+A*(DELV/V))
      C2=C1*R/((V/1000.0)*(DELV/1000.0))+(DELV/V)*RP
     $     +Q*(V/1000.0)*(V/1000.0)*(DELV/1000.0)-C2P
      C3=(A*E+Q*(V/1000.0))*R+B*E*EO*(VO/1000.0)*(VO/1000.0)-C3P
      DISC=C2*C2-4.0*C1*C3
      PI1=(C2+DSQRT(DISC))/(2.0*(V/1000.0)*C1)
      PI2=(C2-DSQRT(DISC))/(2.0*(V/1000.0)*C1)
      PI=PI2
      ENDIF
C
      IF (ROPT.EQ.2) DELV=2.0*DELV
C
      RETURN
      END
C
      SUBROUTINE TINC(SHS,SHL,TM,TV,HF,HV,EXH,IME,IVE,PS,PL,PV,TR)
      IMPLICIT DOUBLE PRECISION (A-H,O-Z)
      DOUBLE PRECISION IME,IVE
C
C.....  THIS SUBROUTINE CALCULATES THE RESIDUAL TEMPERATURE INCREASE
C.....  IN A MATERIAL THAT HAS BEEN RELEASED FROM THE SHOCKED STATE
C.....  AND ESTIMATES THE PERCENTAGES OF VAPORIZED, MELTED, AND SOLID
C.....  MATERIAL DUE TO THE RELEASE PROCESS.
C
C.....  IF WASTE HEAT IS LESS THAN THE ENERGY REQ'D TO START MELT,
C.....  CALCULATE TEMPERATURE RISE USING W.H.=S.H.*(TEMP.INCR.)
```

```
C
      IF (EXH.LT.IME) THEN
      DT=EXH/SHS
      TR=DT
      DEL=0.0
      WRITE(2,50) IME,DEL,EXH
   50 FORMAT('ENERGY REQ, INCIPIENT MELT ... ',E10.4,' JOULES/KG',/,
     $'ENERGY AVAILABLE FOR MELT .... ',E10.4,' JOULES/KG',/,
     $'EXCESS ENERGY AVAILABLE ..... ',E10.4,' JOULES/KG')
      PV=0.0
      PL=0.0
      PS=100.0
      GOTO 100
      ENDIF
C
C.....  IF WASTE HEAT EXCEEDS THE ENERGY REQ'D TO START MELT, BUT IS
C.....  LESS THAN THAT REQ'D TO COMPLETE MELT, RESET THE VALUE OF THE
C.....  ENERGY AVAILABLE FROM THE WASTE HEAT VALUE TO THE VALUE REQ'D
C.....  TO START MELT.  THIS IMPLIES THAT SOME ENERGY IS AVAILABLE FOR
C.....  MELTING A PORTION OF THE MATERIAL.  NOTE: THE TEMPERATURE RISE
C.....  EQUALS THE MELT TEMPERATURE OF THE MATERIAL.
C
      IF (EXH.GE.IME.AND.EXH.LT.IME+HF) THEN
      TR=TM
      DEL=EXH-IME
      REQM=IME+HF
      WRITE(2,60) IME,REQM,DEL
   60 FORMAT('ENERGY REQ, INCIPIENT MELT ... ',E10.4,' JOULES/KG',/,
     $'ENERGY REQ, COMPLETE MELT .... ',E10.4,' JOULES/KG',/,
     $'ENERGY AVAILABLE FOR MELT .... ',E10.4,' JOULES/KG')
      PV=0.0
      PL=100.0*DEL/HF
      PS=100.0-PL
      GOTO 100
      ENDIF
C
C.....  IF THE WASTE HEAT EXCEEDS THE ENERGY REQ'D TO COMPLETELY MELT
C.....  THE MATERIAL, BUT IS LESS THAN THAT REQ'D TO START VAPORIZA-
C.....  TION, COMPUTE THE TEMPERATURE INCREASE CAUSED BY THE EXCESS
C.....  ENERGY AND ADD IT TO THE MELT TEMPERATURE OF THE MATERIAL.
C
      IF (EXH.GE.IME+HF.AND.EXH.LT.IVE) THEN
      DEL=EXH-IME-HF
      DT=DEL/SHL
      TR=TM+DT
      REQM=IME+HF
      WRITE(2,70) IME,REQM,DEL
   70 FORMAT('ENERGY REQ, INCIPIENT MELT ... ',E10.4,' JOULES/KG',/,
     $'ENERGY REQ, COMPLETE MELT .... ',E10.4,' JOULES/KG',/,
     $'EXCESS ENERGY AVAILABLE ..... ',E10.4,' JOULES/KG')
      PV=0.0
      PL=100.0
      PS=0.0
      GOTO 100
      ENDIF
C
C.....  IF WASTE HEAT EXCEEDS THE ENERGY REQ'D TO START VAPORIZATION,
C.....  BUT IS LESS THAN THAT REQ'D TO COMPLETE VAPORIZATION, RESET THE
C.....  VALUE OF THE ENERGY AVAILABLE FROM THE WASTE HEAT VALUE TO THE
C.....  VALUE REQ'D TO START VAPORIZATION.  THIS IMPLIES THAT SOME
C.....  ENERGY IS AVAILABLE FOR VAPORIZING A PORTION OF THE MATERIAL.
C.....  NOTE: THE TEMPERATURE RISE EQUALS THE VAPORIZATION TEMPERATURE
C.....  OF THE MATERIAL.
C
```

```
      IF (EXH.GE.IVE.AND.EXH.LT.IVE+HV) THEN
      DEL=EXH-IVE
      REQV=IVE+HV
      TR=TV
      WRITE(2,80) IVE,REQV,DEL
   80 FORMAT('ENERGY REQ, INCIPIENT VAP .... ',E10.4,' JOULES/KG',/,
     $'ENERGY REQ, COMPLETE VAP ..... ',E10.4,' JOULES/KG',/,
     $'ENERGY AVAILABLE FOR VAP ..... ',E10.4,' JOULES/KG')
      PV=100.0*DEL/HV
      PL=100.0-PV
      PS=0.0
      GOTO 100
      ENDIF
C
      IF (EXH.GE.IVE+HV) THEN
      ECVAP=IVE+HV
      PV=100.0
      PL=0.0
      PS=0.0
      WRITE (2,90) ECVAP
   90 FORMAT('ENERGY REQ, COMPLETE VAP ..... ',E10.4,' JOULES/KG',/,
     $'*** THE MATERIAL IS COMPLETELY VAPORIZED ***')
      GOTO 120
      ENDIF
C
  100 WRITE(2,110) TR,PS,PL,PV
  110 FORMAT('RESIDUAL MATERIAL TEMP ..... ',F10.3,' DEG-C',//,'PERCEN
     $T OF SHOCKED AND RELEASED MATERIAL ...',/,3X,'IN SOLID STATE ... '
     $,F6.2,'%',/,3X,'IN MOLTEN FORM ... ',F6.2,'%',/,3X,'IN VAPOR FORM
     $.... ',F6.2,'%')
C
  120 RETURN
      END
C
      SUBROUTINE TMCALC(V,PS,PL,PV,RP,RT,TR,TM,TV,TS,LP,DP,BHN,TSOL,
     $                  MS,ML,MV,MTARG,HCOPT,SY,SU,UTS,UPS,UTP,UPP,
     $                  MUSM,MSR)
      IMPLICIT DOUBLE PRECISION (A-H,O-Z)
      DOUBLE PRECISION LP,MTARG,MS,ML,MV,MUSM,MSR,MTSR
      INTEGER HCOPT
C
C.....  THIS SUBROUTINE CALCULATES THE MASSES OF SOLID, LIQUID, AND
C.....  GASEOUS TARGET MATERIAL IN THE DEBRIS CLOUD.
C
      LP=LP*2.54
      DP=DP*2.54
      TS=TS*2.54
      T22=0.72*DP
      CST=CS(UTS,UTP)
      CSP=CS(UPS,UPP)
      T1N=CSP+UPS-UPP
      T1D=CST-UTS+UTP
      T1=T1N/T1D
      T2=CST/CSP
      T3=UTS/UPS
      T42=LP*T1*T2*T3
      PI=4.0*ATAN(1.0)
      DS=(1.5*DP*DP*LP)**0.3333333333
C
C.....  NOTE: THE PROJECTILE LENGTH AND DENSITY PASSED TO THE HOLE
C.....        DIAMETER CALCULATOR SUBROUTINES IS THE TOTAL LENGTH OF
C.....        THE PROJECTILE AND ITS AVERAGE MATERIAL DENSITY,
C.....        RESPECTIVELY
C
```

```
      IF (HCOPT.EQ.1) CALL DHOLE1(TS,DP,RP,V,DH)
      IF (HCOPT.EQ.2) CALL DHOLE2(TS,DP,RP,RT,LP,V,BHN,SY,DS,DH)
      IF (HCOPT.EQ.3) CALL DHOLE3(TS,DP,RP,RT,LP,V,BHN,DH)
      IF (HCOPT.EQ.4) CALL DHOLE4(TS,DP,RP,RT,V,SY,DH)
      IF (HCOPT.EQ.5) DH=DP
      MTARG=PI*(DH/2.0)*(DH/2.0)*TS*RT
      MTSR=PI*(DP/2.0)*(DP/2.0)*TS*RT
C
      CALL SORT(TS,T22,T42,TO)
      FSR=TO/TS
C
      IF (FSR.LT.1.0) THEN
      WRITE (2,50) TO,TS
   50 FORMAT(/,'DEPTH OF TARG MATL SUBJ TO S&R = ',F9.4,' CM < TARG THIC
     $KNESS = ',F9.4,' CM.',/,'PROGRAM HALTED IN SUBROUTINE TMCALC.')
      WRITE (*,50) TO,TS
      STOP
      ENDIF
C
      MSR=FSR*MTSR
      MUSM=MTSR-MSR
      MS=(PS/100.0)*MSR
      ML=(PL/100.0)*MSR
      MV=(PV/100.0)*MSR
      TSOL=MTARG-MSR+MS
      TNS=MTARG-TSOL
C
      WRITE (2,20) RP,LP,DP,TS,DH,MTARG,TO,MSR,MUSM,MSR,MS,ML,MV,
     $                TSOL,TNS
   20 FORMAT(/,'AVG PROJ DENSITY ..... ',F9.4,' GM/CU.CM.',/,'TOTAL PR
     $OJ LENGTH ..... ',F9.4,' CM',/,'PROJECTILE DIAMETER .... ',F9.4,
     $' CM',/,'TARG PLATE THICKNESS ... ',F9.4,' CM',/,'TARG PLATE HOLE
     $DIA .... ',F9.4,' CM',//,'MASS OF REMOVED TARG MATL ..... ',
     $F9.4,' GMS',/,'DEPTH OF TARG MATL SUBJ TO S&R ..... ',F9.4,' CM',
     $/,'TOT MASS OF TARG MATL SUBJ TO S&R ... ',F9.4,' GMS',/,'MASS OF
     $UNSH TARGET MATL ..... ',F9.4,' GMS',/,'MASS OF SH AND REL
     $TARG MATL ..... ',F9.4,' GMS',/,3X,'MASS OF S&R SOLID MATL ....
     $..... ',F9.4,' GMS',/,3X,'MASS OF S&R LIQUID MATL ..... ',
     $F9.4,' GMS',/,3X,'MASS OF S&R VAPOR MATL ..... ',F9.4,' GMS'
     $,/,'TOTAL SOLID MASS COMPONENT ..... ',F9.4,' GMS',/,'TOTAL N
     $ON-SOLID COMPONENT ..... ',F9.4,' GMS')
C
      RETURN
      END
C
      SUBROUTINE DHOLE1(TS,DP,RP,V,DH)
      IMPLICIT DOUBLE PRECISION (A-H,O-Z)
C
C.....  THIS SUBROUTINE CALCULATES THE HOLE IN A THIN PLATE DUE TO
C.....  THE NORMAL IMPACT OF A SOLID RIGHT CIRCULAR CYLINDER USING
C.....  KAPPII EQUATION HSSO1 (KAPPII USER'S MANUAL).
C
      A=
      B=
      C=
      T1=DEXP(A*RP)
      T2=1.0-DEXP(-C*TS/DP)
      DHDP=T1*(1.0+B*V*T2)
      DH=DP*DHDP
      IF (DH.LT.DP) DH=DP
      RETURN
      END
C
      SUBROUTINE DHOLE2(TS,DP,RP,RT,LP,V,BHN,SY,DS,DH)
```

```
      IMPLICIT DOUBLE PRECISION (A-H,O-Z)
      DOUBLE PRECISION KT,LP
C
C.....  THIS SUBROUTINE CALCULATES THE HOLE IN A THIN PLATE DUE TO
C.....  THE NORMAL IMPACT OF A SOLID RIGHT CIRCULAR CYLINDER USING
C.....  KAPPII EQUATION HSSO2 (KAPII USER'S MANUAL).
C
      A=
      B=
      E=
      KT=
      FW=
      T1=RT/RP
      T2=RP*V*V/(2.0*E*BHN)
      R1=A*(T1**B)*(T2**0.3333333333)
      U=DSQRT(T1)
      PWR=V*V*(RP/2.0/SY)*U/(1.0+U)
      SV=1.0-DEXP(-1000.0*PWR)
      AR=LP/DP
      IF (AR.GE.1.0) PDP=(SV/U)*(AR-1.0+R1/2.0)
      IF (AR.LE.1.0) PDP=(SV/U)*(R1*DP/DS/2.0)*(AR**0.3333333333)
      P=PDP*DP
      DRC=0.533*(RP/RT)+0.467
      RC=P/DSQRT(DRC)
      Q=1.0-(DP/2.0/RC)**2
      IF (Q.LT.0.0) THEN
      DH=-1.0
      RETURN
      ENDIF
      IF (Q.GE.0.0) THEN
      T=KT*TS+P*(1.0-DSQRT(Q))
      DH=2.0*FW*(RC/P)*DSQRT(T*(2.0*P-T))
      IF (DH.LT.DP) DH=DP
      RETURN
      ENDIF
      END
C
      SUBROUTINE DHOLE3(TS,DP,RP,RT,LP,V,BHN,DH)
      IMPLICIT DOUBLE PRECISION (A-H,O-Z)
      DOUBLE PRECISION K,LP
C
C.....  THIS SUBROUTINE CALCULATES THE HOLE IN A THIN PLATE DUE TO
C.....  THE NORMAL IMPACT OF A SOLID RIGHT CIRCULAR CYLINDER USING
C.....  KAPPII EQUATION HSAO1 (KAPPII USER'S MANUAL).
C
      A=
      B=
      C=
      E=
      F=
      G=
      K=F*((BHN/RP)**G)
      R1=RP/RT
      R2=(3.0*LP)/(2.0*DP)
      R3=(RP*V*V)/(2.0*E*BHN)
      DR=A*(R1**B)*(R2**C)*(R3**0.3333333333)
      R4=(TS/DP)**0.6666666666
      DHDP=1.0+(DR-1.0)*(1.0-DEXP(-K*R4))
      DH=DP*DHDP
      IF (DH.LT.DP) DH=DP
      RETURN
      END
C
      SUBROUTINE DHOLE4(TS,DP,RP,RT,V,SY,DH)
```

```
      IMPLICIT DOUBLE PRECISION (A-H,O-Z)
C
C.....  THIS SUBROUTINE CALCULATES THE HOLE IN A THIN PLATE DUE TO
C.....  THE NORMAL IMPACT OF A SOLID SPHERE USING THE PEN4.V10 HOLE
C.....  DIAMETER EQUATION (BOEING-D180-30550-2).
C
      R1=DP/TS
      R2=1000.0*RP*V*V/SY
      R3=RP/RT
      T1=R1*(R2**0.415)/(R3**0.15)/29.9
      DHTS=11.02*(1.0-DEXP(-T1))
      DH=TS*DHTS
      IF (DH.LT.DP) DH=DP
      RETURN
      END
C
      SUBROUTINE UPPCAL(RPA,RPB,KPA,KPB,COPA,COPB,V1,UPP)
      IMPLICIT DOUBLE PRECISION (A-H,O-Z)
      DOUBLE PRECISION KPA,KPB
C
C.....  THIS SUBROUTINE CALCULATES THE PARTICLE VELOCITY IN A MATERIAL
C.....  'B' DUE TO A SHOCK WAVE THAT HAS ENTERED MATERIAL 'B' FROM AN
C.....  ADJACENT MATERIAL 'A'
C
      A=RPA*KPA-RPB*KPB
      B=RPA*COPA+RPB*COPB+4.0*RPA*KPA*V1
      P1=2.0*RPA*V1*(COPA+2.0*KPA*V1)
      DISC=B*B-4.0*A*P1
      UPP=(B-SQRT(DISC))/(2.0*A)
C
      RETURN
      END
C
      SUBROUTINE SORT(A,B,C,SM)
      IMPLICIT DOUBLE PRECISION (A-H,O-Z)
      SM=A
      IF (SM.GT.B) SM=B
      IF (SM.GT.C) SM=C
      RETURN
      END
C
      SUBROUTINE DCVEL(UFST1,UFSP1,V,MTARG,MPROJ,MPLYR,MTSR,MPSR,MUSTM
     $                 ,MUSPM,PMSSNR,EXT,EXP,FSRP,NPMAT)
      IMPLICIT DOUBLE PRECISION (A-H,O-Z)
      DOUBLE PRECISION MDC,MPROJ,MTARG,MUSTM,MTSR
      DOUBLE PRECISION MUSPM(10),MPSR(10),EXP(10),FSRP(10),MPLYR(10),
     $                  UFSP1(10),PMSSNR(10)
      CHARACTER*1 ALLSR
C
C....   THIS SUBROUTINE COMPUTES DEBRIS CLOUD VELOCITIES AND THE DEBRIS
C....   CLOUD SEMI-CONE ANGLE.  FIRST, A CHECK IS PERFORMED TO SEE IF
C....   ANY UNSHOCKED PROJECTILE MATERIAL REMAINS.
C
      ALLSR='Y'
      DO 10 I=1,NPMAT
      IF (FSRP(I).NE.1) THEN
      ALLSR='N'
      GOTO 100
      ENDIF
   10 CONTINUE
C
C....   IF NO UNSHOCKED PROJECTILE MATERIAL REMAINS, THEN ALL OF THE
C....   PROJECTILE MATERIAL COMBINES WITH THE TARGET MATERIAL TO FORM
C....   THE DEBRIS CLOUD.
```

```
C
      VL=UPST1
      VR=V-UPSP1(NPMAT)
      VCOM=MPROJ*V/(MTARG+MPROJ)
      EIMP=(MPROJ/1000.0)*(V*1000.0)*(V*1000.0)/2.0
      E1=EXT*MTSR/1000.0
      E2=0.0
      DO 20 I=1,NPMAT
      E2=E2+EXP(I)*MPSR(I)/1000.0
   20 CONTINUE
      E3=(MPROJ/1000.0+MTARG/1000.0)*(VCOM*1000.0)*(VCOM*1000.0)/2.0
      DELE=EIMP-E1-E2-E3
      DELM=(MPROJ+MTARG)/1000.0
      VEXP=SQRT(2.0*DELE/DELM)/1000.0
      VEXP1=(VL-VR)/2.0
C
      WRITE(2,30)
   30 FORMAT(/,'NO UNSHOCKED RESIDUAL PROJECTILE FRAGMENT REMAINS.',/,
     $'ANY SOLID PROJECTILE AND TARGET MATERIAL REMAINING',/,'IS LIKELY
     $TO BE FRAGMENTED.')
      WRITE(2,40) VR,VR/V,VCOM,VCOM/V,VL,VL/V,VEXP,VEXP/V,VEXP1,
     $            VEXP1/V
   40 FORMAT(/, DEBRIS CLOUD VELOCITY SUMMARY ...',/,3X,'REAR SURFACE VE
     $LOCITY (VR) .............',F7.3,' KM/SEC (=',F5.3,'V)',/,3X,'CENTER
     $-OF-MASS VELOCITY (VCOM) .........',F7.3,' KM/SEC (=',F5.3,'V)',/,
     $3X,'LEADING EDGE VELOCITY (VL) .............',F7.3,' KM/SEC (=',
     $F5.3,'V)',/,3X,'EXPANSION VEL (VEXP -> ENERGY CONS) ...',F7.3,' KM
     $/SEC (=',F5.3,'V)',/,3X,'EXPANSION VEL (VEXP = (VF-VR)/2) ......',
     $F7.3,' KM/SEC (=',F5.3,'V)')
C
      GOTO 200
C
C....   IF SOME UNSHOCKED PROJECTILE MATERIAL REMAINS, THEN INVOKE THE
C....   ALTERNATIVE DEBRIS CLOUD VELOCITY CHARACTERIZATION SCHEME.
C
  100 CONTINUE
      VL=UPST1
      TPWH=0.0
      TMUSPM=0.0
      MDC=MPROJ+MTARG
      DO 110 I=1,NPMAT
      TPWH=TPWH+EXP(I)*MPSR(I)
      TMUSPM=TMUSPM+MUSPM(I)+PMSSNR(I)
      MDC=MDC-MUSPM(I)-PMSSNR(I)
  110 CONTINUE
      A=2.0+MDC/TMUSPM
  115 B=VL+(MPROJ/TMUSPM)*V
      C1=VL*VL
      C2=(MPROJ/TMUSPM-1.0)*(MPROJ/MDC)*V*V
      C3=2.0*(EXT*MTSR/1000.0+TPWH/1000.0)/1000.0/MDC
      C=C1+C2+C3
      DISC=(B/A)*(B/A)-C/A
      IF (DISC.LT.0.0)THEN
      VL=VL-0.1
      GOTO 115
      ENDIF
      VCOM=B/A-SQRT(DISC)
      VEXP=VL-VCOM
      VRES=(MPROJ*V-MDC*VCOM)/TMUSPM
C
      WRITE(2,120)
  120 FORMAT(/,'SOME UNSHOCKED PROJ MATL REMAINS ...')
      WRITE(2,130) TMUSPM,TMUSPM/MPROJ,VRES,VRES/V
  130 FORMAT(/,3X,'TOT MPROJ,UNSH ...',F7.3,' GMS  (=',F5.3,'MPROJ)',/,
```

```
     $3X,'AVG VP,UNSH ......',F7.3,' KM/S (=',F5.3,'V)',//,'ALL OTHER SO
     $LID PROJECTILE MATERIAL (IF ANY) IS LIKELY TO BE FRAGMENTED.',/,
     $'ANY SOLID TARGET MATERIAL REMAINING IS ALSO LIKELY TO BE FRAGMENT
     $ED.',/,'THE DEBRIS CLOUD CONSISTS OF SHOCKED AND RELEASED PROJECTI
     $LE MATERIAL AND',/,'ALL EJECTED TARGET MATERIAL.')
C
      WRITE(2,140) VCOM,VCOM/V,VL,VL/V,VEXP,VEXP/V
  140 FORMAT(/,'DEBRIS CLOUD VELOCITY SUMMARY ...',/,3X,'DEB CLD CENTER-
     $OF-MASS VEL (VCOM) ...',F7.3,' KM/SEC (=',F5.3,'V)',/,3X,'DEB CLD
     $LEADING EDGE VEL (VL) .......',F7.3,' KM/SEC (=',F5.3,'V)',/,3X,
     $'DEB CLD EXPANSION VEL (VEXP) ........',F7.3,' KM/SEC (=',F5.3,
     $'V)')
C
  200 DCANG=ATAN(VEXP/VCOM)
      DCANG=(180.0/3.141592)*DCANG
C
      WRITE(2,498) DCANG
  498 FORMAT(//,'DEBRIS CLOUD HALF-ANGLE .........',F7.3,' DEG')
C
      RETURN
      END
C
      DOUBLE PRECISION FUNCTION CS(US,UP)
      IMPLICIT DOUBLE PRECISION (A-H,O-Z)
C
C.....  THIS FUNCTION CALCULATES THE SPEED OF A RAREFACTION WAVE IN A
C.....  SHOCKED MEDIUM
C
      T1=(US-UP)/US
      CSQ=US*US*(0.49+T1*T1)
      CS=DSQRT(CSQ)
      RETURN
      END
C
      SUBROUTINE RSINT(NPMAT,UTS,UTP,UPSA,UPPA,LPA,DP,TS,V,LO)
      IMPLICIT DOUBLE PRECISION (A-H,O-Z)
      DOUBLE PRECISION LO,L11,L41,LPTOT,UPPA(10),UPSA(10),CSP(10),
     $VE(10),VD(10),VC(10),TE(10),XE(10),TD(10),TDSUM(10),LPA(10)
C
C.....  THIS SUBROUTINE CALCULATES THE LOCATION WITHIN THE PROJECTILE
C.....  AT WHICH THE TARGET RAREFACTION WAVE OVERTAKES THE PROJECTILE
C.....  SHOCK WAVE
C
      L11=0.72*DP*2.54
      CST=CS(UTS,UTP)
      VB=CST-UTP
      VA=UTS
      TC=(TS/VA)*(VB+VA)/(VB+UTP)
      LPTOT=LPA(1)*2.54
      VC(1)=UTP
      DO 10 I=2,NPMAT
      VC(I)=UPPA(I)
      LPTOT=LPTOT+LPA(I)*2.54
   10 CONTINUE
C
      I=0
   99 CONTINUE
      I=I+1
      CSP(I)=CS(UPSA(I),UPPA(I))
      VE(I)=UPSA(I)-V
C
C.....  CONSIDER THE FIRST MATERIAL LAYER OF THE PROJECTILE.
C
      IF (I.EQ.1) THEN
```

```
      VD(1)=CSP(1)-UTP
      XET=VE(1)*(VD(1)+VC(1))*TC/(VD(1)-VE(1))
      XES=XET
      TET=XET/VE(1)
      TES=TET
      XDT=XET*V/VE(1)
      L41=(XES+XDT)*2.54
      CHKL1=LPA(1)*2.54
      CALL SORT(CHKL1,L11,L41,LO)
C
C.....  IF ONLY ONE PROJECTILE MATERIAL IS INVOLVED, RETURN MIN VALUE
C.....  AS THE LOCATION ALONG THE PROJECTILE AXIS OF THE INTERSECTION
C.....  OF THE RAREFACTION WAVE AND THE SHOCK WAVE.
C
      IF (NPMAT.EQ.1) GOTO 40
C
C.....  IF THERE IS MORE THAN ONE PROJECTILE MATERIAL LAYER AND THE MIN
C.....  VALUE EXCEEDS THE THICKNESS OF THE MATERIAL LAYER, THEN THE
C.....  SHOCK WAVE IS OVERTAKEN AT A POINT BEYOND THE THICKNESS OF THE
C.....  FIRST LAYER.  INITIALIZE ARRAY ENTRIES REQUIRED FOR NEXT LAYER
C.....  CALCULATIONS AND MOVE ON TO THE SECOND MATERIAL LAYER.
C
      IF (NPMAT.GE.2.AND.LO.GT.LPA(1)) THEN
      TE(1)=LPA(1)/(VE(1)+V)
      XE(1)=VE(1)*TE(1)
      TD(1)=(XE(1)+VC(2)*TE(1))/(VD(1)+VC(2))
      COEF=(VC(1)-VC(2))/(VD(1)+VC(2))
      TC(1)=TD(1)+COEF*TC
      GOTO 99
      ENDIF
C
C.....  IF THERE IS MORE THAN ONE PROJECTILE MATERIAL LAYER AND THE MIN
C.....  VALUE LIES WITHIN THE FIRST LAYER, THEN THE SHOCK WAVE IS OVER-
C.....  TAKEN BY A RAREFACTION WAVE WITHIN THE FIRST LAYER.
C
      IF (NPMAT.GE.2.AND.LO.LE.LPA(1)) GOTO 40
      ENDIF
C
C.....  CONSIDER THE REMAINING PROJECTILE LAYERS
C
      IF (I.GE.2) THEN
      VD(I)=CSP(I)-UPPA(I)
      XES=0.0
      TES=0.0
      TDIFF=TC
      DO 20 J=1,I-1
      XES=XES+XE(J)
      TES=TES+TE(J)
      TDIFF=TDIFF+TD(J)-TE(J)
   20 CONTINUE
      XET=VE(I)*(VD(I)+VC(I))*TDIFF/(VD(I)-VE(I))
      XES=XES+XET
      TET=XET/VE(I)
      TES=TES+TET
      XDTP=XET*V/VE(I)
      XDT=XDTP*TES/TET
      L41=(XES+XDT)*2.54
      CHKLI=0.0
      DO 30 J=1,I
      CHKLI=CHKLI+LPA(J)*2.54
   30 CONTINUE
      CALL SORT(CHKLI,L11,L41,LO)
C
C.....  IF THE MIN VALUE EXCEEDS THE CUMULATIVE LENGTH OF THE PROJECTILE
```

```
C.....  MATERIAL THROUGH THE CURRENT LAYER, THEN THE SHOCK WAVE IS OVER-
C.....  TAKEN AT A POINT BEYOND THE THICKNESS OF THE CURRENT LAYER AND LO
C.....  IS SET EQUAL TO THE CURRENT CUMULATIVE LENGTH.  INITIALIZE ARRAY
C.....  ENTRIES REQUIRED FOR NEXT LAYER CALCULATIONS AND MOVE ON TO THE
C.....  NEXT MATERIAL LAYER (UNLESS THIS IS THE FINAL MATERIAL LAYER IN
C.....  WHICH CASE RETURN THE TOTAL PROJECTILE LENGTH AS LO).
C
      IF (LO.EQ.CHKLI) THEN
      IF (I.EQ.NPMAT) THEN
      LO=CHKLI
      GOTO 40
      ENDIF
      IF (I.LT.NPMAT) THEN
      TE(I)=LPA(I)/(VE(I)+V)
      XE(I)=VE(I)*TE(I)
      TD(I)=(XE(I)+VC(I+1)*TE(I))/(VD(I)+VC(I+1))
      TD(I)=TD(I)+(VC(I)-VC(I+1))*TDIFF/(VD(I)+VC(I+1))
      GOTO 99
      ENDIF
      ENDIF
C
C.....  IF THE MIN VALUE LIES WITHIN THE CURRENT LAYER, THEN THE SHOCK
C.....  WAVE IS OVERTAKEN BY A RAREFACTION WAVE WITHIN THE CURRENT LAYER.
C
      IF (LO.LT.CHKLI) GOTO 40
      ENDIF
C
   40 RETURN
      END
C
      SUBROUTINE PMCALC(I,UPS,UTS,UPP,UTP,RP,PS,PL,PV,TS,LP,DP,TSOL,
     $MS,ML,MV,MPLYR,MUSM,MSR,FSR,PGMSTP,ISTOP,LO,CHKL)
      IMPLICIT DOUBLE PRECISION (A-H,O-Z)
      DOUBLE PRECISION LP,LO,LSR,MPLYR,MS,ML,MV,MSR,MUSM
      CHARACTER*1 PGMSTP
C
C.....  THIS SUBROUTINE CALCULATES THE MASSES OF SOLID, LIQUID, AND
C.....  GASEOUS PROJECTILE MATERIAL IN THE DEBRIS CLOUD.
C
      PI=4.0*ATAN(1.0)
      LP=LP*2.54
      MPLYR=PI*(DP/2.0)*(DP/2.0)*LP*RP
C
      IF (CHKL.GT.LO) THEN
      LSR=LP-(CHKL-LO)
      PGMSTP='Y'
      ENDIF
      IF (CHKL.LE.LO) THEN
      LSR=LP
      PGMSTP='N'
      ENDIF
      FSP=LSR/LP
      MSR=FSR*MPLYR
      MUSM=MPLYR-MSR
      MS=(PS/100.0)*MSR
      ML=(PL/100.0)*MSR
      MV=(PV/100.0)*MSR
      TSOL=MUSM+MS
      TNS=MPLYR-TSOL
C
      WRITE (2,100) RP,LP,DP,MPLYR
  100 FORMAT(/,'PROJECTILE LAYER DENSITY ..... ',F9.4,' GM/CU.CM.',/,
     $'PROJECTILE LAYER LENGTH ..... ',F9.4,' CM',/,'PROJECTILE LAYER D
     $IAMETER .... ',F9.4,' CM',/,'PROJECTILE LAYER MASS ..... ',F9.4
```

```
     $,' GMS')
C
      WRITE (2,200) LO,LSR,MUSM,MSR,MS,ML,MV,TSOL,TNS
  200 FORMAT(/,'PROJ LENGTH WHERE RMAVE HITS SWAVE .... ',F9.4,' CM',/,
     $'LENGTH OF PROJ LYR MATL SUBJ TO S&R ... ',F9.4,' CM',/,'MASS OF U
     $NSH PROJ LYR MATERIAL ..... ',F9.4,' GMS',/,'MASS OF SH AND REL
     $ PROJ LYR MATL ..... ',F9.4,' GMS',/,3X,'MASS OF S&R SOLID LYR MA
     $TL ..... ',F9.4,' GMS',/,3X,'MASS OF S&R LIQUID LYR MATL .....
     $... ',F9.4,' GMS',/,3X,'MASS OF S&R VAPOR LYR MATL ..... ',
     $F9.4,' GMS',/,'TOTAL SOLID LAYER MASS COMPONENT ..... ',F9.4,
     $' GMS',/,'TOTAL NON-SOLID LAYER COMPONENT ..... ',F9.4,' GMS')
C
      ISTOP=I
      RETURN
      END
```

APPENDIX B -- Input File INDATA

---MAT'L---	-----CO----	-----K-----	---RHO----	--GAMO----	---BHN----
--EL.MOD.-	-----NU----	--ALFA----	---CPS----	---CPL----	---EPS----
--T.MELT--	--T.VAP---	--H.FUS---	--H.VAP---	--ALFA----	--BETA----
--YLDSTR--	-ULTSTR---	--ROPT----			
AL					
ALUMINUM	5.380	1.340	2.712	2.130	120.0
0.103E+08	0.35	0.240E-04	0.235	0.255	0.005
660.0	2450.0	95.0	2450.0	5.0	5.0
290.0	434.02				
A1					
2XXX ALUM	5.350	1.340	2.800	2.000	120.0
0.106E+08	0.33	0.209E-04	0.212	0.242	0.005
640.0	2450.0	85.0	2450.0	5.0	5.0
314.0	433.02				
A2					
5XXX ALUM	5.310	1.340	2.670	2.000	84.0
0.101E+08	0.33	0.225E-04	0.215	0.245	0.005
641.0	2450.0	85.0	2450.0	5.0	5.0
211.0	312.02				
A3					
6XXX ALUM	5.380	1.340	2.700	2.000	93.0
0.100E+08	0.33	0.233E-04	0.212	0.242	0.005
652.0	2450.0	85.0	2450.0	5.0	5.0
202.0	268.02				
A4					
7XXX ALUM	5.290	1.340	2.810	2.000	150.0
0.103E+08	0.33	0.221E-04	0.217	0.245	0.005
636.0	2450.0	85.0	2450.0	5.0	5.0
479.0	531.02				
BE					
BERYLLIUM	7.975	1.124	1.820	1.160	120.0
0.419E+08	0.08	0.140E-04	0.570	0.832	0.005
1281.0	2884.0	260.0	8195.0	5.0	5.0
225.0	300.02				
CD					
CADMIUM	2.307	1.640	8.640	2.270	24.0
0.672E+07	0.33	0.343E-04	0.058	0.063	0.005
321.0	765.0	13.5	212.0	5.0	5.0
34.0	52.02				
CU					
COPPER	3.940	1.489	8.930	2.000	37.0
0.190E+08	0.34	0.170E-04	0.097	0.114	0.005
1083.0	2590.0	49.0	1150.0	5.0	5.0
240.0	340.02				
EP					
EPOXY	3.020	1.520	1.180	0.800	-1.0
0.650E+06	0.50	0.500E-04	0.250	0.285	-1.0
350.0	-1.0	-1.0	-1.0	-1.0	-1.0
-1.0	-1.02				
FE					
IRON	4.580	1.490	7.870	1.570	95.0
0.290E+08	0.30	0.120E-04	0.120	0.150	0.005
1539.0	3035.0	65.0	1591.0	5.0	5.0

```
     469.0      550.02
-------------------------------------------------------------------
PB
LEAD             2.030      1.470     11.340      2.770        7.0
 0.200E+07        0.45 0.293E-04      0.031      0.036      0.005
     327.0     1740.0        6.0      210.0       10.0       10.0
       9.0       17.02
-------------------------------------------------------------------
LX
LEXAN            2.750      1.480      1.180      0.860       37.0
 0.345E+06        0.50 0.650E-04      0.290      0.315       -1.0
     225.0       -1.0       -1.0       -1.0       -1.0       -1.0
      -1.0       -1.02
-------------------------------------------------------------------
MO
MOLYBDENUM       5.173      1.220     10.200      1.520      200.0
 0.460E+08        0.31 0.061E-04      0.079      0.104      0.005
    2610.0     5555.0       70.0     1242.0        5.0        5.0
     350.0      450.02
-------------------------------------------------------------------
NI
NICKEL           4.667      1.530      8.860      1.800      200.0
 0.330E+08        0.30 0.143E-04      0.130      0.157      0.005
    1454.0     2865.0       74.0     1523.0        5.0        5.0
      59.0      317.02
-------------------------------------------------------------------
PT
PLATINUM         3.680      1.500     21.370      2.940       70.0
 0.277E+08        0.39 0.110E-04      0.037      0.042      0.005
    1769.0     4349.0       26.0      632.0       10.0       10.0
     100.0      200.02
-------------------------------------------------------------------
S1
304 STEEL        4.590      1.550      7.910      1.670      237.0
 0.284E+08        0.28 0.112E-04      0.110      0.125      0.005
    1425.0     3035.0       65.0     1590.0        5.0        5.0
     250.0      500.02
-------------------------------------------------------------------
S2
430 STEEL        4.680      1.550      7.830      1.670      251.0
 0.299E+08        0.29 0.104E-04      0.110      0.125      0.005
    1470.0     3035.0       65.0     1590.0        5.0        5.0
     275.0      480.02
-------------------------------------------------------------------
S3
4340 STEEL       4.570      1.550      7.830      1.670      290.0
 0.290E+08        0.30 0.112E-04      0.110      0.125      0.005
    1510.0     3070.0       65.0     1590.0        5.0        5.0
     469.0      745.02
-------------------------------------------------------------------
TA
TANTALUM         3.374      1.201     16.650      1.690      200.0
 0.260E+08        0.35 0.065E-04      0.033      0.039      0.005
    2996.0     5425.0       38.0     1007.0       10.0       10.0
     288.0      380.02
-------------------------------------------------------------------
SN
TIN              2.560      1.520      7.280      1.850        4.0
 0.603E+07        0.33 0.269E-04      0.058      0.062      0.005
     235.0     2450.0       14.0      580.0       10.0       10.0
      23.0       31.02
-------------------------------------------------------------------
TI
TITANIUM         4.786      1.049      4.512      1.100      330.0
```

```
 0.180E+08      0.30 0.100E-04      0.150      0.167      0.005
    1676.0    3260.0       99.0    2182.0        5.0        5.0
     810.0    1013.02
-------------------------------------------------------------------
W
TUNGSTEN        4.150      1.237     19.170      1.480      400.0
 0.590E+08      0.30 0.040E-04      0.035      0.046      0.005
    3410.0    5900.0       53.0    1054.0       10.0       10.0
    1379.0    1517.02
-------------------------------------------------------------------
ZN
ZINC            3.042      1.500      7.140      2.150       82.0
 0.108E+08      0.33 0.274E-04      0.100      0.115      0.005
     420.0     907.0       25.0     420.0       10.0       10.0
     138.0     183.02
-------------------------------------------------------------------
AU
GOLD            3.060      1.570     19.240      3.100       33.0
 0.124E+08      0.42 0.161E-04      0.034      0.038      0.005
    1063.0    2960.0       16.0     413.0       10.0       10.0
      95.0     125.02
-------------------------------------------------------------------
AG
SILVER          3.230      2.500     10.490      2.500       25.0
 0.120E+08      0.37 0.211E-04      0.062      0.071      0.005
     961.0    2210.0       25.0     554.0       10.0       10.0
      55.0     175.02
-------------------------------------------------------------------
MG
MAGNESIUM       4.490      1.240      1.740      1.500       45.0
 0.640E+07      0.29 0.300E-04      0.295      0.336      0.005
     650.0    1110.0       88.0    1326.0        5.0        5.0
     197.0     278.02
-------------------------------------------------------------------
XX
-------------------------------------------------------------------
```

APPENDIX C -- Output File IMPOUT

```
HYPERVELOCITY IMPACT OF A   38.240 GM MULTI-MATERIAL PROJECTILE ON A
ALUMINUM   TARGET AT A 10.00 KM/SEC IMPACT VELOCITY

TARGET MATERIAL PROPERTIES ...

   MAT = ALUMINUM
   CO  =   5.380 KM/S
   K   =   1.340
   RHO =   2.712 GM/CU.CM.
   TS  =    .317 CM

PROJECTILE MATERIAL PROPERTIES (DP =   2.540 CM) ...

   MAT  1 = ALUMINUM
   CO     =   5.380 KM/S
   K      =   1.340
   RHO    =   2.712 GM/CU.CM.
   LP     =    .254 CM

   MAT  2 = 4340 STEEL
   CO     =   4.570 KM/S
   K      =   1.550
   RHO    =   7.830 GM/CU.CM.
   LP     =    .254 CM

   MAT  3 = TUNGSTEN
   CO     =   4.150 KM/S
   K      =   1.237
   RHO    =  19.170 GM/CU.CM.
   LP     =    .254 CM

***** TARGET MATERIAL RELEASE CALCULATION *****

INITIAL CONDITIONS FOR TARGET MATERIAL ...
   PARTICLE VELOCITY ..... UP =    5.000 KM/S
   SHOCK WAVE SPEED ..... US =   12.080 KM/S
   HUGONIOT IMPACT PRESSURE .... PH =  163.805 GPA =  1.617 MBAR
   HUGONIOT IMPACT ENERGY ..... EH =  .1250E+08 JOULES/KG
   SPECIFIC VOLUME AT REST ..... V0 =       .369 CU.CM./GM
   SPECIFIC VOLUME AT IMPACT ... V1 =       .216 CU.CM./GM

PARAMETERS REQUIRED FOR CALCULATING TARGET MATERIAL RELEASE FROM SHOCKED
STATE USING THE TILLOTSON EQUATION OF STATE:
   TARG MATL ELASTIC MODULUS ..... E    = .7102E+11 N/SQ.M.
   TARG MATL POISSON RATIO ..... NU   =      .350
   TARG MATL BULK MODULUS ..... K    = .7891E+11 N/SQ.M.
   TARG MATL LIN. COEF. OF THERM. EXP. ... ALFA = .2400E-04 /DEG-C
   TARG MATL SP HEAT (SOLID) ..... CPS  =      .235 CAL/GM/DEG-C
   TARG MATL SP HEAT (LIQUID) ..... CPL  =      .255 CAL/GM/DEG-C
   TARG MATL AMB M-GRUN COEF (CAL,INP) ... GAM0 =    2.129, 2.130
   TARG MATL YIELD STRENGTH ..... SY   =   290.000 MPA
   TARG MATL ULT STRENGTH ..... SU   =   434.000 MPA
   TARG MATL BRN HDNS NO ..... BHN  =   120.000
   TARG MATL MELT TEMPERATURE ..... TM   =    660.00 DEG-C
   TARG MATL VAPOR TEMPERATURE ..... TV   =   2450.00 DEG-C
   TARG MATL HEAT OF FUSION ..... HF   =     95.00 CAL/GM
   TARG MATL HEAT OF VAPORIZATION ..... HV   =   2450.00 CAL/GM
   TARG MATL INICPIENT MELT ENERGY ..... IME  = .6492E+06 JOULES/KG
   TARG MATL INCIPIENT VAPOR ENERGY ..... IVE  = .2958E+07 JOULES/KG

ADDITIONAL PARAMETERS REQUIRED FOR CALCULATING MATERIAL RELEASE FROM
SHOCKED STATE USING THE TILLOTSON EQUATION OF STATE:
   AA  =   .7850E+11 N/SQ.M.
   BB  =   .4831E+11 N/SQ.M.
```

```
   A    =    .5000
   B    =   1.6292
   ALP  =   5.0000
   BET  =   5.0000
   EOI  =    .6687E+07 JOULES/KG
   EOM  =   1.0000
   EO   =    .6687E+07 JOULES/KG
   ES   =    .2958E+07 JOULES/KG
   HV   =    .1026E+08 JOULES/KG
   ESP  =    .1321E+08 JOULES/KG
   VS   =    .4170 CU.CM./GM
   EPS  =    .0050

END-STATE CALCULATION RESULTS USING THE TILLOTSON EOS ...
MATERIAL FIN SP VOL (VF) .....        .494 CU.CM./GM
MATERIAL SHOCK ENERGY ........  .1250E+08 JOULES/KG
MATERIAL ENERGY RECOVERED ....  .9992E+07 JOULES/KG
WASTE HEAT GENERATED .........  .2508E+07 JOULES/KG
ENERGY REQ, INCIPIENT MELT ...  .6492E+06 JOULES/KG
ENERGY REQ, COMPLETE MELT ....  .1047E+07 JOULES/KG
EXCESS ENERGY AVAILABLE ......  .1461E+07 JOULES/KG
RESIDUAL MATERIAL TEMP .......   2028.692 DEG-C

PERCENT OF SHOCKED AND RELEASED MATERIAL ...
   IN SOLID STATE ...    .00%
   IN MOLTEN FORM ... 100.00%
   IN VAPOR FORM ....    .00%

FREE SURF VEL (UP+UR) ........ 10.652 KM/SEC
FREE SURF VEL (2.0*UP) ....... 10.000 KM/SEC

AVG PROJ DENSITY .......    9.9040 GM/CU.CM.
TOTAL PROJ LENGTH ......     .7620 CM
PROJECTILE DIAMETER ....    2.5400 CM
TARG PLATE THICKNESS ...     .3175 CM
TARG PLATE HOLE DIA ....    5.3722 CM

MASS OF REMOVED TARG MATL ...........   19.5174 GMS
DEPTH OF TARG MATL SUBJ TO S&R ......     .3175 CM
TOT MASS OF TARG MATL SUBJ TO S&R ...    4.3631 GMS
MASS OF UNSH TARGET MATL ............     .0000 GMS
MASS OF SH AND REL TARG MATL ........    4.3631 GMS
   MASS OF S&R SOLID MATL ...........     .0000 GMS
   MASS OF S&R LIQUID MATL ..........    4.3631 GMS
   MASS OF S&R VAPOR MATL ...........     .0000 GMS
TOTAL SOLID MASS COMPONENT ..........   15.1543 GMS
TOTAL NON-SOLID COMPONENT ...........    4.3631 GMS

***** PROJECTILE MATERIAL RELEASE CALCULATIONS, LAYER NO. 1 *****

INITIAL CONDITIONS FOR PROJECTILE LAYER NO.  1 MATERIAL ...
   PARTICLE VELOCITY ..... UP =    5.000 KM/S
   SHOCK WAVE SPEED ...... US =   12.080 KM/S
   SHOCK PRESSURE ........ PH =  163.805 GPA =  1.617 MBAR
   SHOCK ENERGY .......... EH =  .1250E+08 JOULES/KG
   SPECIFIC VOLUME (AT REST) ... V0 =       .369 CU.CM./GM
   SPECIFIC VOLUME (SHOCKED) ... V1 =       .216 CU.CM./GM

PARAMETERS REQUIRED FOR CALCULATING RELEASE OF PROJ LAYER NO.  1 MATERIAL
FROM SHOCKED STATE USING THE TILLOTSON EQUATION OF STATE:
   MATL ELASTIC MODULUS ..... E    = .7102E+11 N/SQ.M.
   MATL POISSON RATIO ....... NU   =      .350
   MATL BULK MODULUS ........ K    = .7891E+11 N/SQ.M.
   MATL LIN. COEF. OF THERM. EXP. ... ALFA = .2400E-04 /DEG-C
```

```
   MATL SP HEAT (SOLID) ..... CPS  =      .235 CAL/GM/DEG-C
   MATL SP HEAT (LIQUID) ..... CPL  =      .255 CAL/GM/DEG-C
   MATL AMB M-GRUN COEF (CAL,INP) ... GAMO =    2.129, 2.130
   MATL YIELD STRENGTH ..... SY   =   290.000 MPA
   MATL ULT STRENGTH ..... SU   =   434.000 MPA
   MATL BRN HDNS NO ..... BHN  =   120.000
   MATL MELT TEMPERATURE ..... TM   =    660.00 DEG-C
   MATL VAPOR TEMPERATURE ..... TV   =   2450.00 DEG-C
   MATL HEAT OF FUSION ..... HF   =     95.00 CAL/GM
   MATL HEAT OF VAPORIZATION ..... HV   =   2450.00 CAL/GM
   MATL INICPIENT MELT ENERGY ..... IME  = .6492E+06 JOULES/KG
   MATL INCIPIENT VAPOR ENERGY ..... IVE  = .2958E+07 JOULES/KG

ADDITIONAL PARAMETERS REQUIRED FOR CALCULATING MATERIAL RELEASE FROM
SHOCKED STATE USING THE TILLOTSON EQUATION OF STATE:
   AA  =   .7850E+11 N/SQ.M.
   BB  =   .4831E+11 N/SQ.M.
   A   =   .5000
   B   =  1.6292
   ALF =  5.0000
   BET =  5.0000
   EOI =   .6687E+07 JOULES/KG
   EOM =  1.0000
   EO  =   .6687E+07 JOULES/KG
   ES  =   .2958E+07 JOULES/KG
   HV  =   .1026E+08 JOULES/KG
   ESP =   .1321E+08 JOULES/KG
   VS  =   .4170 CU.CM./GM
   EPS =   .0050

END-STATE CALCULATION RESULTS USING THE TILLOTSON EOS ...
MATERIAL FIN SP VOL (VF) .....       .494 CU.CM./GM
MATERIAL SHOCK ENERGY ........  .1250E+08 JOULES/KG
MATERIAL ENERGY RECOVERED ....  .9992E+07 JOULES/KG
WASTE HEAT GENERATED .........  .2508E+07 JOULES/KG
ENERGY REQ, INCIPIENT MELT ...  .6492E+06 JOULES/KG
ENERGY REQ, COMPLETE MELT ....  .1047E+07 JOULES/KG
EXCESS ENERGY AVAILABLE ......  .1461E+07 JOULES/KG
RESIDUAL MATERIAL TEMP .......   2028.692 DEG-C

PERCENT OF SHOCKED AND RELEASED MATERIAL ...
   IN SOLID STATE ...    .00%
   IN MOLTEN FORM ... 100.00%
   IN VAPOR FORM ....    .00%

PROJECTILE LAYER DENSITY .....    2.7120 GM/CU.CM.
PROJECTILE LAYER LENGTH ......     .2540 CM
PROJECTILE LAYER DIAMETER ....    2.5400 CM
PROJECTILE LAYER MASS ........    3.4904 GMS

PROJ LENGTH WHERE RWAVE HITS SWAVE ....     .7009 CM
LENGTH OF PROJ LYR MATL SUBJ TO S&R ...     .2540 CM
MASS OF UNSH PROJ LYR MATERIAL ........     .0000 GMS
MASS OF SH AND REL PROJ LYR MATL ......    3.4904 GMS
   MASS OF S&R SOLID LYR MATL .........     .0000 GMS
   MASS OF S&R LIQUID LYR MATL ........    3.4904 GMS
   MASS OF S&R VAPOR LYR MATL .........     .0000 GMS
TOTAL SOLID LAYER MASS COMPONENT ......     .0000 GMS
TOTAL NON-SOLID LAYER COMPONENT .......    3.4904 GMS

***** PROJECTILE MATERIAL RELEASE CALCULATIONS, LAYER NO. 2 *****

INITIAL CONDITIONS FOR PROJECTILE LAYER NO.  2 MATERIAL ...
   PARTICLE VELOCITY ........... UP =    3.359 KM/S
```

```
   SHOCK WAVE SPEED ..... US =    9.777 KM/S
   SHOCK PRESSURE ..... PH =  257.156 GPA =  2.539 MBAR
   SHOCK ENERGY ..... EH =  .5642E+07 JOULES/KG
   SPECIFIC VOLUME (AT REST) ... V0 =       .128 CU.CM./GM
   SPECIFIC VOLUME (SHOCKED) ... V1 =       .084 CU.CM./GM

PARAMETERS REQUIRED FOR CALCULATING RELEASE OF PROJ LAYER NO.  2 MATERIAL
FROM SHOCKED STATE USING THE TILLOTSON EQUATION OF STATE:
   MATL ELASTIC MODULUS ..... E    = .1999E+12 N/SQ.M.
   MATL POISSON RATIO ..... NU   =      .300
   MATL BULK MODULUS ..... K    = .1666E+12 N/SQ.M.
   MATL LIN. COEF. OF THERM. EXP. ... ALFA = .1120E-04 /DEG-C
   MATL SP HEAT (SOLID) ..... CPS  =      .110 CAL/GM/DEG-C
   MATL SP HEAT (LIQUID) ..... CPL  =      .125 CAL/GM/DEG-C
   MATL AMB M-GRUN COEF (CAL,INP) ... GAM0 =    1.553, 1.670
   MATL YIELD STRENGTH ..... SY   =   469.000 MPA
   MATL ULT STRENGTH ..... SU   =   745.000 MPA
   MATL BRN HDNS NO ..... BHN  =   290.000
   MATL MELT TEMPERATURE ..... TM   =  1510.00 DEG-C
   MATL VAPOR TEMPERATURE ..... TV   =  3070.00 DEG-C
   MATL HEAT OF FUSION ..... HF   =    65.00 CAL/GM
   MATL HEAT OF VAPORIZATION ..... HV   =  1590.00 CAL/GM
   MATL INICPIENT MELT ENERGY ..... IME  = .6953E+06 JOULES/KG
   MATL INCIPIENT VAPOR ENERGY ..... IVE  = .1784E+07 JOULES/KG

ADDITIONAL PARAMETERS REQUIRED FOR CALCULATING MATERIAL RELEASE FROM
SHOCKED STATE USING THE TILLOTSON EQUATION OF STATE:
   AA  =   .1635E+12 N/SQ.M.
   BB  =   .2165E+12 N/SQ.M.
   A   =   .5000
   B   =  1.0525
   ALF =  5.0000
   BET =  5.0000
   EOI =   .1447E+08 JOULES/KG
   EOM =  1.0000
   EO  =   .1447E+08 JOULES/KG
   ES  =   .1784E+07 JOULES/KG
   HV  =   .6656E+07 JOULES/KG
   ESP =   .8439E+07 JOULES/KG
   VS  =   .1444 CU.CM./GM
   EPS =   .0050

END-STATE CALCULATION RESULTS USING THE TILLOTSON EOS ...
MATERIAL FIN SP VOL (VF) .....       .142 CU.CM./GM
MATERIAL SHOCK ENERGY .....  .5642E+07 JOULES/KG
MATERIAL ENERGY RECOVERED ....  .4211E+07 JOULES/KG
WASTE HEAT GENERATED .....  .1431E+07 JOULES/KG
ENERGY REQ, INCIPIENT MELT ...  .6953E+06 JOULES/KG
ENERGY REQ, COMPLETE MELT ....  .9674E+06 JOULES/KG
EXCESS ENERGY AVAILABLE .....  .4639E+06 JOULES/KG
RESIDUAL MATERIAL TEMP .....   2396.557 DEG-C

PERCENT OF SHOCKED AND RELEASED MATERIAL ...
   IN SOLID STATE ...    .00%
   IN MOLTEN FORM ... 100.00%
   IN VAPOR FORM ....    .00%

PROJECTILE LAYER DENSITY .....    7.8300 GM/CU.CM.
PROJECTILE LAYER LENGTH .....     .2540 CM
PROJECTILE LAYER DIAMETER ....    2.5400 CM
PROJECTILE LAYER MASS .....   10.0775 GMS

PROJ LENGTH WHERE RWAVE HITS SWAVE ....     .7009 CM
LENGTH OF PROJ LYR MATL SUBJ TO S&R ...     .2540 CM
```

```
MASS OF UNSH PROJ LYR MATERIAL .....      .0000 GMS
MASS OF SH AND REL PROJ LYR MATL .....   10.0775 GMS
   MASS OF S&R SOLID LYR MATL .....       .0000 GMS
   MASS OF S&R LIQUID LYR MATL .....     10.0775 GMS
   MASS OF S&R VAPOR LYR MATL .....       .0000 GMS
TOTAL SOLID LAYER MASS COMPONENT .....    .0000 GMS
TOTAL NON-SOLID LAYER COMPONENT .....    10.0775 GMS

***** PROJECTILE MATERIAL RELEASE CALCULATIONS, LAYER NO. 3 *****

INITIAL CONDITIONS FOR PROJECTILE LAYER NO.  3 MATERIAL ...
   PARTICLE VELOCITY ..... UP =    2.559 KM/S
   SHOCK WAVE SPEED ..... US =    7.315 KM/S
   SHOCK PRESSURE ..... PH =  358.834 GPA =  3.542 MBAR
   SHOCK ENERGY ..... EH =  .3274E+07 JOULES/KG
   SPECIFIC VOLUME (AT REST) ... V0 =       .052 CU.CM./GM
   SPECIFIC VOLUME (SHOCKED) ... V1 =       .034 CU.CM./GM

PARAMETERS REQUIRED FOR CALCULATING RELEASE OF PROJ LAYER NO.  3 MATERIAL
FROM SHOCKED STATE USING THE TILLOTSON EQUATION OF STATE:
   MATL ELASTIC MODULUS ..... E    = .4068E+12 N/SQ.M.
   MATL POISSON RATIO ..... NU   =      .300
   MATL BULK MODULUS ..... K    = .3390E+12 N/SQ.M.
   MATL LIN. COEF. OF THERM. EXP. ... ALFA = .4000E-05 /DEG-C
   MATL SP HEAT (SOLID) ..... CPS  =      .035 CAL/GM/DEG-C
   MATL SP HEAT (LIQUID) ..... CPL  =      .046 CAL/GM/DEG-C
   MATL AMB M-GRUN COEF (CAL,INP) ... GAM0 =    1.448, 1.480
   MATL YIELD STRENGTH ..... SY   =  1379.000 MPA
   MATL ULT STRENGTH ..... SU   =  1517.000 MPA
   MATL BRN HDNS NO ..... BHN  =   400.000
   MATL MELT TEMPERATURE ..... TM   =  3410.00 DEG-C
   MATL VAPOR TEMPERATURE ..... TV   =  5900.00 DEG-C
   MATL HEAT OF FUSION ..... HF   =    53.00 CAL/GM
   MATL HEAT OF VAPORIZATION ..... HV   =  1054.00 CAL/GM
   MATL INICPIENT MELT ENERGY ..... IME  = .4996E+06 JOULES/KG
   MATL INCIPIENT VAPOR ENERGY ..... IVE  = .1201E+07 JOULES/KG

ADDITIONAL PARAMETERS REQUIRED FOR CALCULATING MATERIAL RELEASE FROM
SHOCKED STATE USING THE TILLOTSON EQUATION OF STATE:
   AA  =   .3302E+12 N/SQ.M.
   BB  =   .2476E+12 N/SQ.M.
   A   =   .5000
   B   =   .9481
   ALF = 10.0000
   BET = 10.0000
   EOI =   .2574E+07 JOULES/KG
   EOM =  1.0000
   EO  =   .2574E+07 JOULES/KG
   ES  =   .1201E+07 JOULES/KG
   HV  =   .4412E+07 JOULES/KG
   ESP =   .5613E+07 JOULES/KG
   VS  =   .0590 CU.CM./GM
   EPS =   .0050

END-STATE CALCULATION RESULTS USING THE TILLOTSON EOS ...
MATERIAL FIN SP VOL (VF) .....       .055 CU.CM./GM
MATERIAL SHOCK ENERGY ........  .3274E+07 JOULES/KG
MATERIAL ENERGY RECOVERED ....  .2564E+07 JOULES/KG
WASTE HEAT GENERATED .........  .7095E+06 JOULES/KG
ENERGY REQ, INCIPIENT MELT ...  .4996E+06 JOULES/KG
ENERGY REQ, COMPLETE MELT ....  .7215E+06 JOULES/KG
ENERGY AVAILABLE FOR MELT ....  .2099E+06 JOULES/KG
RESIDUAL MATERIAL TEMP .......   3410.000 DEG-C
```

```
PERCENT OF SHOCKED AND RELEASED MATERIAL ...
   IN SOLID STATE ...   5.40%
   IN MOLTEN FORM ...  94.60%
   IN VAPOR FORM ....    .00%

PROJECTILE LAYER DENSITY .....   19.1700 GM/CU.CM.
PROJECTILE LAYER LENGTH ......     .2540 CM
PROJECTILE LAYER DIAMETER ....    2.5400 CM
PROJECTILE LAYER MASS ........   24.6725 GMS

PROJ LENGTH WHERE RWAVE HITS SWAVE ....     .7009 CM
LENGTH OF PROJ LYR MATL SUBJ TO S&R ...     .1929 CM
MASS OF UNSH PROJ LYR MATERIAL ........    5.9316 GMS
MASS OF SH AND REL PROJ LYR MATL ......   18.7409 GMS
   MASS OF S&R SOLID LYR MATL .........    1.0128 GMS
   MASS OF S&R LIQUID LYR MATL ........   17.7281 GMS
   MASS OF S&R VAPOR LYR MATL .........     .0000 GMS
TOTAL SOLID LAYER MASS COMPONENT ......    6.9444 GMS
TOTAL NON-SOLID LAYER COMPONENT .......   17.7281 GMS


MASS DISTRIBUTION SUMMARY ...
   PROJECTILE LAYER NO.  1 ... SOLID ....     .00 GMS
                               UNSH ....     .00 GMS
                               SNR .....     .00 GMS
                               S&R .....     .00 GMS
                              LIQUID ...    3.49 GMS
                              VAPOR ....     .00 GMS
   PROJECTILE LAYER NO.  2 ... SOLID ....     .00 GMS
                               UNSH ....     .00 GMS
                               SNR .....     .00 GMS
                               S&R .....     .00 GMS
                              LIQUID ...   10.08 GMS
                              VAPOR ....     .00 GMS
   PROJECTILE LAYER NO.  3 ... SOLID ....    6.94 GMS
                               UNSH ....    5.93 GMS
                               SNR .....     .00 GMS
                               S&R .....    1.01 GMS
                              LIQUID ...   17.73 GMS
                              VAPOR ....     .00 GMS
   TARGET MATERIAL ..........  SOLID ....   15.15 GMS
                               FRAG ....   15.15 GMS
                               S&R .....     .00 GMS
                              LIQUID ...    4.36 GMS
                              VAPOR ....     .00 GMS

SOME UNSHOCKED PROJ MATL REMAINS ...

   TOT MPROJ,UNSH ...  5.932 GMS  (= .155MPROJ)
   AVG VP,UNSH ..... 11.053 KM/S (=1.105V)

ALL OTHER SOLID PROJECTILE MATERIAL (IF ANY) IS LIKELY TO BE FRAGMENTED.
ANY SOLID TARGET MATERIAL REMAINING IS ALSO LIKELY TO BE FRAGMENTED.
THE DEBRIS CLOUD CONSISTS OF SHOCKED AND RELEASED PROJECTILE MATERIAL AND
ALL EJECTED TARGET MATERIAL.

DEBRIS CLOUD VELOCITY SUMMARY ...
   DEB CLD CENTER-OF-MASS VEL (VCOM) ...  6.114 KM/SEC (= .611V)
   DEB CLD LEADING EDGE VEL (VL) ....... 10.652 KM/SEC (=1.065V)
   DEB CLD EXPANSION VEL (VEXP) ........  4.539 KM/SEC (= .454V)


DEBRIS CLOUD HALF-ANGLE ..... 36.589 DEG
```

DISTRIBUTION LIST
(WL-TR-94-7039)

Eglin AFB Offices:

WL/MNSA	**10**
WL/MNOI (STINFO Facility)	**1**
WL/CA-N	**1**

HQ Defense Nuclear Agency/SPSP
Attn: Mr Tony Frederickson
6801 Telegraph Rd
Alexandria VA 22310-3398
2

DASIAC
2560 Huntington Ave, Suite 500
Alexandria VA 22303-1490
1

Space and Missile Systems Center/MGWE
Attn: Mr Mehdi Kavary
P. O. Box 92960
Los Angeles CA 90009-2960
1

DTIC/DDAC
Cameron Station
Alexandria VA 22304-6145
1

BMDO/AQT
The Pentagon
Attn: Lt Col Charles Martin
Washington DC 20301-7000
1

USA Space & Strategic Defense Command
CSSD-SL-L
Attn: Dr Robert Becker
PO BOX 1500
Huntsville AL 35807-3801
1